Shipboard Aggregate Power Monitoring

by

Keith P. Douglas

ARCHIVES

B.S. Systems Engineering, United States Naval Academy, 1997
Master of Engineering Management, Old Dominion University, 2004

Submitted to the Department of Mechanical Engineering in Partial Fulfillment of the Requirements for the Degrees of

Naval Engineer
and
Master of Science in Mechanical Engineering
at the
MASSACHUSETTS INSTITUTE OF TECHNOLOGY
June 2009

Signature of Author_____
Department of Mechanical Engineering
May 8, 2009

Certified by _____
Robert W. Cox
Assistant Professor of Electrical and Computer Engineering, UNC Charlotte
Thesis Supervisor

Certified by_____
Steven B. Leeb
Professor of Electrical Engineering and Computer Science & Mechanical Engineering
Thesis Supervisor

Certified by _____
James Paris, Doctoral Candidate
Department of Electrical Engineering and Computer Science
Thesis Reader

Accepted by _____
David E. Hardt
Chairman, Department Committee on Graduate Students
Department of Mechanical Engineering

Shipboard Aggregate Power Monitoring

by

Keith P. Douglas

Submitted to the Department of Mechanical Engineering
on May 8, 2009 in Partial Fulfillment of the
Requirements for the Degrees of

Naval Engineer

And

Master of Science in Mechanical Engineering

ABSTRACT

Modern naval warships rely on vast arrays of sensor networks to evaluate the performance of mission critical systems. Although these sensor networks enable increased levels of automation, they are costly to install and to maintain. The power distribution network offers an alternative solution for tracking the performance of mission critical systems. Research conducted at Massachusetts Institute of Technology's Laboratory for Electromagnetic and Electronic Systems (LEES) has proven that the power distribution network contains vital information that can provide performance monitoring and automatic diagnostic functions.

This thesis will address the issue of sensor-count reduction through the application of Non-Intrusive Load Monitoring (NILM) technology. Theoretical studies and field experiments will be presented in order to demonstrate the NILM's ability to correlate load activity with power measured from an aggregate level in the distribution system. Additionally, a critical evaluation is conducted on the current NILM configuration's ability to perform automated classification. Findings will be supported using data collected from NILMs monitoring power flow on board the U.S. Coast Guard Cutter ESCANABA (WMEC-907).

Thesis Supervisor: Robert W. Cox
Title: Assistant Professor of Electrical and Computer Engineering, UNC Charlotte

Thesis Advisor: Steven B. Leeb
Title: Professor of Electrical Engineering and Computer Science & Mechanical Eng.

The author would like to acknowledge the following organizations and individuals for their assistance. Without them this thesis would not have been possible.

- Dr. Steven Leeb who was always willing to listen and provide excellent advice. It was refreshing to have an advisor so passionate about his work.
- Dr. Robert Cox for his incredible patience and support. Thanks for fielding all my phone calls.
- Jim Paris who was always available to help with all computer-related issues, whether they were Linux questions or reformatting hard drives.
- Warit Wichakool for all of his technical assistance and hardware support throughout the various installations on the USCG Cutter ESCANABA.
- Jeremy Leghorn and Greg Elkins- my Navy buddies. We definitely had some memorable field installations and trips to LBES.
- The Officers and crew of the USCGC ESCANABA (WMEC-907). Specifically, LT Andrew Goshorn who went far past expectations in allowing the MIT LEES research team access to the ship.
- My lovely wife, Stacey, and my two beautiful kids, Hayden and Mia. Their warm smiles and support gave me the strength I needed to complete this task.

Table of Contents

List of Figures

List of Tables

This Page Intentionally Left Blank

Chapter 1

Introduction

1. 1 Background

The Non-Intrusive Load Monitor (NILM) is a device used to measure raw current and voltage from a single point in an electrical distribution system (Figure 1-1). These measurements are converted (preprocessed) into real and reactive power (Figure 1-2) and their associated harmonics. When applied to a given electro-mechanical system, the power measurements provide vital system information that can be used to determine the overall "health" of not only the electrical components (i.e. motors), but also the mechanical components (i.e. pumps, filters, valves, etc.) of a given system.

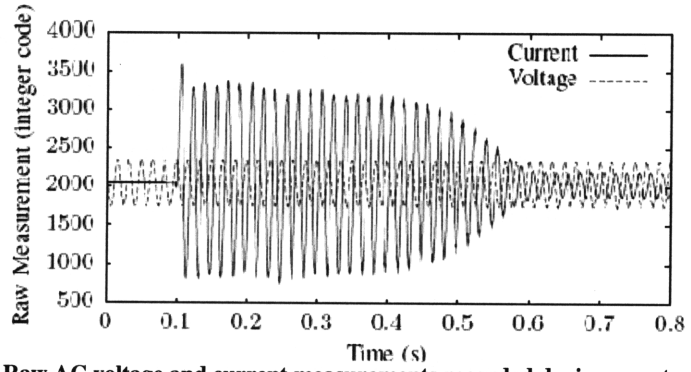

Figure 1-1: Raw AC voltage and current measurements recorded during a motor start-up. (1)

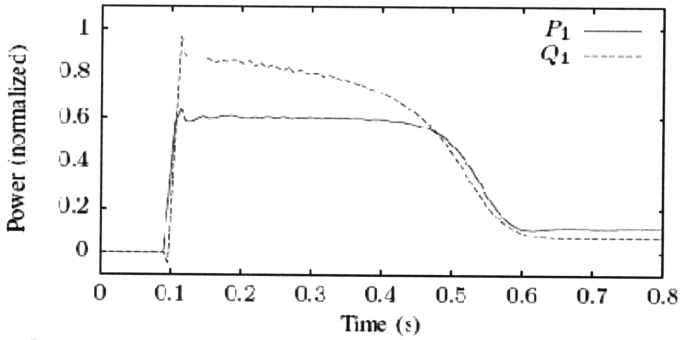

Figure 1-2: Preprocessed spectral power envelopes of motor transient in Figure 1-1. The high frequency content associated with the raw data has been removed. Preprocessor information is typically used for NILM applications that involve real-time detection and classification algorithms. (1)

The NILM's effectiveness in shipboard power-based evaluation and monitoring has been demonstrated on several occasions. Early research focused on collecting power data from individual loads (auxiliary seawater system, sewage system, reverse osmosis), then analyzing the archived data to determine correlations between system operation and power signatures. (2) (3) (4) More recently, research efforts have focused on applying the knowledge gained from individual load monitoring to modern state and parameter estimation algorithms to provide system "health" information for user interfaces and diagnostic tools. (5) (6) (7)

Figure 1-3 shows a NILM layout, where multiple loads are monitored via a single NILM. As the NILM moves further "upstream" to monitor multiple loads from a single point, it becomes less "intrusive". However, there are practical limitations to how far "upstream" the NILM can effectively perform such tasks as event detection and system diagnostics. From a designer's perspective, there are necessary tradeoffs that impact the NILM's performance in real world applications. This thesis will address the tradeoffs that affect the likely performance of the NILM in shipboard power systems. Additionally, current event detection and classification methods will be scrutinized using both local and upstream data collected during recent field studies on the USCGC ESCANABA (WMEC-907) and the U.S. Navy's Land Based Engineering Site (LBES) in Philadelphia, Pennsylvania.

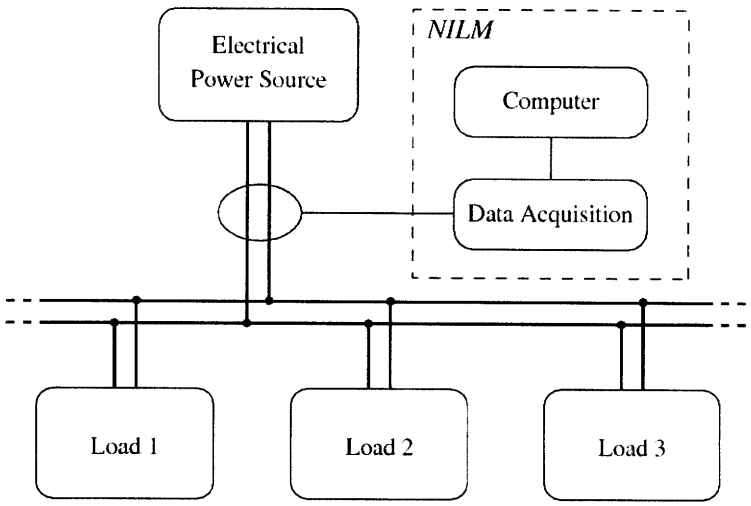

Figure 1-3: Typical system layout for a NILM used to monitor multiple loads. (1)

1.2 Motivation for Research

The U.S. Department of the Navy spends approximately $4 billion a year to maintain its existing fleet (8). In an effort to lower the costs associated with maintaining an aging fleet, the navy enterprise has incorporated policy aimed at reducing lifecycle maintenance costs. In May of 1998, the Chief of Naval Operations instituted a condition-based maintenance (CBM) policy (9), which focused on eliminating waste associated with traditional navy maintenance practices that relied on preventative maintenance strategies.

During the same time period as CBM implementation, the Smart Ship concept was also gaining momentum (10). The focus of the Smart Ship project was to identify key enablers for reducing manning and workload. Initially, 61 enabling technologies were identified and installed on the navy's prototype Smart Ship, the USS YORKTOWN (CG 48). These enablers were divided into seven core technologies, one of which was the Integrated Condition Assessment System (ICAS) (11).

ICAS is the U.S. Navy's CBM program of record; it is currently installed on 95 surface ships (10). The ICAS provides the capability to collect, monitor, and trend machinery data via various types of sensors located within the systems of interest. This information can then be used locally by ship's force to diagnose equipment or sent to intermediate maintenance facilities for diagnosis and trend analysis. However, in order for ICAS to realize its full potential, it must continue to grow and increase its capabilities to meet the needs of the future navy.

One area for potential improvement in ICAS technology is sensor count reduction. ICAS relies on an extensive array of sensors to provide the vital information regarding component status. As the sensor count grows, so does the complexity and costs associated with maintaining the very system designed to reduce maintenance costs. The USS San Antonio (LPD-17) has 7023 signals associated with the Machinery Control System (MCS), while the amphibious assault ships have over 12,000 signals. The Navy's Future Surface Combatant (DDG 1000) is projected to have up to 33,000 control signals. (12)

For a little more than a decade, researchers at the Massachusetts Institute of Technology (MIT) have analyzed ways to monitor shipboard systems using the Non-Intrusive Load Monitor (NILM). The NILM is a system that can determine the operating schedule of electrical loads in a target system using centralized measurements (13). By monitoring the power signatures associated with individual loads from an electrical node, the NILM has the potential to drastically reduce sensor count currently associated with U.S. Navy vessels. This sensor count reduction combined with the existing ICAS architecture could prove tremendously beneficial to the Navy's condition based maintenance program.

1.3 Objective and Outline

Previous shipboard research involving the NILM relied on dedicated component monitoring. This approach allowed researchers to effectively demonstrate several basic diagnostic indicators for mechanical loads based on electrical power signatures. Current research has focused on using the NILM to conjointly monitor several loads from an aggregate point in the electrical power system. The objective of this research is to explore how well the NILM can determine load composition within shipboard aggregate power systems using spectral envelope estimates.

The thesis consists of five chapters including the introduction and conclusions. Chapter 2 takes an in-depth look at three key challenges that must be addressed when designing aggregate power monitoring systems. Methods for aggregate event detection that are identified in Chapter 2 are applied in Chapter 3, which uses data gathered from the Navy's Land Based Engineering Site (LBES) in Philadelphia, Pennsylvania. Chapter 4 provides a brief description of the most current NILM configuration, which uses a software package, *Ginzu*, to perform automated classification and diagnostics. Lessons learned from a recent deployment of the USCGC ESCANABA (WMEC-907) with this particular NILM installed are also explored.

Chapter 2

Aggregate Power System Monitoring

The power distribution network can be exploited not only as a means for power distribution, but also as a means for providing useful diagnostic system monitoring. This chapter focuses on recent research conducted to demonstrate how well the NILM performs in an aggregate environment, where the objective is to minimize the number of NILM monitors required to capture useful system information for diagnostic monitoring. Figures and equations provided throughout this chapter were taken from (1), which was co-authored by the author of this thesis.

Ideally, a single NILM would be able to perform diagnostic monitoring of an entire ship; however, there are practical limitations that prevent this level of "non-intrusiveness". Although not all inclusive, the following three areas heavily influence the NILM's ability to perform aggregate diagnostic monitoring and are the focal point of this chapter:

- First, the NILM samples a continuous signal (i.e. current), which results in quantization. This quantization is the result of the analog-to-digital conversion (ADC), where the analog signal must be converted into finite digital data output. For a given NILM hardware configuration, the power range it observes is bounded by the sensor and ADC card selection. As the NILM is moved further "upstream" in the power distribution system, the corresponding power range increases. The larger power range results in different hardware selection, which ultimately influences the NILM's ability to accurately detect smaller transients.
- Second, the NILM is susceptible to external signals that distort underlying information in acquired signals. This includes random measurement noise and other distortions such as possible electromagnetic noise.
- Third, the NILM must be capable of disaggregating loads of interest. For example, there may be two induction motors of similar size associated with separate systems. Detection techniques that rely on power level changes alone may not be capable of distinguishing

the two motors. Additionally, random power changes due to such loads as cycling lube oil heaters may mask transients of interest for a given detection algorithm.

2.1 NILM System

Figure 2-1 illustrates how continuous signals (current and voltage) are (1) sensed, (2) sampled, and then (3) processed to perform various load monitoring functions. A typical NILM configuration consists of an enclosed sensor box, external power connections to include current transducers and voltage sensing lines, and a personal laptop computer for data processing and archiving.

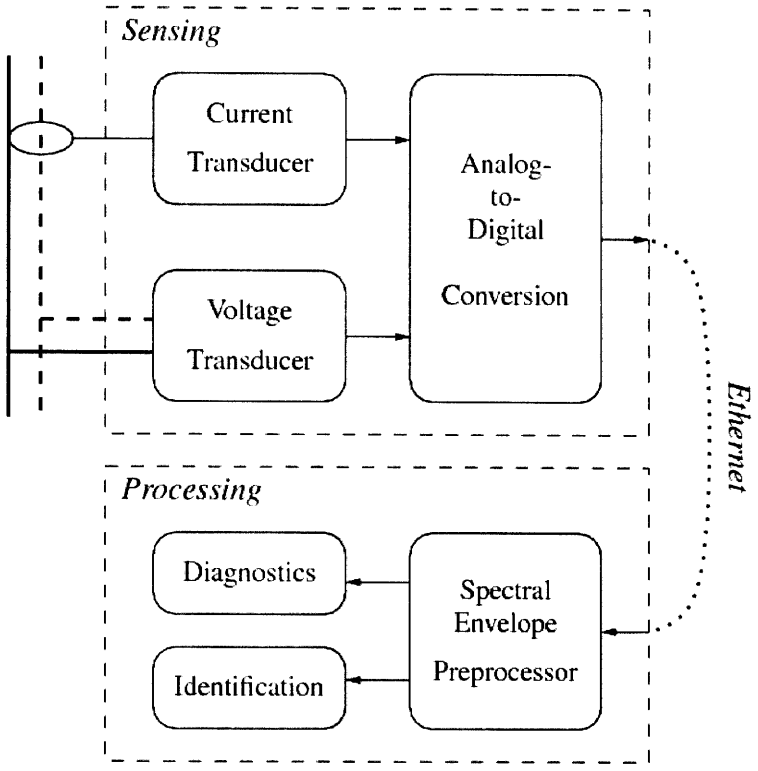

Figure 2-1: NILM data acquisition and processing diagram.

Acquired data in the form of current and voltage is first converted into digital form through an analog-to-digital converter. The quantized signal from the converter is passed to a personal computer (PC) via Ethernet for preprocessing. Preprocessed data extracts useful information from the raw data signal for detection, classification, and diagnostic functions. Figure 2-2

provides an internal view of a NILM sensor box. Figure 2-3 displays the physical layout of an entire NILM install.

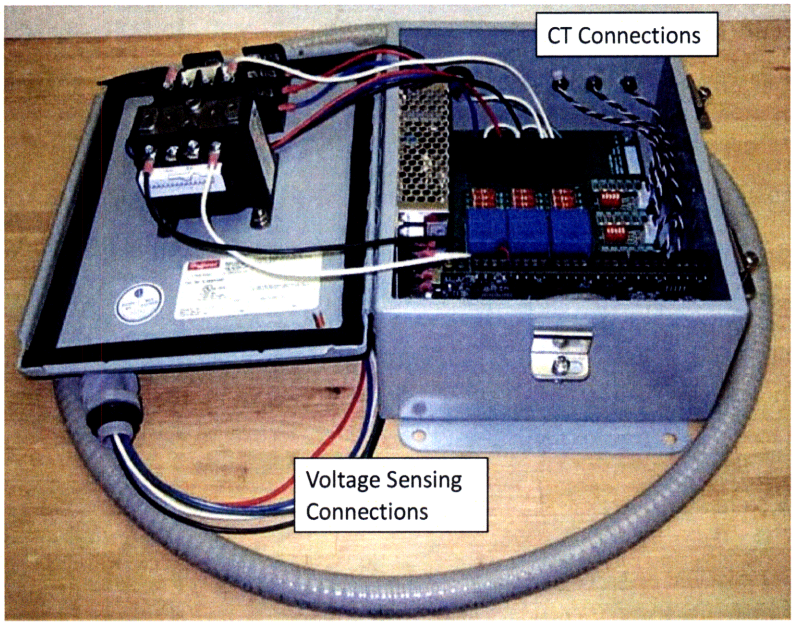

Figure 2-2: Integrated NILM sensor box courtesy of NEMOmetrics. Sensor box includes connections for power, current signals, as well as an Ethernet connection to connect to an external PC.

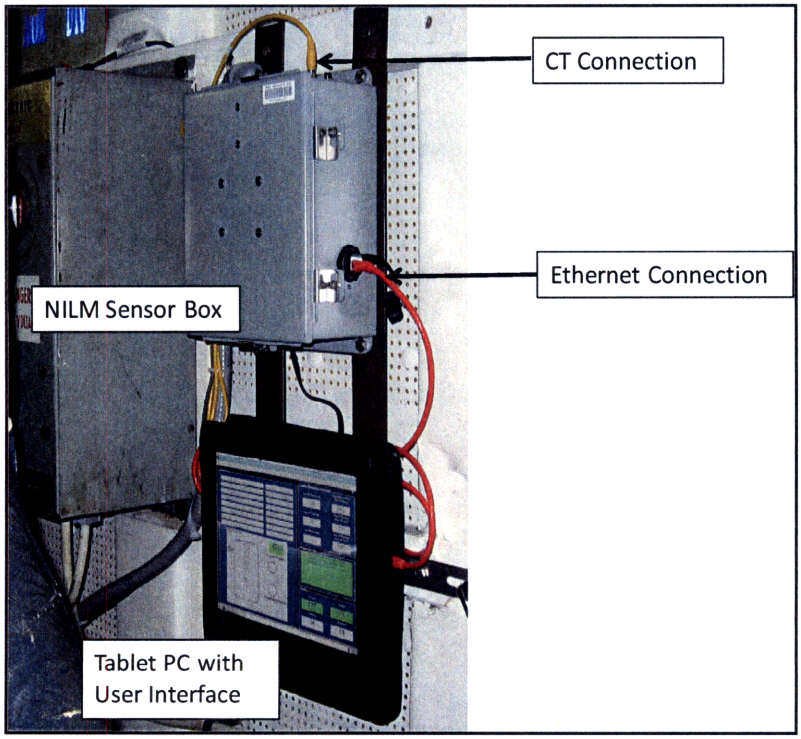

Figure 2-3: NILM layout for installation on USCGC ESCANABA (WMEC-907).

2.1.1 Data Acquisition

Data acquisition measures the current and voltage that supplies power to a particular load or group of loads within a system. Although voltage and current are both sensed, this discussion will focus on current alone. A majority of the information that is used for NILM applications is derived from the current signal. A current transducer such as the one shown in Figure 2-4 is placed around a particular phase to sense the incoming primary current, I_P. The I_P is converted into a smaller signal by a conversion ratio K_N. The output of the CT is referred to as the secondary current, I_S. TABLE 2-1 lists commonly used current transducers for NILM applications.

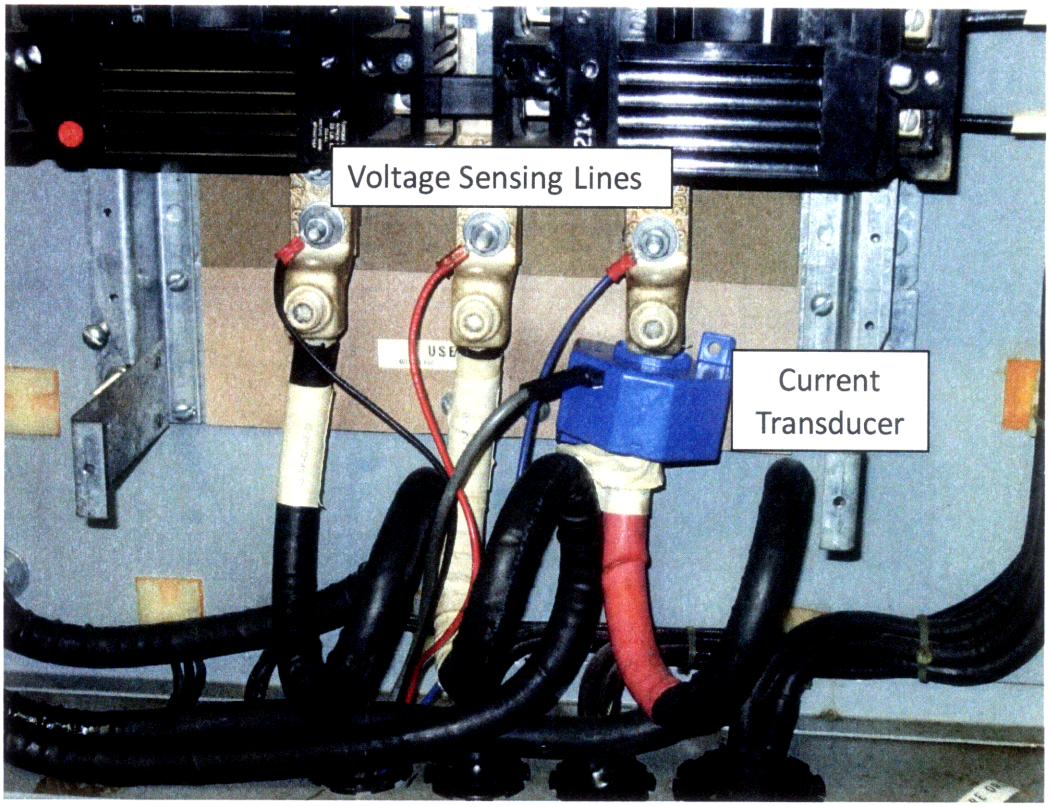

Figure 2-4: Interior view of Power Panel 2-82-3. The LA-205-S current transducer (CT) and three voltage sensing lines are annotated.

TABLE 2-1: TYPICAL CURRENT TRANSDUCERS AND CONVERSION RATIOS

Model	Maximum Primary Current	K_N
LA-55	$\pm 50\ A$	1/1000
LA-150	$\pm 150\ A$	1/2000
LA-205	$\pm 200\ A$	1/2000
LA-305	$\pm 300\ A$	1/2500

The secondary output I_S is fed to a burden resistor R_M to ground. R_M is proportional to I_P and can be represented as follows:

$$V_M = I_S * R_M = I_P * K_N * R_M \quad 2\text{-}1$$

For an LA-55 CT, a 50 Ω burden resistor, and an I_P of ± 50 A,

$$V_M = \pm 50\ A * \frac{1}{1000} * 50\ \Omega \quad 2\text{-}2$$

$$\approx \pm 2.5\ V \quad 2\text{-}3$$

The continuous amplitudes from the incoming signal,V_M, are applied to an ADC card. The ADC samples the signal at a rate of 8000 samples per second. The process of converting the continuous signal into digital data with finite precision results in quantization. The number of quantization levels L can be derived based on the number of significant binary bits B available for a particular ADC card. For instance, if B =3 bits, there are 2^B quantization levels or 8 discrete levels. The effect of quantization on an incoming continuous signal is shown in Figure 2-5. As the bit level increases, the digital output closely resembles that of the incoming continuous waveform.

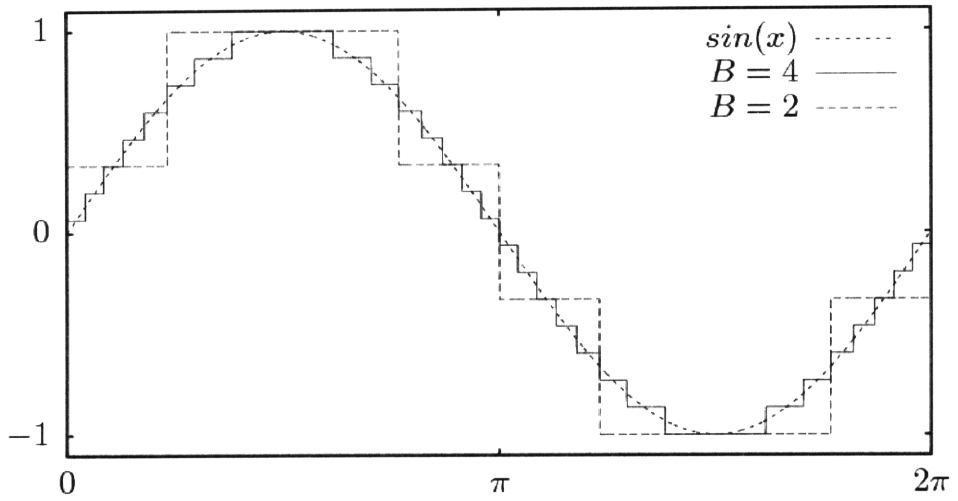

Figure 2-5: Illustration of quantization error introduced during the signal processing through the ADC. The continuous function, sin(x), is compared to a 2 bit and 4 bit discrete output from an ADC.

In (1), a detailed discussion on the various ADC cards typically used for NILM applications is provided. Currently, the LabJack UE9 Ethernet-based card is the standard for NILM installations. This card provides design flexibility by offering Ethernet connection with a downstream PC. Its predecessor, the PCI-1710, required the downstream computer to be placed near the sensor box to accommodate its PCI card. The LabJack UE9 has the following specifications:

- Voltage range (V_R) of $\pm 5\ V$
- Counts output range of 0 to 65520[1]
- 12 bits (B)

One way to describe the accuracy of a given ADC card is by measured voltage per least significant bit (LSB), where

$$V_{M,LSB} = \frac{|V_R|}{2^B} \qquad 2\text{-}4$$

[1] The software associated with the LabJack outputs 16-bit values; however, there are only 12 significant bits. The lower 4 bits have zeros for placeholders. This results in the count output range listed.

Using the LabJack and a 12 bit ADC converter,

$$V_{M,LSB} = \frac{((+5\,V) - (-5\,V))}{2^{12}} \quad 2\text{-}5$$

$$\approx 2.441\,mV/bit \quad 2\text{-}6$$

This represents the maximum accuracy for a particular ADC over its entire input voltage range. Note that in applications, the full V_R may not be achieved; this value is dependent upon the burden resistor and current transducer that is chosen. Recall from 2-3 that the measured range was only $\pm\,2.5\,V$, which results in a loss of half of the available V_R. This loss in resolution can be mitigated by careful selection of burden resistors, CTs, and ADC cards for a given NILM.

Another useful way to describe the accuracy of an ADC card is to determine the primary current per LSB, $I_{P,LSB}$. Using the components in the example above,

$$I_{P,LSB} = \frac{V_{M,LSB}}{K_N * R_M} \quad 2\text{-}7$$

$$I_{P,LSB} = \frac{2.441\,mV/bit}{1/1000 * 50\,\Omega} \quad 2\text{-}8$$

$$\approx 48.82\,mA/bit \quad 2\text{-}9$$

which yields an associated primary current value in amps/bit. Data resolution may also be described by a comparison of a target load current I to $I_{P,LSB}$. The number of least significant bits N corresponding to the target load can be computed as

$$N = \frac{I}{I_{P,LSB}} \quad 2\text{-}10$$

The effective number of bits B_E is found by

$$N = 2^{B_E} \quad 2\text{-}11$$

$$B_E = \log_2(N) \quad 2\text{-}12$$

$$B_E = \log_2\left(\frac{I}{I_{P,LSB}}\right) \quad 2\text{-}13$$

For instance, if I = $\pm$ 5 A for the same ADC, burden resistor, and CT as described for Equation 2-9,

$$B_E = \log_2\left(\frac{(+5\,A - (-5\,A))}{48.82\,mA/bit}\right) \quad 2\text{-}14$$

$$\approx 7.68\,bits \quad 2\text{-}15$$

Fully expanded, Equation 2-13 yields

$$B_E = \log_2\left(\frac{I * K_N * R_M * 2^B}{|V_R|}\right) \quad 2\text{-}16$$

2.1.2 Spectral Envelope Preprocessor

The NILM utilizes a preprocessor to extract spectral power envelopes from incoming raw voltage and current waveforms. "Preprocessing exposes energy consumption and harmonic signatures that are relatively uniquely associated with the physical task performed by a load." (1) Similar to radio transmissions using amplitude modulation, the target information is carried on a 60 Hz (for typical shipboard distribution systems) waveform with varying amplitude. The carrier waveform is removed, revealing the power spectrum and its vital information. The resulting envelope is used to identify loads and perform diagnostics.

Reference (14) described that the current signal $x(t)$ could be decomposed using Fourier integrals into the in-phase spectral envelopes a_k and the quadrature spectral envelopes b_k:

$$a_k(t) = \frac{2}{T}\int_t^{t-T} x(\tau)\sin(k\omega\tau)\,d\tau \quad 2\text{-}17$$

$$b_k(t) = \frac{2}{T}\int_t^{t-T} x(\tau)\cos(k\omega\tau)\,d\tau \quad 2\text{-}18$$

where the averaging period T is one or more periods of the line frequency, and the $\sin(k\omega\tau)$is phase-locked to the voltage measurement using a Kalman filter. (15) The integer k corresponds to the harmonic index. For NILM applications, $k = 1$ corresponds to real and reactive power terms. The a_k term provides real power P when scaled based on the front-end data acquisition configuration. Similarly, reactive power Q is computed using the b_k term and the appropriate scale factors. Figure 1-2 illustrates a preprocessor envelope for an induction motor.

2.1.3 Load Classification and Diagnostics

To realize the full potential of the NILM for shipboard applications, there must be intelligent software solutions that are capable of distracting, classifying, and diagnosing transients. Methods for identifying when a transient occurs often rely on steady state power levels and transient power signatures. Typically, transients are noted when a load turns on and off.

Diagnostics require accurate classification of transients within a monitored system. Once properly identified, algorithms can be used to look for "unusual" behavior. Take the CHT system for example. An exemplar or power "fingerprint" may be used to detect when a vacuum pump is turned on. A diagnostic algorithm could then look for unusual behavior, such as excessive run times or improper power levels. Information may then be displayed to the operator to indicate improper operations.

Matching the transient signatures relies on finding unique aspects of a load's power usage. When scaling to larger NILM applications, the ability to discern these unique features is diminished as the number of loads increases. Smarter methods for extracting individual load information may be necessary. This is addressed in further detail in Section 2.5.

2.2 Measurement Accuracy

In order to successfully perform load identification and diagnostics of the aggregate power signal, the NILM must maintain a certain degree of accuracy with respect to data measurements. Recall from previous discussion, that the designer bounds the NILM's power range when

choosing burden resistors, CTs, and ADC cards. As the NILM moves further "upstream", load currents increase resulting in a loss in resolution for smaller loads in the aggregate. One method for evaluating the NILM's performance to disaggregate loads in the "upstream" is to observe how well it detects and classifies target loads.

Two NILMs were installed on the USCGC ESCANABA on February 14, 2009 to measure the effectiveness of the NILM to disaggregate load information. A "downstream" NILM was installed at the CHT control panel, while an "upstream" NILM was placed at a node in the electrical distribution system that feeds the CHT control panel and other downstream loads. The objective was to describe how well the NILM disaggregates and reports the operations of individual electrical loads using aggregate current at the service entry to a power panel that supports multiple loads.

The upstream node for the installation was power panel P 2-282-3 (Figure 2-6), which is located in Auxiliary Machinery Room #1, centerline, against bulkhead 82. It receives power directly from the 450 VAC, 60 hertz, 3φ, 800 amps 1S main distribution switchboard. The panel's isolation breaker has a current trip set point of 150 amps and is located on the 1S distribution board. Panel loads range from the CHT control panel (largest load 1.7 HP vacuum pump) to the 40 HP fin stabilizer motor. The complete list of loads along with ratings is:

- Wastewater Discharge Pump #1 Motor (5 HP)
- Fin Stabilizer #2 Motor (40 HP)
- Reverse Osmosis Disconnect Switch (15 kW)
- HVAC Hot Water Circulation Pump #2 Motor (1.5 HP)
- Potable Water Service Pump #1 Motor (7.5 HP)
- Potable Water Service Pump #2 Motor (7.5 HP)
- CHT Control Panel (Two 1.5 HP Vacuum Pump Motors and Two 2 HP Discharge Pump Motors)

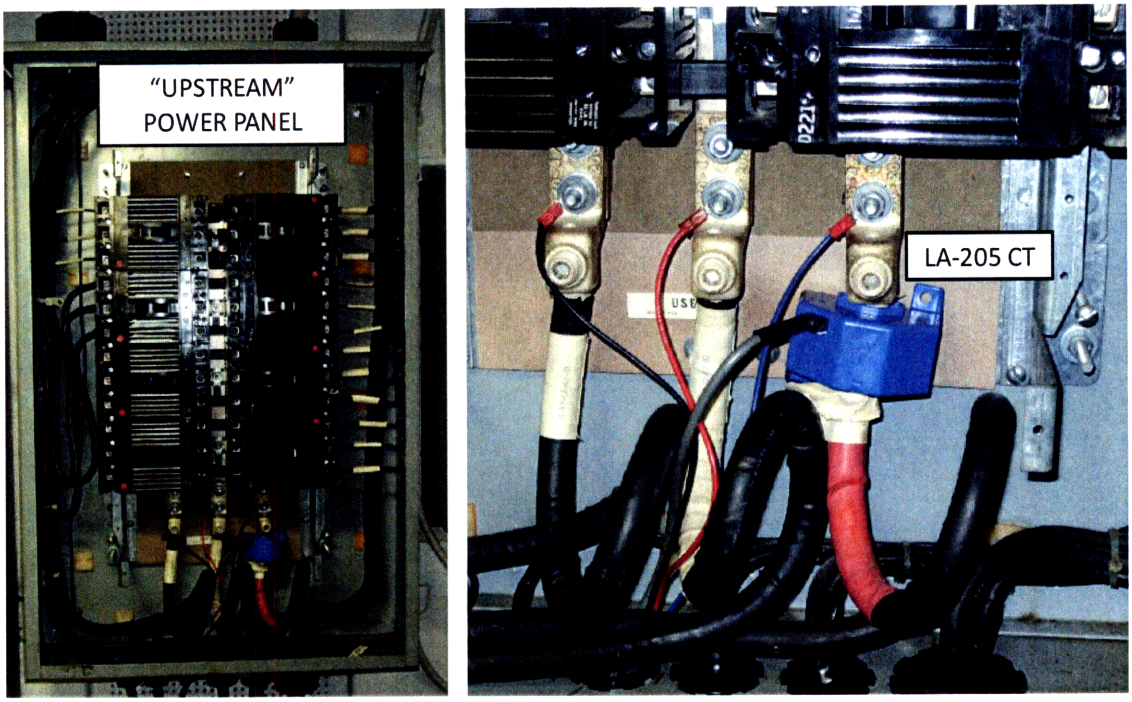

Figure 2-6: Interior view of P-2-282-3 (left) and close-up view of bottom portion of panel (right).

The downstream NILM was placed at the local control panel of the CHT system (Figure 2-7). The control panel receives power from the upstream power panel, P-2-282-3. The primary purpose of the control panel is to provide various control signals to the CHT system, as well as provide power to the system's vacuum and discharge pumps.[2] Three CTs were installed in order to obtain differently scaled raw data locally. The three channels were connected to differently sized burden resistors to create the variation in data scaling.

[2] Further explanation on the control panel can be found in Chapter 4.

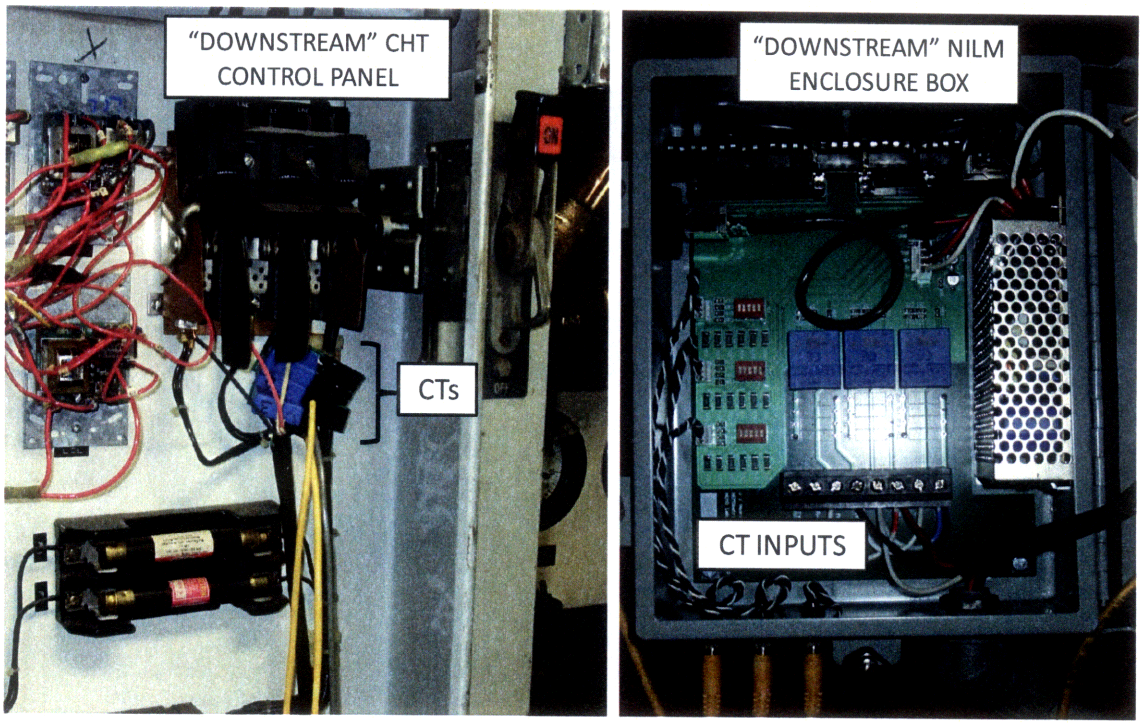

Figure 2-7: Interior view of CHT Control Panel (left) showing three CTs connected to a single phase of line current. Interior view of NILM enclosure box (right) shows the physical location of CT inputs from the control panel.

A single run of CHT vacuum pump transients were captured locally on all three channels, as well as "upstream". Although three different local configurations were installed, the following discussion will focus only on the downstream configuration with the highest bit resolution. TABLE 2-2 lists the NILM front-end components that provide the greatest disparity between "upstream" and "downstream" scaling.

TABLE 2-2: FIELD EXPERIMENT NILM COMPARISON

	Downstream	Upstream
Current Transducer	LA-55	LA-205
K_N	1/1000	1/2000
R_M	155Ω	5Ω
V_R	$\pm 5V$	$\pm 5V$
B	12 bits	12 bits

2.2.1 Raw Data

The degree of closeness with which the "upstream" NILM can measure a "downstream" load is diminished due to selection of the current transducer and analog-to-digital conversion system required to accommodate the "upstream" dynamic power range. Consider a local transient such as a vacuum pump start, which has a 5A current amplitude. Using Equation 2-16 and the NILM configurations in TABLE 2-2, the effective number of bits $B_{E,D}$ of the raw current for the downstream configuration is

$$B_{E,D} = \log_2\left(\frac{5 * \frac{1}{1000} * 155 * 2^{12}}{10}\right) \quad 2\text{-}19$$

$$B_{E,D} \approx 8.31\ bits \quad 2\text{-}20$$

Similarly, the effective number of bits $B_{E,U}$ of the raw current in the upstream is

$$B_{E,U} = \log_2\left(\frac{5 * \frac{1}{2000} * 5 * 2^{12}}{10}\right) \quad 2\text{-}21$$

$$B_{E,U} \approx 2.36\ bits \quad 2\text{-}22$$

This reveals approximately 6 bits of data accuracy is lost, which results in significant degradation of the raw current measured signal. Figure 2-8 shows raw data measurements for a portion of a vacuum pump's transient (shutoff) taken by the two configurations described in TABLE 2-2. Note how small changes of current in the aggregate may be lost in the raw data measurements due to the quantization that occurs due to reduced accuracy.

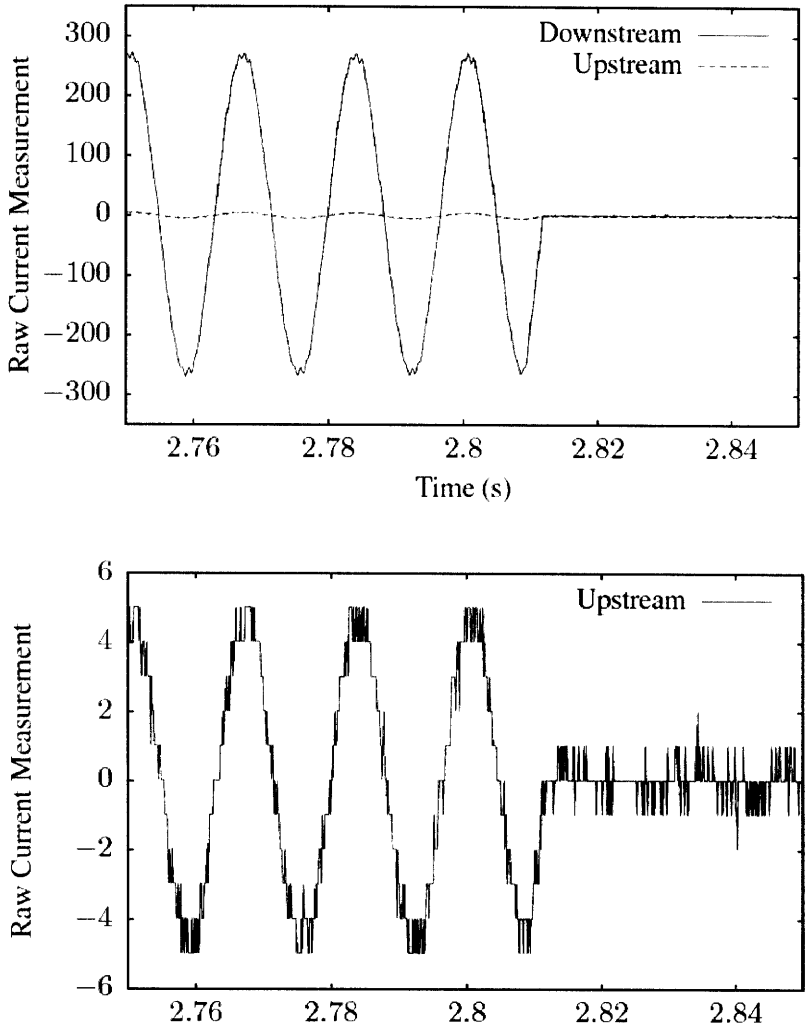

Figure 2-8: Two NILM configurations recording the same transient. Top plot shows raw data captured on both configurations on same scale. Bottom plot is a close-up view of the upstream configuration raw data capture revealing quantization error.

2.2.2 Spectral Envelope Accuracy

Current NILM analysis methods rely solely on preprocessor output, not raw data measurements. Proper (5) and Branch (7) each utilized "prep" output to perform detection, classification, and diagnostic analysis for both the CHT system and Reverse Osmosis (RO). More specifically, the first harmonic indices of real and reactive power have proven to be fruitful signatures for shipboard NILM applications.

Recall from Equations 2-17 and 2-18 that P_1 and Q_1 are calculated using the time-average over a 60 Hz period. Similar to a low-pass filter, as the preprocessor averages the raw data it removes some of the higher frequency content. This results in a "smoother" power data stream, which consequently reduces the raw data quantization error. Although this is not rigorously proven, shipboard NILM aggregate results show strong evidence of this "smoothing" effect. Based on these indications, the "prep "output is less susceptible to the data quantization and scaling issues that reduce raw data accuracy.

Figure 2-9 shows the preprocessor output comparison between the downstream and upstream NILM using the same raw data compared previously in Figure 2-8. Although the raw data shows significant quantization in the upstream, the preprocessor yields very similar results in the upstream and downstream output. These results indicate that the preprocessor output maintains the power information necessary to perform analyses such as load detection and diagnostics.

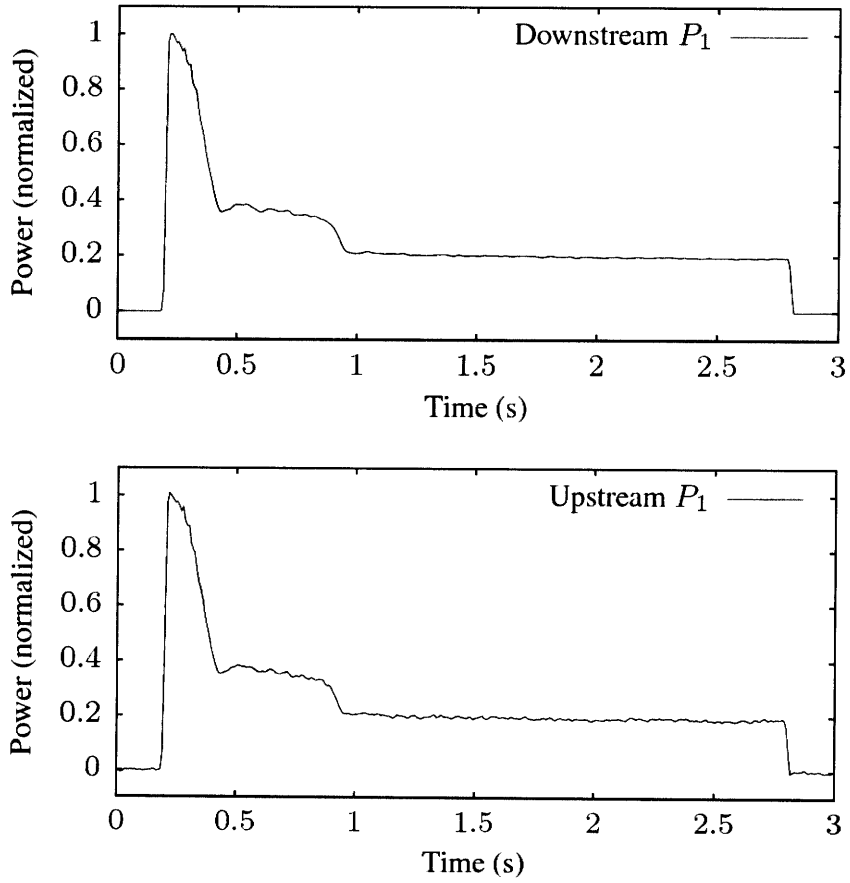

Figure 2-9: Preprocessor spectral envelope comparison for raw data captured in Figure 2-8.

2.3 Measurement Distortion

Alteration of the measured voltage and current waveforms in any matter may adversely impact NILM performance. Distortion may be generated internally from the NILM system or coupled from external sources; this falsification of measured data may be carried throughout the data acquisition and processing stages, resulting in improper classification and diagnostics. Unwanted energy such as thermally generated white noise, electromagnetic coupling, or magnetic interference must be mitigated throughout the design process.

In (1), Paris describes two general categories of distortion related to NILM applications: (1) uncorrelated noise and (2) correlated noise and coupled signals. A brief description of these two sources is described for the reader; however, for additional information on these topics refer to (1) and (16).

2.3.1 Uncorrelated Noise

One form of uncorrelated noise that may occur within the system and which serves as a model for additive noise in general is additive white Gaussian noise (AWGN). This type of noise is characterized by a constant spectral density, which implies the energy associated with the noise is evenly distributed across all frequencies. Furthermore, the noise is normally distributed around a mean of zero. The NILM utilizes a Kalman filter to reduce error associated with the zero-crossing of the voltage measurement. The robust design of the Kalman filter results in high noise rejection (15), and so the NILM is largely unaffected by noise in the voltage input.

Current measured by the preprocessor is also susceptible to this particular noise. However, the NILM's spectral envelope calculations remove the higher frequency content of the incoming waveforms. Since the noise energy is equally distributed across all frequencies, the spectral output only contains a small portion of the energy associated with the noise. Based on these informal discussions and analysis of field results, it is highly unlikely that this type of noise will impact the scalability of the NILM.

2.3.2 Electromagnetic Interference

Noise sources external to the NILM may also impose a risk to its overall performance. One potential source is from electromagnetically coupled sources. Electromagnetic energy may be generated from such sources as current-carrying wire or power generators. As the number of loads for a NILM application increases, the NILM's susceptibility to this type of energy increases.

One method for mitigating risk associated with externally coupled energy is proper shielding techniques. The NILM's enclosure box helps isolate the data acquisition components from these externally-generated emissions. Additional ways to reduce susceptibility include smart layout designs. The NILM's modular design, which allows physical separation between data acquisition components and processing hardware, is also an important aspect in electromagnetic compatibility. Based on previous field studies, which includes several installations on Coast Guard ships, as well as installations at the LBES facility, the NILM does not appear highly susceptible to electromagnetic interference in practice.

2.4 Disaggregation

Perhaps the most challenging issue facing aggregate power monitoring is disaggregation of loads of interest. The obvious benefit created by monitoring more loads from a single NILM is sensor count reduction. However, this imposes new challenges when it comes to extracting target loads. The complexity associated with disaggregation is not constant from one site installation to the next. It is very dependent upon the type of information that must be obtained in order to fulfill the requirements for a particular NILM installation. For example, one NILM application may only require properly identifying the status of multiple pumps within a fluid system. This scenario could most likely be addressed using steady state power levels and finite state modeling. A different application may require loading information of a particular system such as the low pressure air compressor (LPAC) system. Since LPAC loading results in variation in the compressor cycling, a different approach than that used for pump status will be required.

2.4.1 Methods

Disaggregation is the act of separating a known entity into component parts. In order for the NILM to disaggregate load transients within the collective signal, it must identify a unique feature or metric that distinguishes the known entity from all other loads and background variations within the signal. Common methods used to detect and classify individual events rely on steady-state power changes, finite state modeling, and transient behavior. These approaches typically utilize first order power and reactive power to achieve the desired results. More advanced approaches may include higher order harmonics, as well as frequency analysis. Current research is also exploring the use of machine learning algorithms that are capable of analyzing multiple features (i.e. period, amplitude, frequency content) to detect specific loads within a system.

Recent field studies have relied heavily on steady-state power levels in conjunction with transient behaviors to perform detection and classification of loads. Proper (5) used these methods to perform automated classification on the vacuum-assisted sewage system, which includes two different types of pumps within the system. Results from these studies showed the validity in this type of analysis. As the NILM scales to monitor more loads, the chance for transient overlap increases, which could adversely affect the NILM's ability to extract individual loads. Furthermore, higher levels of system monitoring result in higher overall power levels; these levels will introduce greater levels in power variation. Ultimately, the increased variations could mask the transients of interest.

Depending upon the size of the site being monitored, the overlap issue may be inconsequential. The number of loads may be small enough that the risk associated with transient overlap may be ignored. For larger site installations, smarter software solutions that take into account sequential steps for a given process may be implemented. For instance, Bennett (4) identified the NILM's ability to identify multiple steps within a gas turbine motor start-up procedure. One step in particular included a +28 VDC signal that opened a vent valve downstream of the exhaust fan for the propulsion turbine. Although the actuator signal is too small to see in the aggregate level, the associated start-up of the vent fan, which occurs nearly immediately following the actuator

signal, could be used to classify the turbine start-up. In general cases where overlap is expected based on system procedures, the multiple events may be treated as one using a classifier designed to detect the multiple events.

Steady-state power variations may also managed using techniques similar to those used for overlap issues. Jones (6) identified high frequency oscillations associated with lube oil heaters during his research. The magnitude of these oscillations in the aggregate is capable of masking smaller loads of interest. One solution to this problem is to use a filter, such as a notch filter, to remove the cycling heater masking effect. Another useful type of signal processing filter is the median filter, because it preserves the sharp edges of the power signal, which is often used for transient identification.

2.4.2 ESCANABA Experimental Data

To demonstrate the capability of the NILM to disaggregate loads, two monitoring systems were installed on the USCGC ESCANABA in September 2008. An "upstream" NILM (Figure 2-10) was placed at P-2-282-3; a "downstream" NILM was installed at the CHT control panel.[3] Data was collected over a two month period while the ship was deployed, then retrieved for analysis in November 2008.

[3] Refer to Section 2.2, Measurement Accuracy, for further details on P-2-282-3.

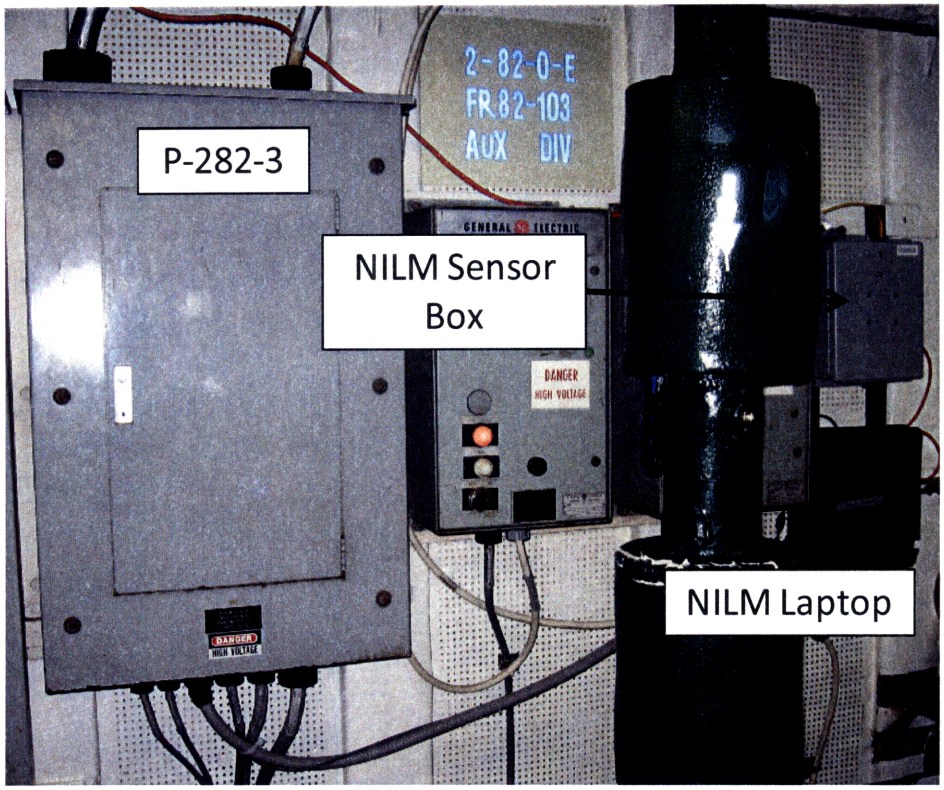

Figure 2-10: Upstream NILM System. The sensor box receives the raw current and voltage signals from the panel, samples the data at 8 kHz, and sends the resulting data to the computer via Ethernet.

Based on the data acquisition components listed in TABLE 2-3 , the dynamic current range for the upstream NILM is larger than the downstream NILM by a factor of 2. This results in an effective bit increase (Equation 2-16) of approximately 1 bit from upstream to downstream, which does not introduce significant quantization error.

TABLE 2-3: SENSOR CONFIGURATION FOR DISAGGREGATION EXPERIMENT

	Upstream	Downstream
Transducer	LA-205	LA-150
K_N	1/2000	1/2000
R_M	50 Ω	100 Ω

The objective of this experiment was to determine whether the relatively small transients associated with the CHT vacuum pump could be reliably identified in the upstream data. Figures Figure 2-11throughFigure 2-13 show data captured from October 22, 2008 from 0430-0500. The downstream plots show three distinct vacuum pump runs with no additional loads. Upstream

plots display the vacuum pump runs along with additional loads on a steady 35 kW power level. The closer view of the first CHT pump run (Figure 2-12) displays the additional transient event in the upstream during the CHT pump run. Additionally, it illustrates how the large amplitude steady-state variations relative to downstream data may prevent proper classification.

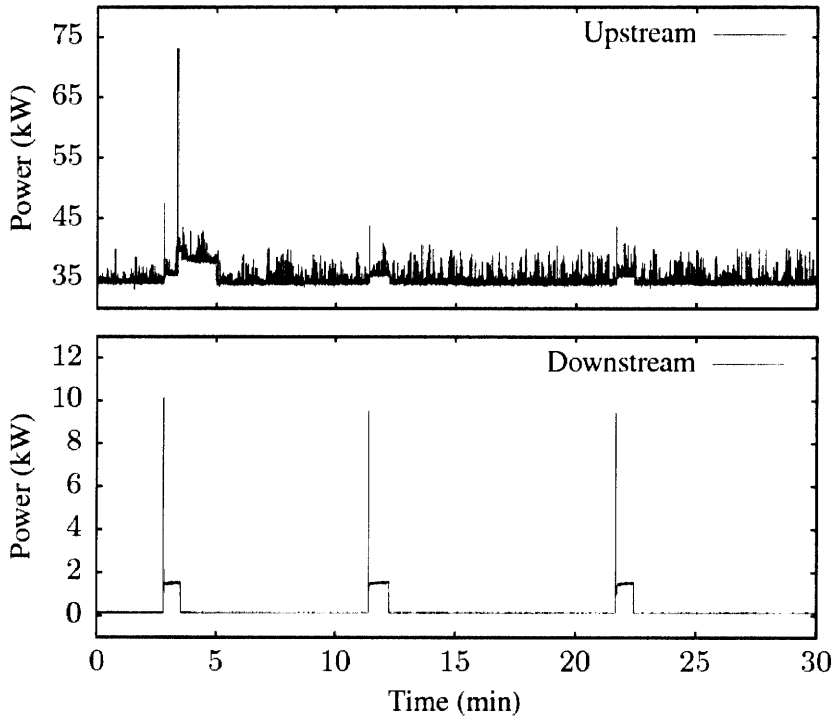

Figure 2-11: Full window time-aligned comparison of downstream data (bottom) and upstream (data). Three vacuum pump transients are shown in the downstream (bottom). The three vacuum pump transients along with additional transients and noise are visible upstream (top) on top of a steady 35 kW load.

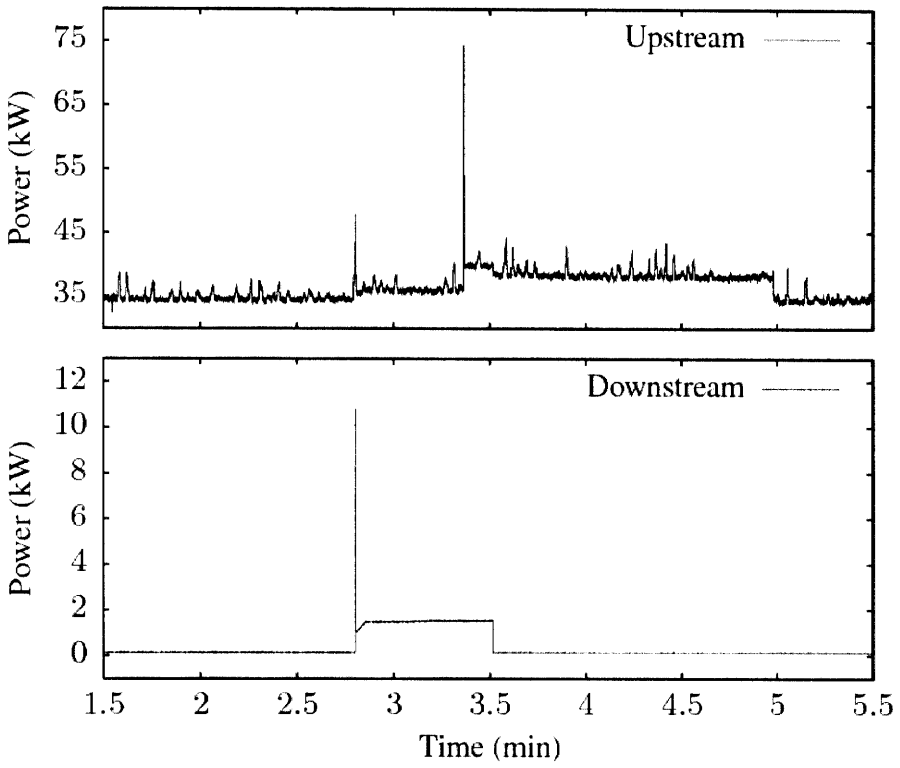

Figure 2-12: Closer view of the first CHT pump run, with a larger unrelated transient captured in the upstream data.

Figure 2-13 illustrates how the general shape of the downstream transient is maintained in the aggregate. Assuming the transient shape is unique, classification may still be possible in the upstream. The following section will discuss potential solutions to load classification using transient exemplars or "fingerprints" to match with similar waveforms in the aggregate.

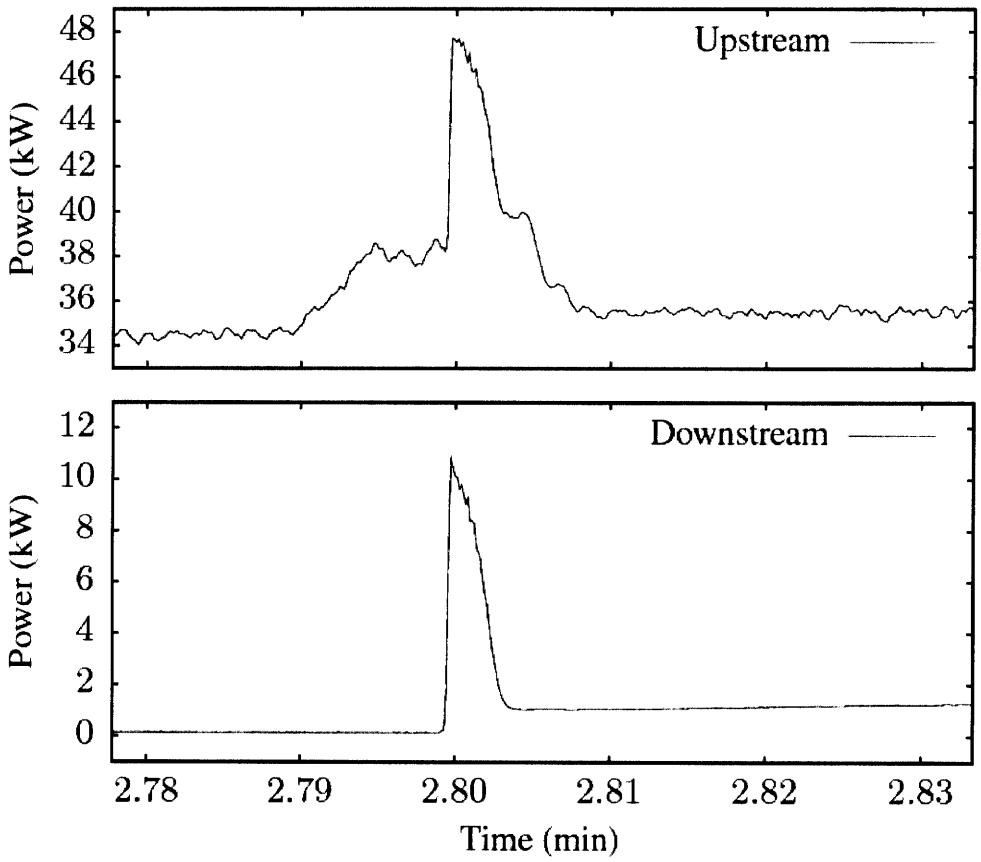

Figure 2-13: Detailed view of the start-up transient of the CHT pump. Note the general shape is still present in the upstream data.

2.4.3 Matching Waveforms

One common method used to determine the similarity in two sampled waveforms, $f[n]$ and $g[n]$, is to determine the Euclidean distance, D, defined as

$$D^2 = \sum_{n \in N} (f[n] - g[n])^2 \qquad 2\text{-}23$$

When expanded,

$$D^2 = \sum ((f[n])^2 - 2f[n]g[n] + (g[n])^2) \qquad 2\text{-}24$$

$$= \sum f[n]^2 + \sum g[n]^2 - 2\sum f[n]g[n] \qquad 2\text{-}25$$

As an inner product, this becomes

$$D^2 = (f \cdot f) + (g \cdot g) - 2(f \cdot g) \qquad 2\text{-}26$$

$$= |f|^2 + |g|^2 - 2(f \cdot g) \quad \text{2-27}$$

If the waveforms match, $D = 0$, and the equation reduces to

$$0 = |f|^2 + |g|^2 - 2(f \cdot g) \quad \text{2-28}$$

If the amplitudes match, $|f| = |g|$, so

$$f \cdot g = \frac{2|g|^2}{2} \quad \text{2-29}$$

$$\frac{f \cdot g}{|g|^2} = 1 \quad \text{2-30}$$

So, given an input signal, $f[n]$, and an exemplar, $g[n]$, if the two waveforms match the figure of merit, M, approaches 1.0. As M approaches 1, it can be reasonably assumed that the two waveforms are similar in amplitude and shape. This is an important attribute for disaggregation methods in the presence of many differently-sized loads that may share similar shapes, which is often the case with shipboard systems that contain multiple induction motors.

When an exemplar is chosen for a given load, it will contain a minimal number of indices to capture the load's characteristic of interest. This exemplar can "slide" across the data stream and a value for M computed. As the exemplar approaches a feature in the data stream that matches in shape and amplitude, the metric M will approach 1.0.

A faster method of computing the same metric is based on cross-correlation (16). Given two waveforms x and y, cross-correlation is defined as:

$$(x \star y)[n] = \sum_{m=-\infty}^{\infty} x^*[m]y[n+m] \quad \text{2-31}$$

where x^* denotes the complex conjugate of x. For real numbers, this represents the same basic operation as the dot product $(x \cdot y)$. Cross-correlation can be computed using the discrete Fourier transform $\mathcal{F}$ using the relation

$$\mathcal{F}\{x \star y\} = \mathcal{F}^*\{x\}\mathcal{F}\{y\} \quad \text{2-32}$$

Application and Results

The cross-correlation method was attempted using data from the patrol period. The candidate transient was a vacuum pump startup. First, an exemplar was extracted from the downstream data sample and the DC offset was removed (Figure 2-14).

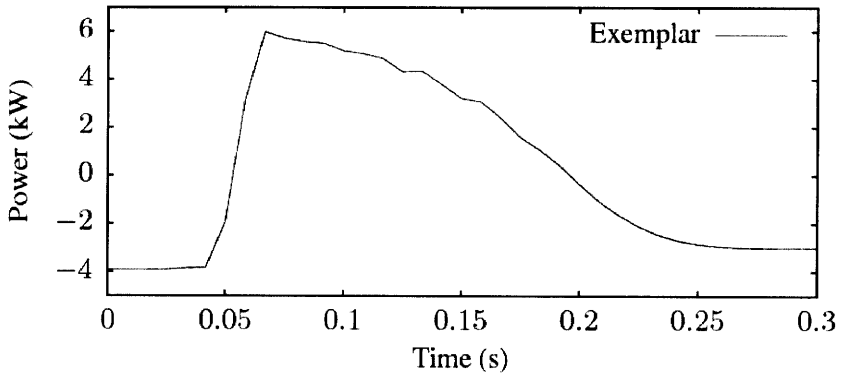

Figure 2-14: Exemplar used to match CHT vacuum pump startup transient.

Then, the correlation was computed using the exemplar and the full window of data from Figure 2-11. First, the downstream data was analyzed. Figure 2-15 reveals a positive match between the exemplar and downstream data. As expected, the correlation value approaches 1.0 as the exemplar "slides" over the transient in the downstream data stream. A peak-detection algorithm with a threshold of ± 0.1 was used in this application.

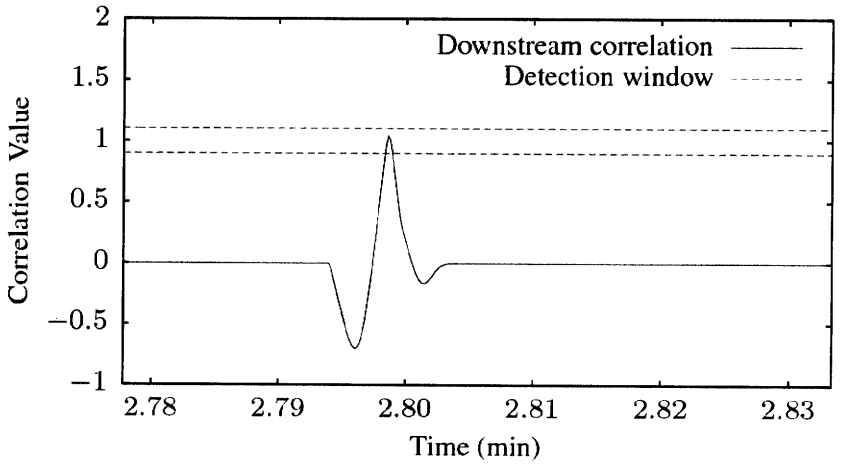

Figure 2-15: Positive exemplar match in the downstream data.

Next, the exemplar extracted from the downstream data was used to perform cross-correlation in the upstream data. Figure 2-16 illustrates the results. Again, the method correctly identified the transient of interest even with the steady-state 35 kW power level and other transient events.

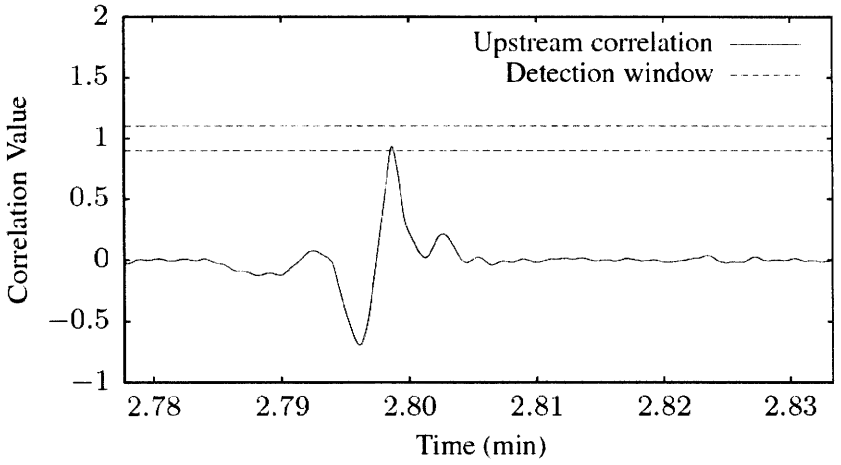

Figure 2-16: Positive exemplar match against a CHT pump startup in the upstream data.

Finally, Figure 2-17 shows an example of the correlation method correctly distinguishing a non-CHT pump startup transient in the upstream. Although the correlation value approaches and passes through the peak detection window, the peak occurs at a higher correlation value, which is easily distinguishable using the peak detection algorithm.

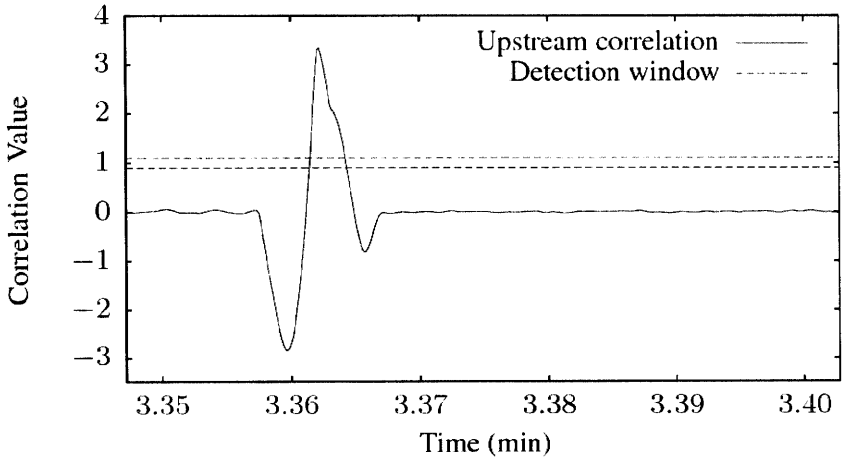

Figure 2-17: Positive exemplar mismatch against a non-CHT event.

For this particular case, the cross-correlation technique correctly identified all pump matches. Similar analysis was conducted on 21 disjoint hours over a three-week period from October 10 to October 20. For every CHT pump transient found in the clean downstream data, the same event was correctly identified in the upstream data. Furthermore, there were no false positives or negatives, indicating that this method can quickly and reliably disaggregate target loads even in the presence of large variations and unrelated transients.

Chapter 3

LBES Aggregate Power Analysis

Methods of disaggregation are examined using field data collected from the Navy's Land Based Engineering Site (LBES) located in Philadelphia, Pennsylvania. The facility contains a fully functional ARLEIGH BURKE (DDG-51) main machinery space, which is used by the navy for crew certifications and also serves as a test site for various mechanical, electrical, and software upgrades. NILM research has been conducted at the LBES site over the past few years with emphasis on local diagnostic indicators and supervisory control ((17) (6) (4) (18)).

LBES studies began with NILM installations on the fuel oil (FO) and low pressure air compression (LPAC) systems in 2005 (18). This was followed with additional NILM installations to monitor the General Electric LM 2500 gas turbines used for propulsion, along with various supervisory control systems associated with the turbines (17). Additional loads monitored through NILM at LBES include fuel oil service pumps (FOSPs), lube oil service pumps (LOSPs), and gas turbine generators (GTGs). In 2007, Jones (6) installed two NILM systems on the main switchboards supplying power to all of the auxiliary system loads previously mentioned. In June 2008, data was collected from the switchboard NILMs and various service loads. The focus of this section is to examine how well cross correlation and peak detection methods perform disaggregation of the various downstream loads in the upstream data.

3.1 Aggregate (3SA) Description

Although two NILMs were installed upstream at the LBES site, only one (3SA) will be used for the purpose of this study, since all target loads are on 3SA. The CT chosen for this installation differs from the previously described CTs (i.e. LA 55-P, 205-S). This particular CT, the Fluke i3000, is a split-core CT that clamps around the current-carrying wire. The decision to use the

clamp style was made based on the site engineer's request to avoid breaking electrical connections in the switchboard (6) .

Selection of the Fluke i3000 resulted in the necessity to use an amplifier circuit to increase the signal level into the PCI-1710 ADC. The CT offers three current ranges: 30A, 300A, and 3000A. Based on potential currents at the switchboard, the 3000A range was chosen. Unlike typical NILM CTs, this particular device converts the primary current I_P to voltage using K_N = 0.1 mV/A; there is no burdened resistor required upstream of the ADC. This results in extremely small output voltages that require amplification. Amplification was achieved using an amplifier card designed by Professor Robert Cox (6). The amplifier card receives I_S and splits the signal into two levels, Channels 1 and 2. The output of channel 1 is amplified by a factor of 10, while the output of channel 2 is amplified by a factor of 100. For the purposes of upstream NILM discussion at LBES, the two outputs of the amplifier cards will be called measured voltage ranges V_M. This follows data acquisition nomenclature defined in previous sections for NILMs equipped with burdened resistors.

A sample power plot is provided in Figure 3-1 to illustrate the relative difference in scaling between channels 1 and channel 2 data. There are two factors that influence the scale difference. First, the obvious, is the difference in amplification of each signal prior to reaching the ADC. Second, the designers chose to select different gains for each channel. Recall the PCI-1710 card was used for this installation. This card offers selectable voltage ranges, V_R. Channel 1 was set to +/- 2.5 V; channel 2 was set to +/- 10V. Based on these scale factors, raw count output from the ADC of channel 2 is approximately 2.5 times that from channel 1for a given I_P. A summary table of the two NILM arrangements is provided in TABLE 3-1below. This chapter will use the channel 1 data only, since it has a higher degree of scaling involved, which yields the most conservative analyses.

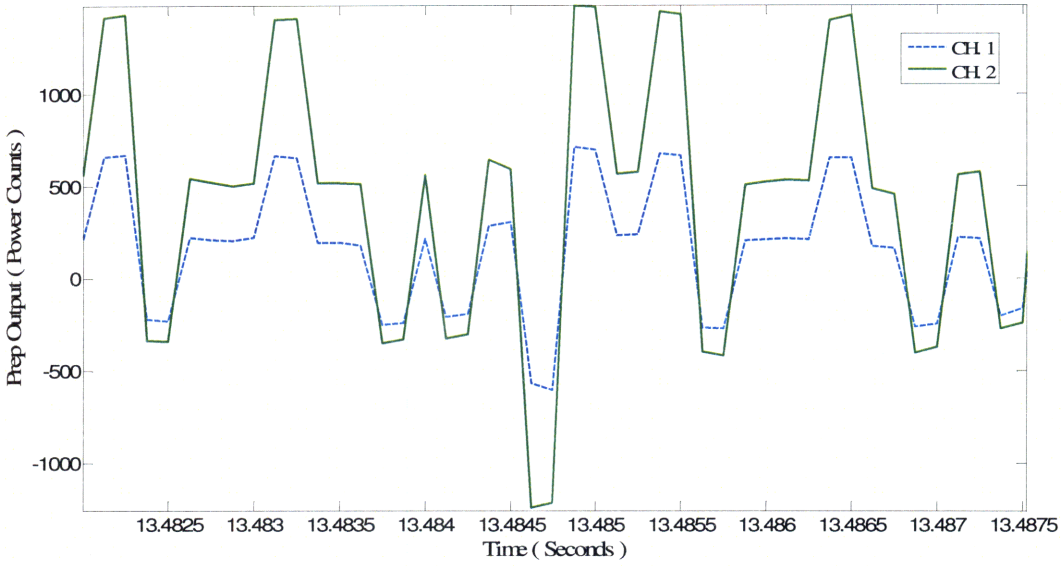

Figure 3-1: Power plot of both channels available for 3SA. The direct current (d.c.) bias was removed from each signal to provide a comparative illustration of the scale difference between the two channels.

TABLE 3-1: 3SA NILM CONFIGURATION

	Upstream CH.1	Upstream CH.2
Current Transducer	Fluke i3000	Fluke i3000
K_N	.1 mV/A	.1 mV/A
R_M	N/A	N/A
G	10	100
V_R	+/- 2.5 V	+/- 10 V
Bits	12	12

3.2 LOSP 2A

Two LOSPs, LOSP 2A and 2B, are piped to a common header supply lubricating oil the main reduction gears and the shaft thrust bearing. Each pump is a two-speed variety with motor ratings of 30/60 HP (slow/fast). LOSP 2A is monitored using a 20Ω burdened resistor and a LEM LA-305S current transducer. The LA-305S has a K_N value of 1/2500 with a maximum primary current range of +/- 300 amps. The NILM uses a PCI-1710 ADC with a V_R of +/- 5V.

TABLE 3-2: LOSP 2A NILM CONFIGURATION

	LOSP 2A
Current Transducer	LEM LA-305S
K_N	1/2500
R_M	20 Ω
V_R	+/- 5V
Bits	12

Recall from Chapter 2 that the effective bits calculation provides a good measure of the data quantization from the local NILM to further upstream. The effective bits, B_E, for channel 1 of 3SA, $B_{E,U}$ may be written as

$$B_{E,U} = \log_2\left(\frac{I * K_N * G * 2^B}{|V_R|}\right) \quad 3\text{-}1$$

where G is the gain from the amplifier card. Using an I_P of +/- 72 amps for the LOSP[4], $B_{E,U}$ for 3SA channel 1 is

$$B_{E,U} = \log_2\left(\frac{72 * 1e-04 * 10 * 2^{12}}{5}\right) \quad 3\text{-}2$$

$$\approx 5.882\ bits \quad 3\text{-}3$$

Equation 2-16 yields the following downstream $B_{E,D}$:

$$B_{E,D} = \log_2\left(\frac{72 * 1/2500 * 20 * 2^{12}}{10}\right) \quad 3\text{-}4$$

$$\approx 7.965\ bits \quad 3\text{-}5$$

The difference in effective bits between the channel 1 data $B_{E,U}$ and the downstream LOSP 2A data $B_{E,D}$ is only 2.2 bits.

[4] Full load amperage rating for high speed operation (4).

3.2.1 LOSP 2A OFF to SLOW Cross Correlation Results

Data obtained on June 19, 2008, between 1030 and 1200 was analyzed. During this time period, four locally-monitored loads were cycled along with additional transients in the aggregate. Figures 3-2 through 3-4 provide comparisons of the time-aligned spectral power envelopes captured both upstream and downstream. Cross correlation and peak detection methods described in Chapter 2 were used to extract the LOSP 2A OFF/SLOW transient from the aggregate.

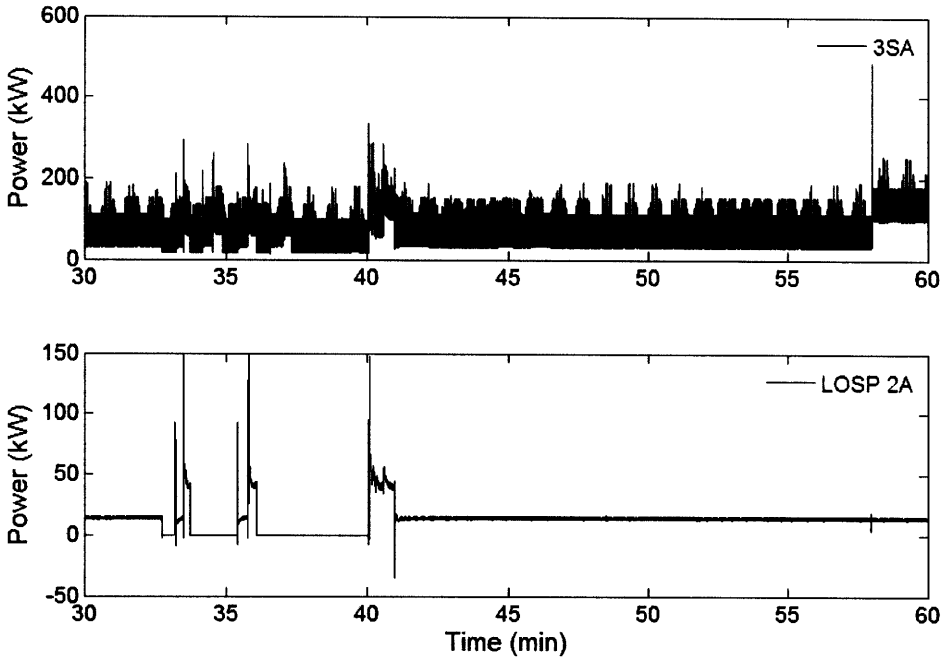

Figure 3-2: Time-aligned power spectral plots of 3SA (upstream) and LOSP 2A (downstream). Note the aggregate contains additional load starts including LOSP 2B transients, which are highlighted in the follow-on figure.

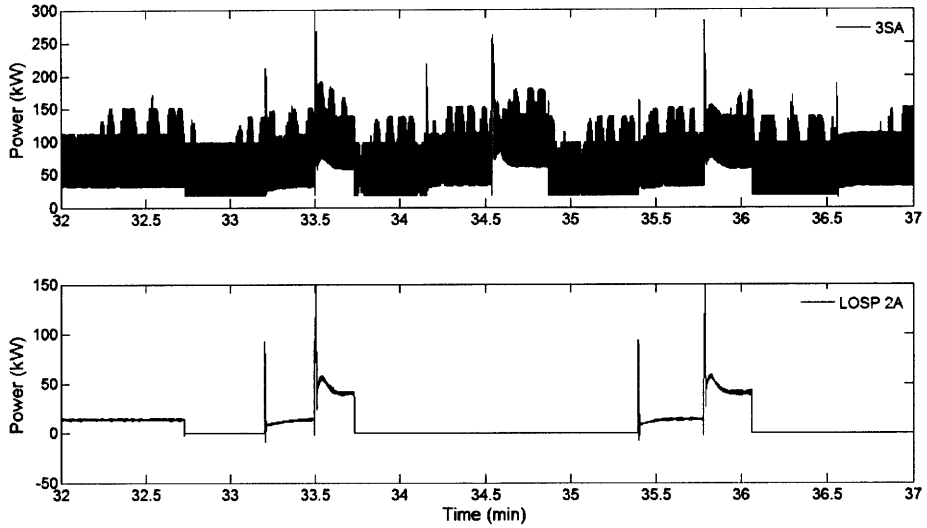

Figure 3-3: Closer view of aggregate and downstream power plots. The aggregate contains LOSP 2A and LOSP 2B transients. The lower plot shows LOSP 2A cycle through its various states of operation (OFF/SLOW/FAST).

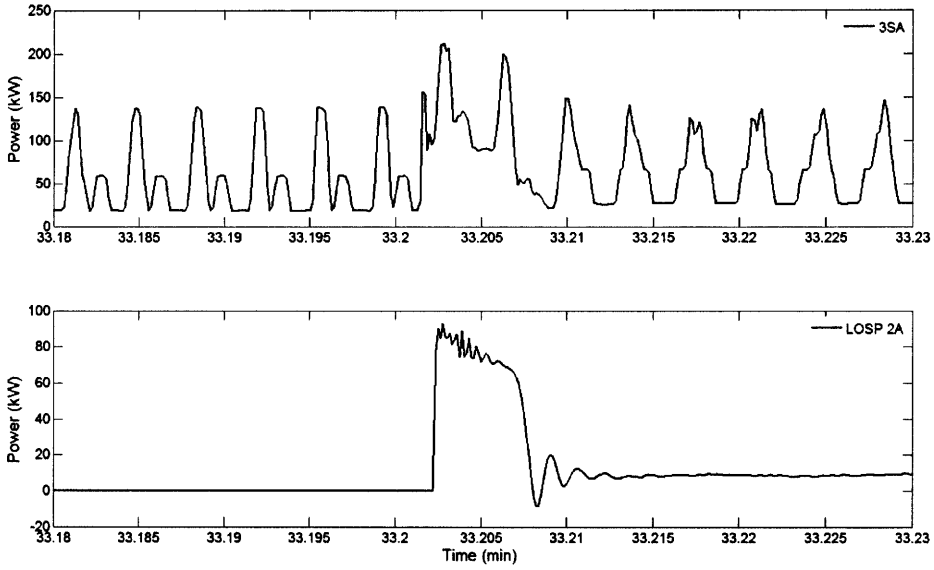

Figure 3-4: Detailed view of the startup transient from OFF to SLOW speed. Aggregate contains a higher frequency cycling load that was identified to be Lube Oil heaters by Jones (6).

In order to conduct the cross correlation technique, a detailed exemplar of the transient of interest is required. Figure 3-4 shows a detailed view of the downstream transient of interest along with the time-aligned upstream data. The sample exemplar for OFF to SLOW Speed was extracted from the downstream data, and then the DC offset was removed. The resulting template is shown in Figure 3-5.

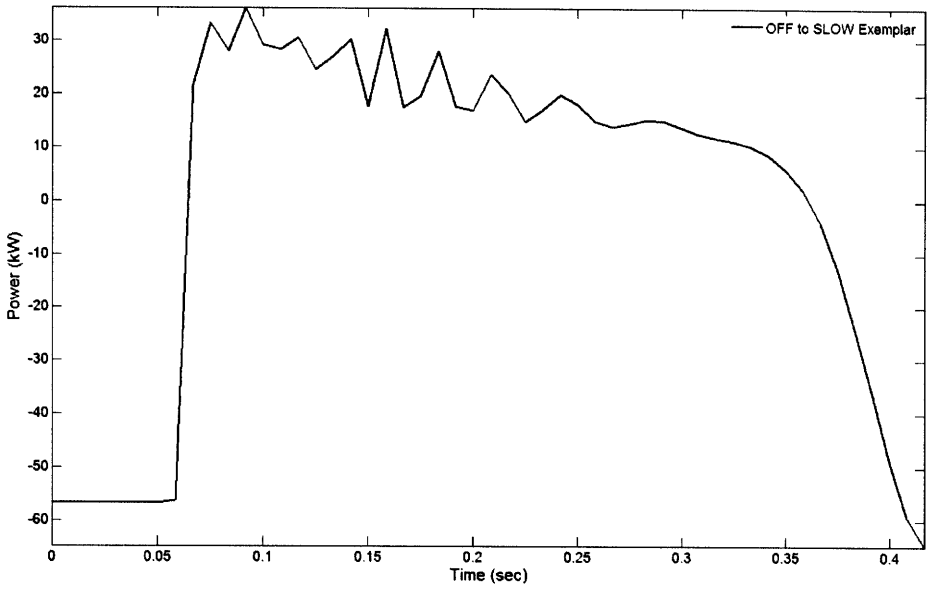

Figure 3-5: Exemplar used for LOSP 2A OFF to SLOW transient.

Next, cross-correlation was computed using this exemplar against full hour windows of downstream and upstream data. Recall from Chapter Two, that a strong correlation is indicated by a local maxima near $y = 1.0$ for a given time t. A peak detection window between 0.9 and 1.1 was used as the threshold for a positive match. Figures 3-6 and 3-7 show the results for the downstream correlation. Each OFF to SLOW event was correctly identified and all other events fell outside of the detection range.

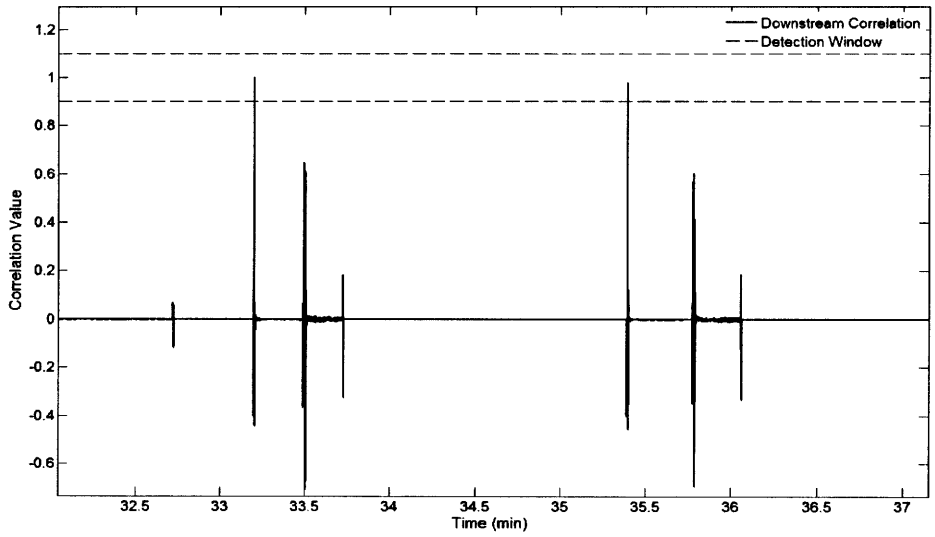

Figure 3-6: Detection window of downstream correlation with multiple transient. The two spikes within the threshold values were both correctly identified LOSP starts (OFF to SLOW). The spikes below the threshold window correspond to SLOW to FAST and FAST to OFF events.

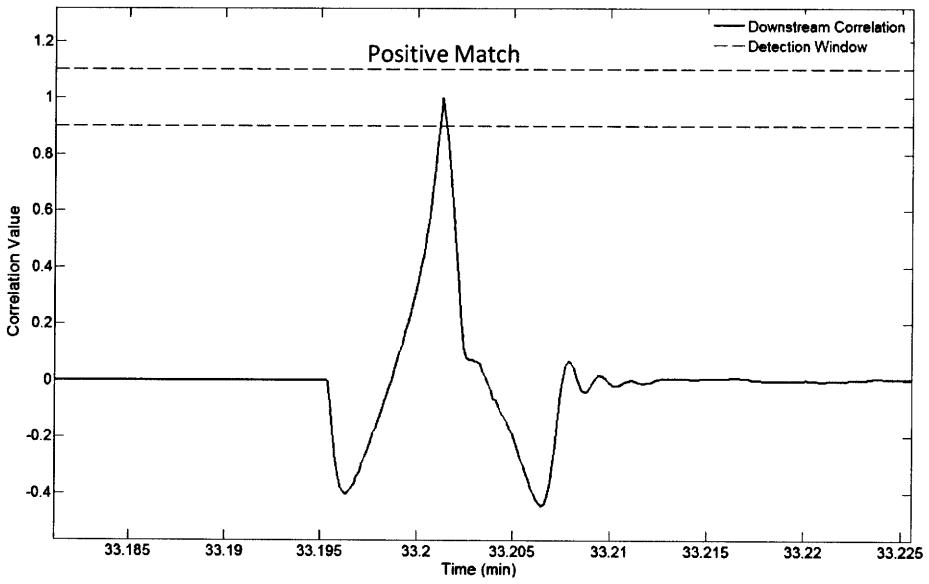

Figure 3-7: Exemplar match against a LOSP start transient recorded in the downstream.

After downstream analysis, the exemplar was cross correlated in the upstream data. Figure 3-8 shows a positive match for the LOSP 2A OFF/SLOW transient in the aggregate. Figure 3-9 shows a positive mismatch that corresponds to a LOSP 2A SLOW/FAST transient. **All LOSP 2A OFF/SLOW transients were correctly identified in the aggregate with no false positives or negatives.**

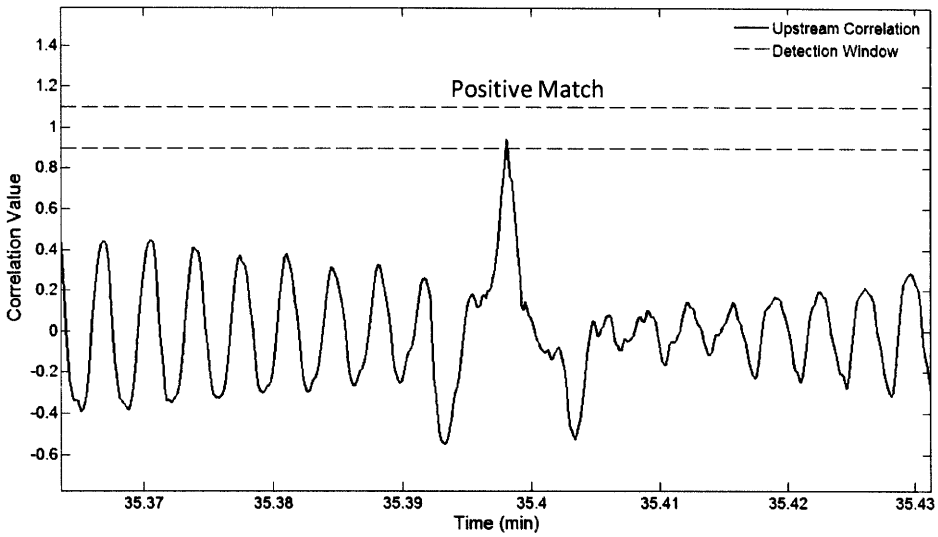

Figure 3-8: Upstream correlation window for positive LOSP 2A OFF/SLOW match.

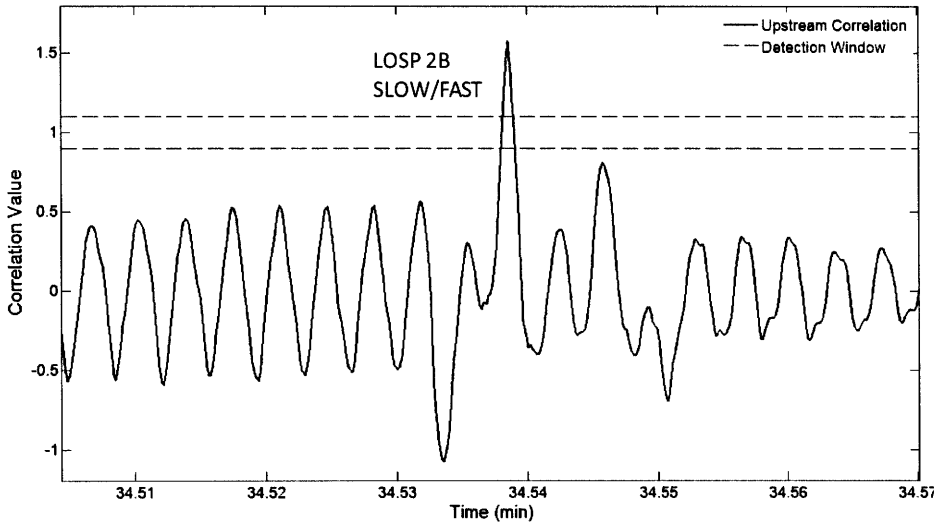

Figure 3-9: Positive mismatch in upstream data for LOSP 2A OFF/SLOW.

3.2.2 LOSP 2A SLOW to FAST Cross Correlation Results

The transient due to a shift in speed from SLOW to FAST of the LOSP was scrutinized next. An exemplar was extracted from the downstream data. The same data samples used for the previous

discussion on OFF to SLOW were used for this study. Refer to Figure 3-2 for the power plot results. The exemplar chosen for this transient is provided as Figure 3-10.

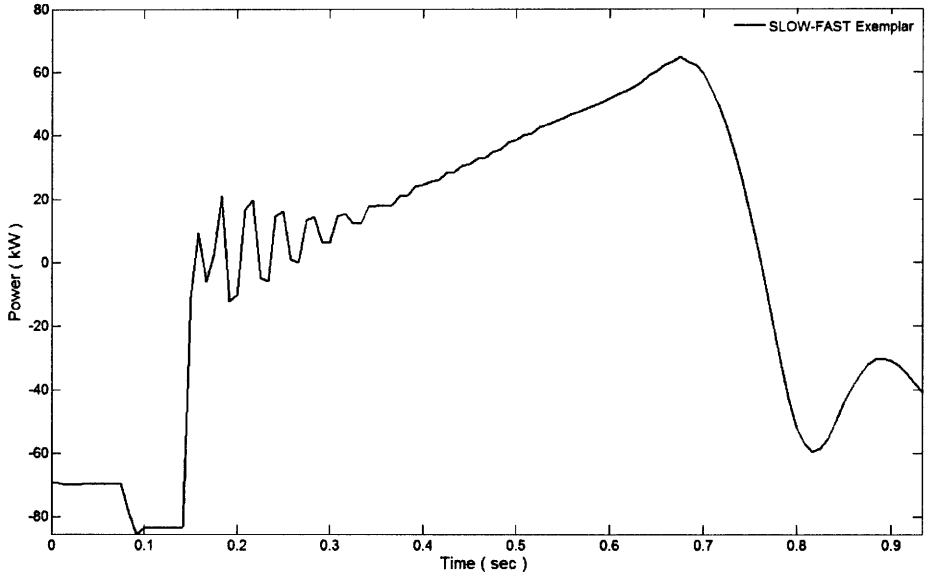

Figure 3-10: Exemplar used to match SLOW to FAST transient of LOSP 2A.

Figures 3-11 and 3-12 are results from the cross-correlation method using downstream data and upstream data, respectively. Again, the detection method correctly identified the transient of interest both downstream and upstream. There were no false positives or negatives revealed.

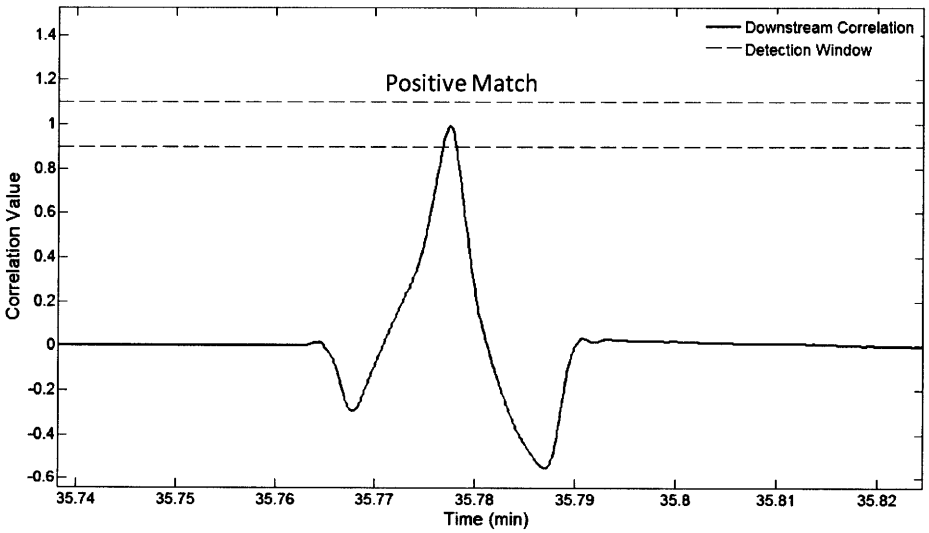

Figure 3-11: Positive match between exemplar and downstream LOSP 2A SLOW/FAST transient. Each candidate transient (SLOW/FAST) was correctly identified; there were no false positives.

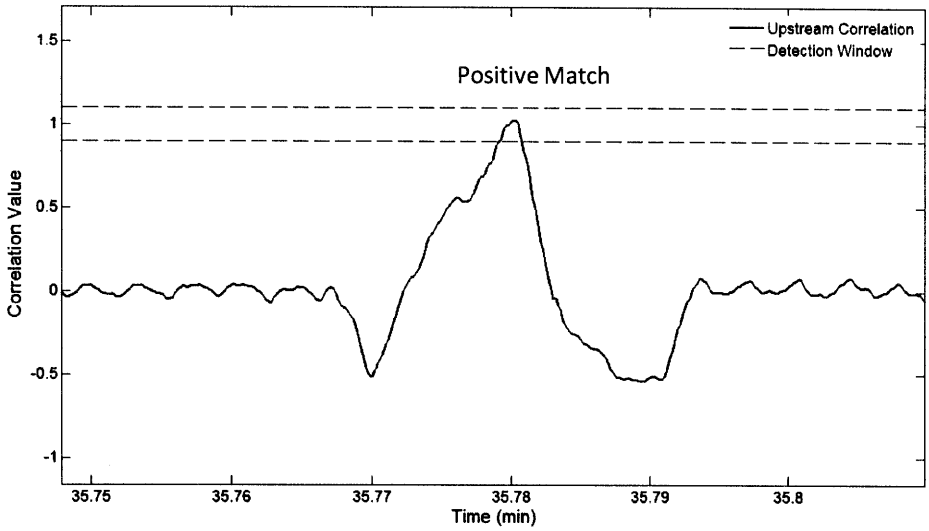

Figure 3-12: Positive match between exemplar and upstream LOSP 2A SLOW/FAST transient.

3.3 Low Pressure Air Compressor (LPAC) Number 2

The LPAC provides compressed air at approximately 125 psig to the LBES low pressure air system. The low pressure air serves to operate various valves and provide pneumatic power for certain plant equipment. The compressor is an Ingersoll-Rand NAXI 100-4A driven by a 35 HP squirrel cage motor rated for 35 full load amps (4). NILM summary is listed in TABLE 3-3. Using the 35 amp full load rating, $B_{E,U} = 4.841$ bits and $B_{E,D} = 7.689$ bits.

TABLE 3-3: NR 2 LPAC NILM CONFIGURATION[5]

	Nr 2 LPAC
Current Transducer	LEM LA-305S
K_N	1/2500
R_M	36 Ω
V_R	+/- 5V
Bits	12

3.3.1 LPAC Nr 2 Correlation Results

Figure 3-13 is a time-aligned spectral power plot of downstream and upstream data recorded on June 19, 2008 between 1100 and 1200. Two LPAC Nr 2 compressor start-ups and shut-downs were recorded in the upstream and downstream data during this window. This performance does not represent normal operation of the LPAC unit, but was conducted to provide known transients for research. During normal operation, the compressor remains energized and the air system is under load. (6) Figure 3-14 is a close-up view of a complete compressor cycle captured locally and upstream.

[5] A pressure transducer was also installed to provide compressor discharge pressure measurements. However, this is not relevant to this discussion.

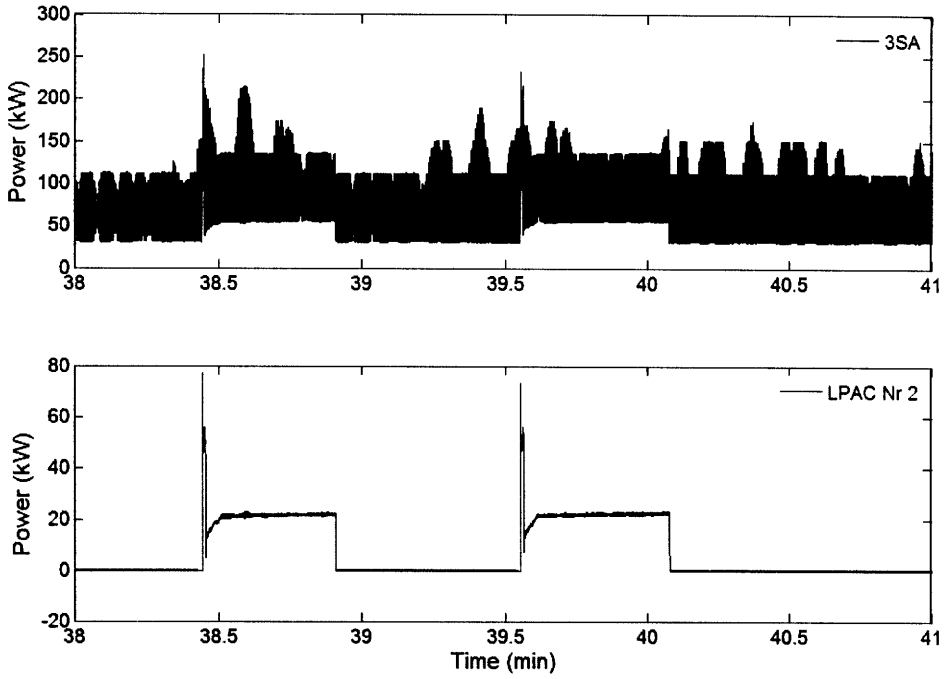

Figure 3-13: Time-aligned full power plot of 3SA and local LPAC Nr 2 NILM. Two transients on bottom plot are compressor cycles from OFF to ON, then back OFF.

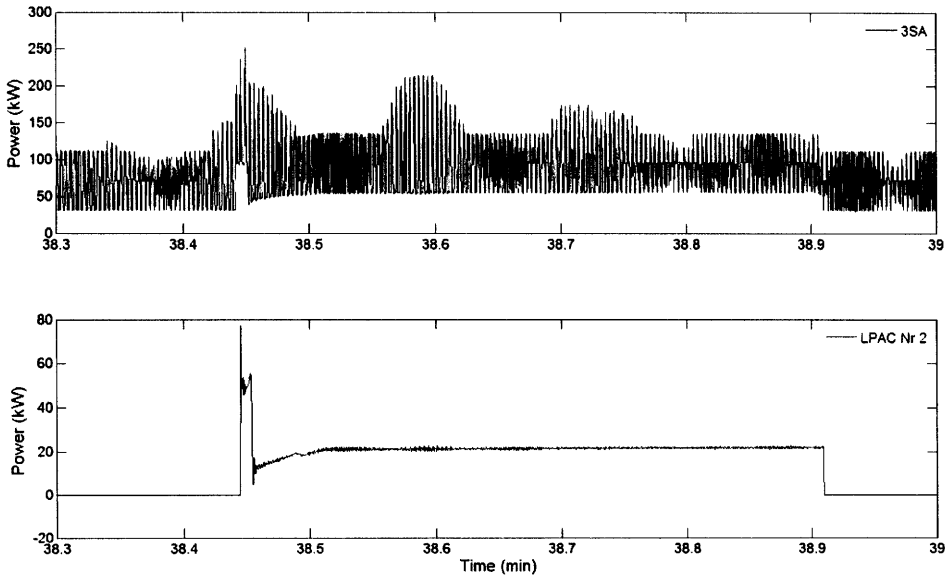

Figure 3-14: Closer view of LPAC Nr 2 compressor cycle.

The cross-correlation method was used on the downstream data, followed by the upstream data. The exemplar in Figure 3-15 was extracted from the downstream data. The downstream data yielded positive exemplar matches for all target transients (Figure 3-16); however, there were many false positives identified in the aggregate (Figure 3-17 and Figure 3-18). Several different exemplars were extracted from the downstream data in an attempt to find a better "fingerprint". However, the "cleanest" results for the upstream aggregate were derived using the exemplar in Figure 3-15.

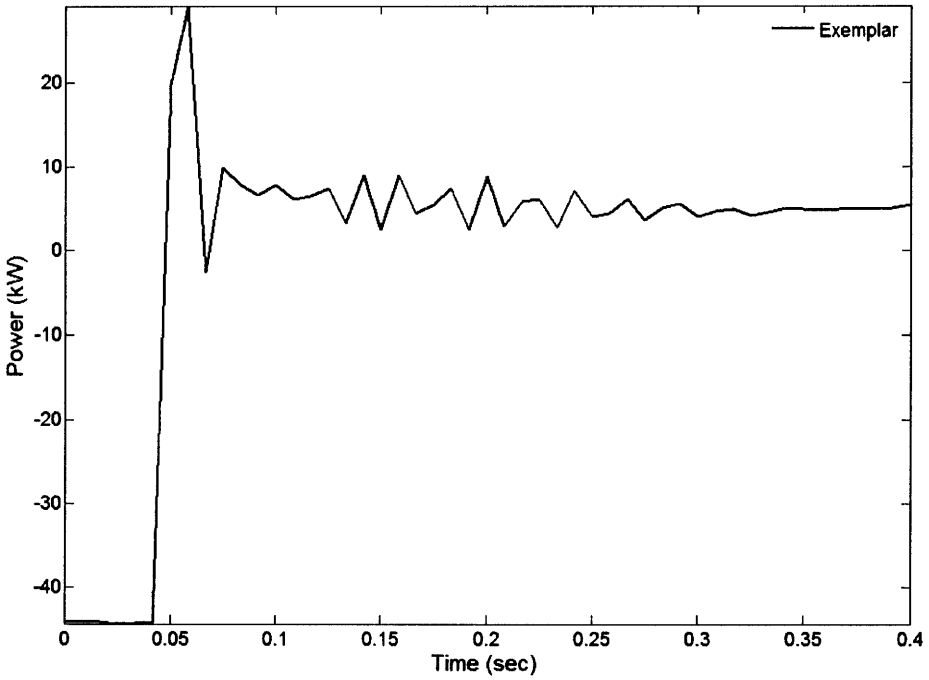

Figure 3-15: LPAC Nr2 exemplar extracted from downstream data.

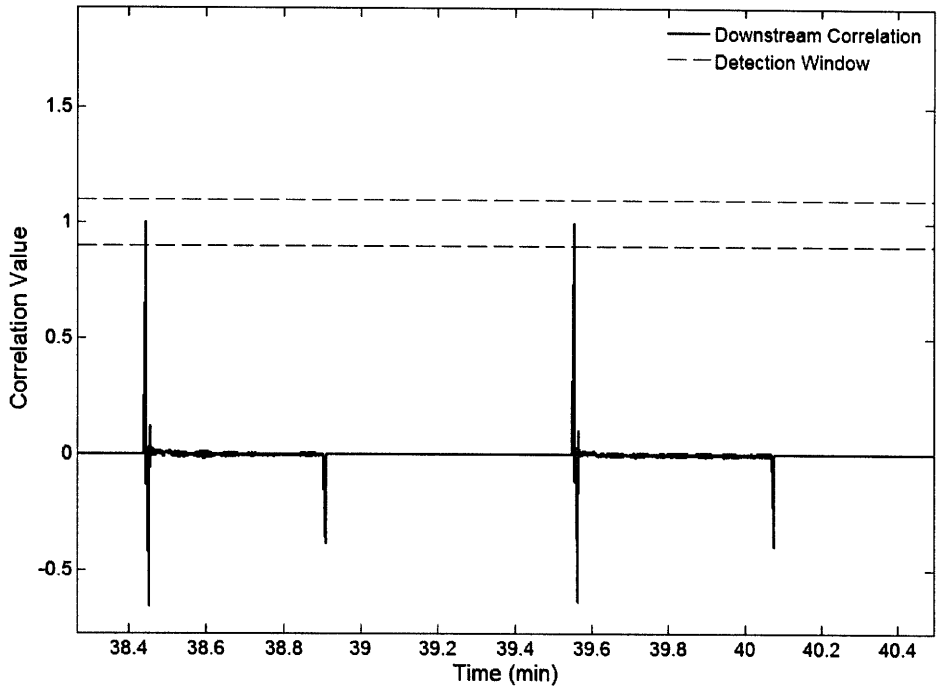

Figure 3-16: Positive exemplar matches with two LPAC compressor start-ups in the downstream data.

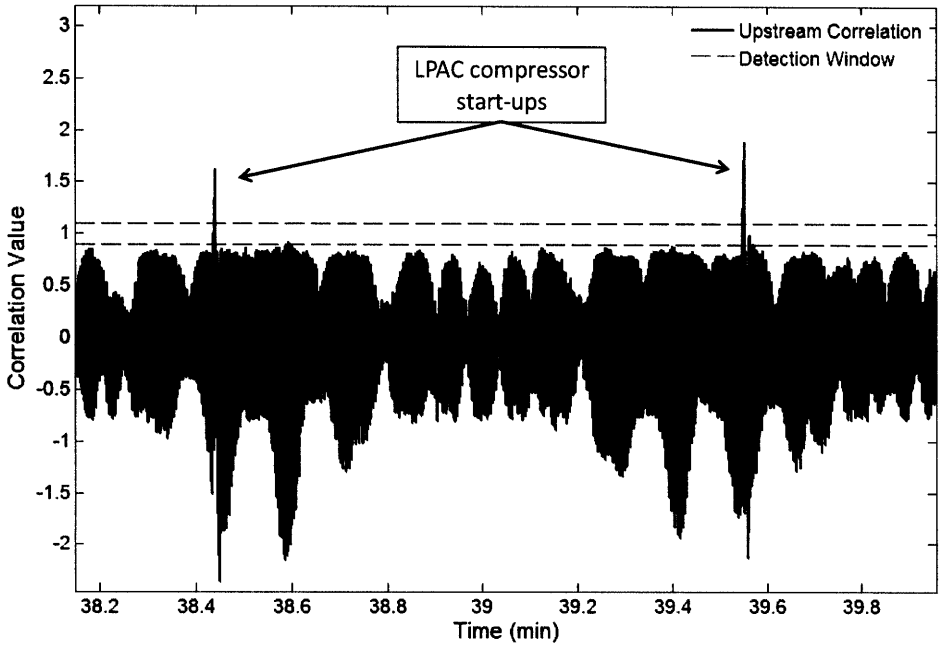

Figure 3-17: Close-up view of the upstream correlation results. Data captured around the actual target transients.

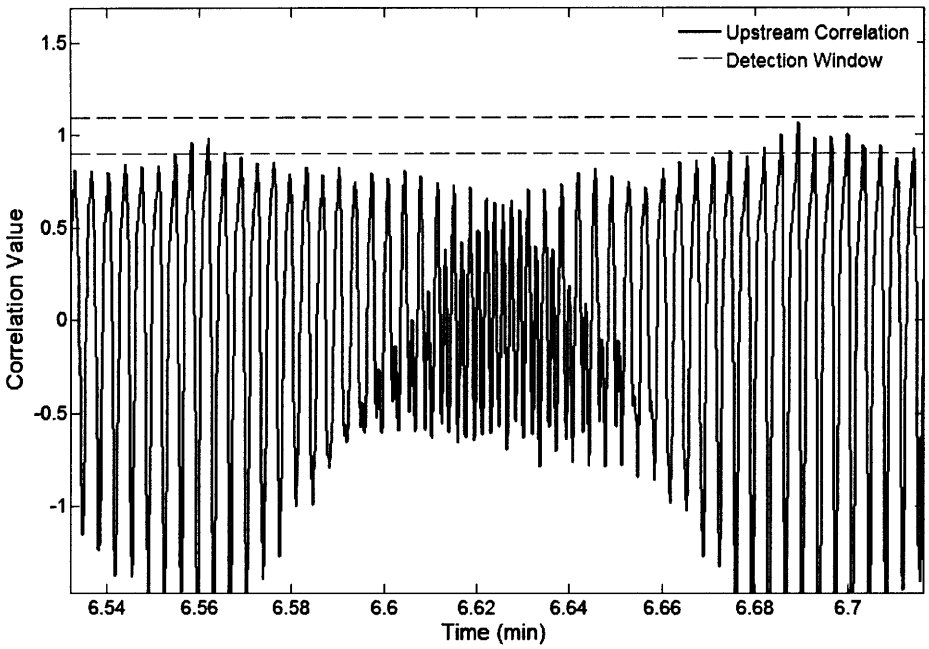

Figure 3-18: Detailed view of upstream correlation results. All correlation values within detection window were falsely identified as positives.

3.4 Fuel Oil Service Pump 2A

The fuel oil service pumps (FOSPs) supply fuel to the gas turbine motors and to the gravity drain tank used by the gas turbine generators. Each FOSP is coupled to a two speed motor. During normal operations, only one pump is required to meet system demand. FOSP 2A is monitored locally by a NILM with configurations listed in TABLE 3-4. Based on a 10 A full load rating for the FOSP motor, the $B_{E,D}$ = 7.965 bits and $B_{E,U}$ = 3.034 bits, which is nearly 5 bits difference. This would result in significant quantization in the raw data; however, preliminary studies in Chapter 2 indicate the preprocessor output is largely unaffected by the quantization.

TABLE 3-4: FOSP 2A NILM CONFIGURATION

	FOSP 2A
Current Transducer	LEM LA-55S
K_N	1/1000
R_M	61 Ω
V_R	+/- 5V
Bits	12

Similar to the results for the LPAC Nr 2 correlation, the cross correlation method correctly labeled transients in the downstream; however, it failed to correctly label FOSP 2A transients in the upstream. Figures 3-19 and 3-20 provide time-aligned spectral plots of both downstream and upstream data. It seems fairly evident from the close-up view that the FOSP transient cannot be "seen" by the naked eye due to the large cycling loads present in the aggregate.

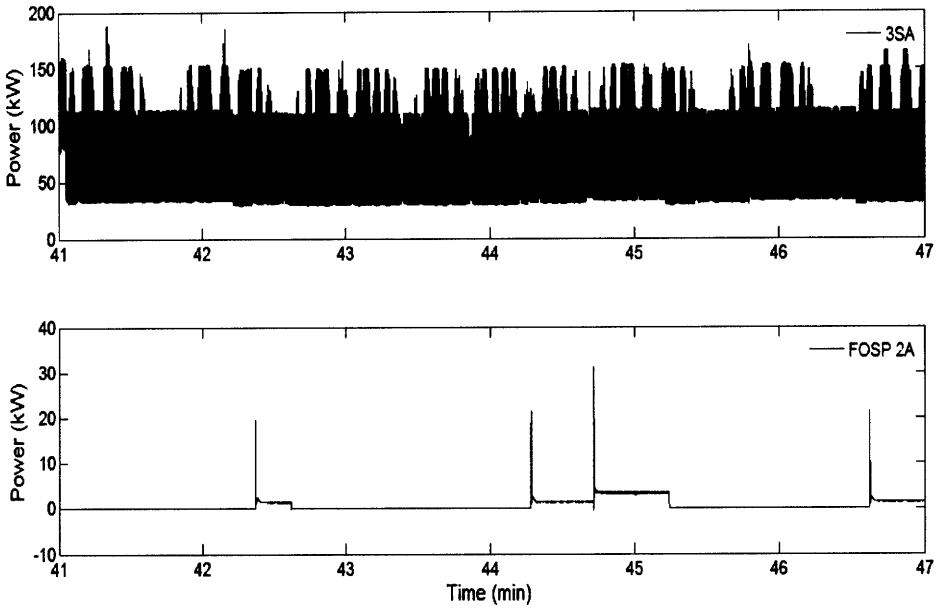

Figure 3-19: Time aligned plots of upstream(top) and downstream(bottom) data. Transients in bottom plot are FOSP 2A

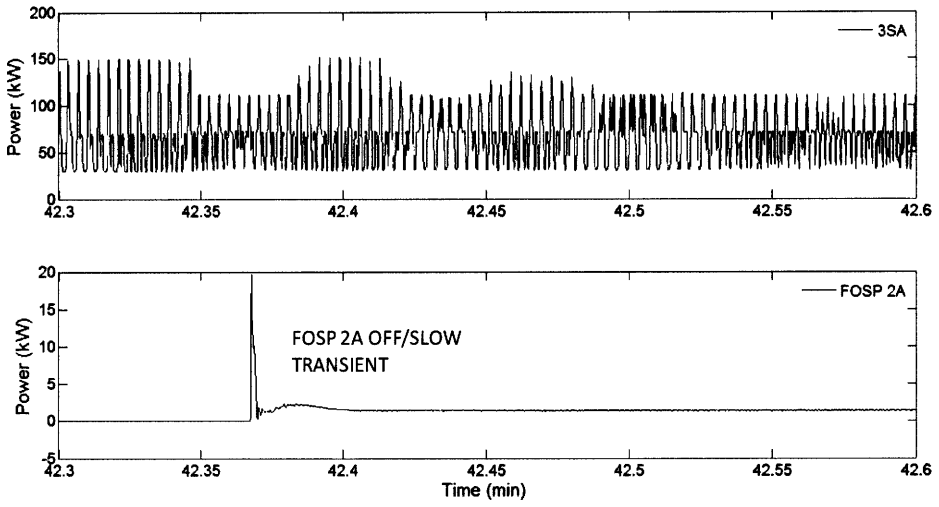

Figure 3-20: Close-up view of the power spectral plots for downstream and upstream data. The cycling load upstream masks the FOSP transient.

The exemplar chosen for the FOSP 2A OFF/SLOW transient is provided in Figure 3-21. Various exemplars were examined to include leading edge only, trailing edge only, and full exemplars. Each yielded similar poor results when cross-correlated with the upstream data. The downstream cross-correlation yielded positive matches and mismatches, with no false identifications. A positive match is shown in Figure 3-22.

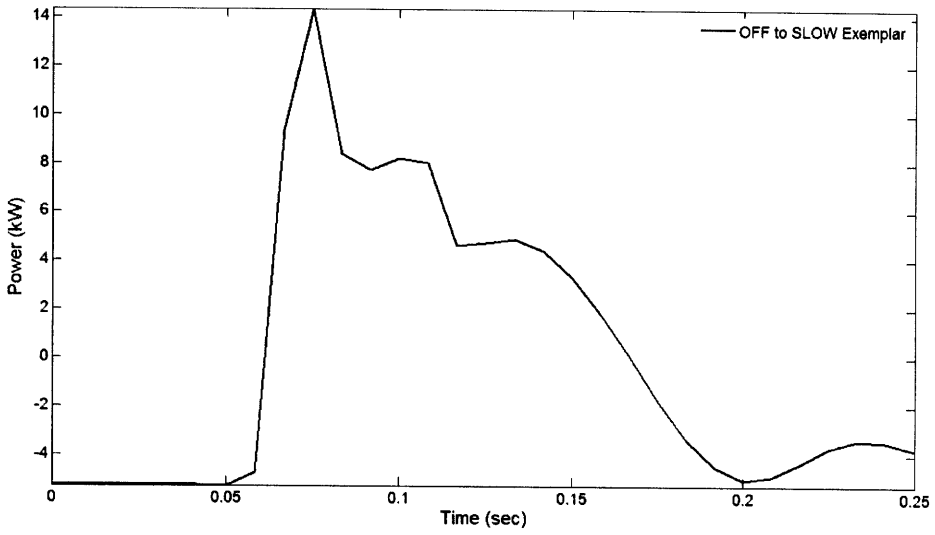

Figure 3-21: FOSP 2A OFF/SLOW exemplar extracted from downstream data.

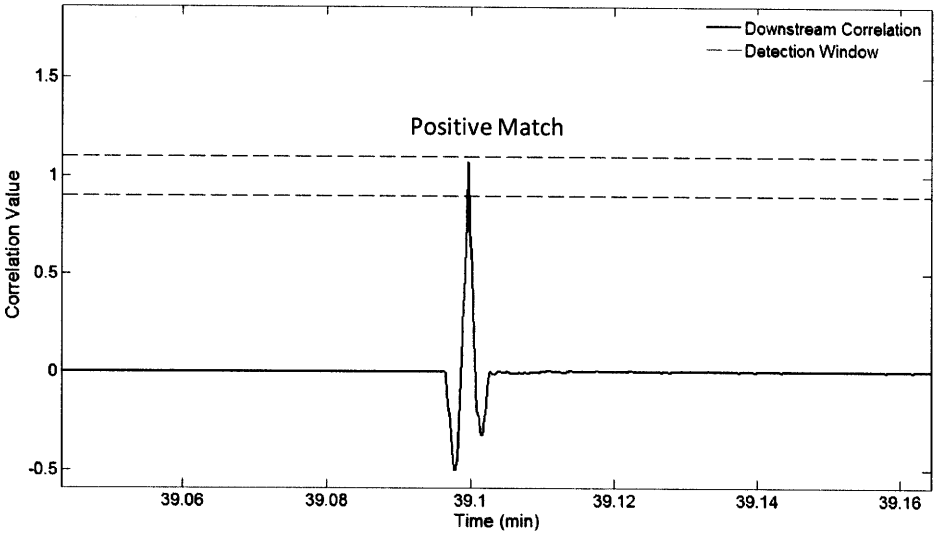

Figure 3-22: Positive cross-correlation match for a FOSP 2A OFF/SLOW transient.

The cross-correlation results for the upstream are illustrated in Figures 3-23 and 3-24. Notice that the cross-correlation value does approach 1.0 near the target transient; however, several false positives are also generated.

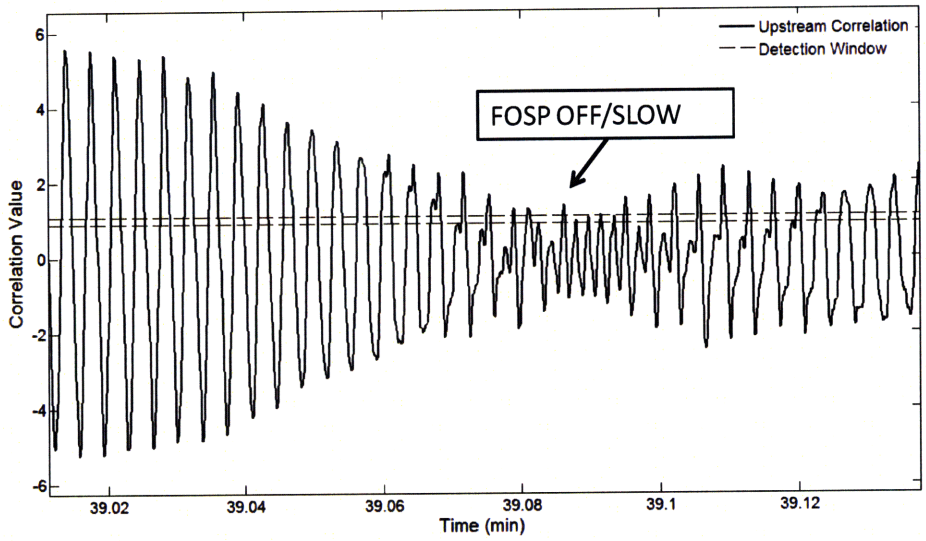

Figure 3-23: Close-up view of cross-correlation results in the aggregate data stream. The FOSP 2A OFF/SLOW transient is indicated.

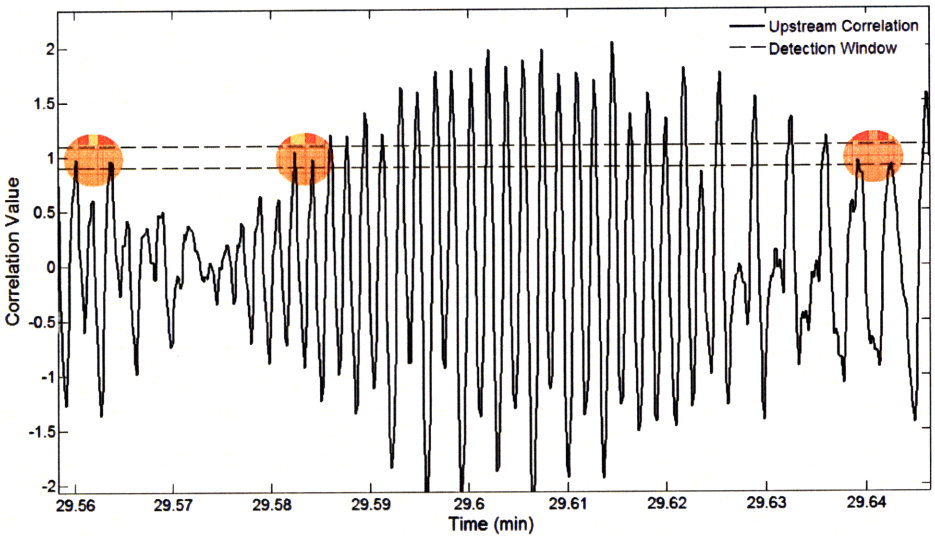

Figure 3-24: Cross-correlation results in upstream data showing false positive identifications (highlighted in red).

3.5 Gas Turbine Propulsion Main Engine Controller

The gas turbine propulsion main engine (GTM) controller NILM monitors a total of four loads. The first load, power panel P 1-282-1, receives 440 VAC and steps it down to 120 VAC. This panel supplies the remaining three loads, which include two Universal Engine Controllers (UECs) and the Shaft Control Unit. The UECs primary function is to provide control and

monitoring of the GTM to include such functions as power level control and overspeed protection. The SCU primarily provides local control to shaft components, the controllable reversible pitch propeller, and other auxiliary equipment. For a detailed explanation of these loads refer to (4). The NILM is arranged with one voltage tap on the power panel and four current channels for each load (TABLE 3-5).

TABLE 3-5: GTM NILM CONFIGURATION

	Panel	UEC 2A & 2B	SCU
Current Transducer	LEM LA-205S	LEM LA-55S	LEM LA-55S
K_N	1/2000	1/1000	1/1000
R_M	67 Ω	130 Ω	130 Ω
V_R	+/- 2.5 V	+/- .625 V	+/- 1.25 V
Bits	12	12	12

This discussion will focus on a normal GTM start sequence. The "upstream" panel will be the 120 VAC panel P-1-282-2, which supplies power to both UECs and the SCU. Current amplitudes associated with transients generated from the SCU and UECs are approximately 1 to 3 amps. Using 2A, the $B_{E,U} \approx 0.712$ bits. In other words, the signals are too small for aggregate monitoring. A logical alternative from a design perspective is to use the power panel that directly feeds the load. Using 2A for I, the $B_{E,U,PANEL} \approx 5.778$ bits. $B_{E,D,UEC} \approx 9.734$ bits and $B_{E,D,SCU} \approx 8.734$ bits.

A normal GTM start sequence is illustrated in Figure 3-25. The process begins with the opening of the starter air regulating valve (SARV), which is accomplished via a + 28 VDC signal supplied from the UEC. Next, the UEC opens the fuel oil service valves (FOSVs) to allow fuel supply to the engine. At the same time, the GTM igniters are energized (shown in Panel). The SARV is closed next by the UEC. The SCU supplies a +28 VDC signal to a relay to open the GTM vent damper, while the GTM cooling fan is energized. The cooling fan has a 130 HP motor and produces a significant voltage-sag, which is seen in all three power plots.

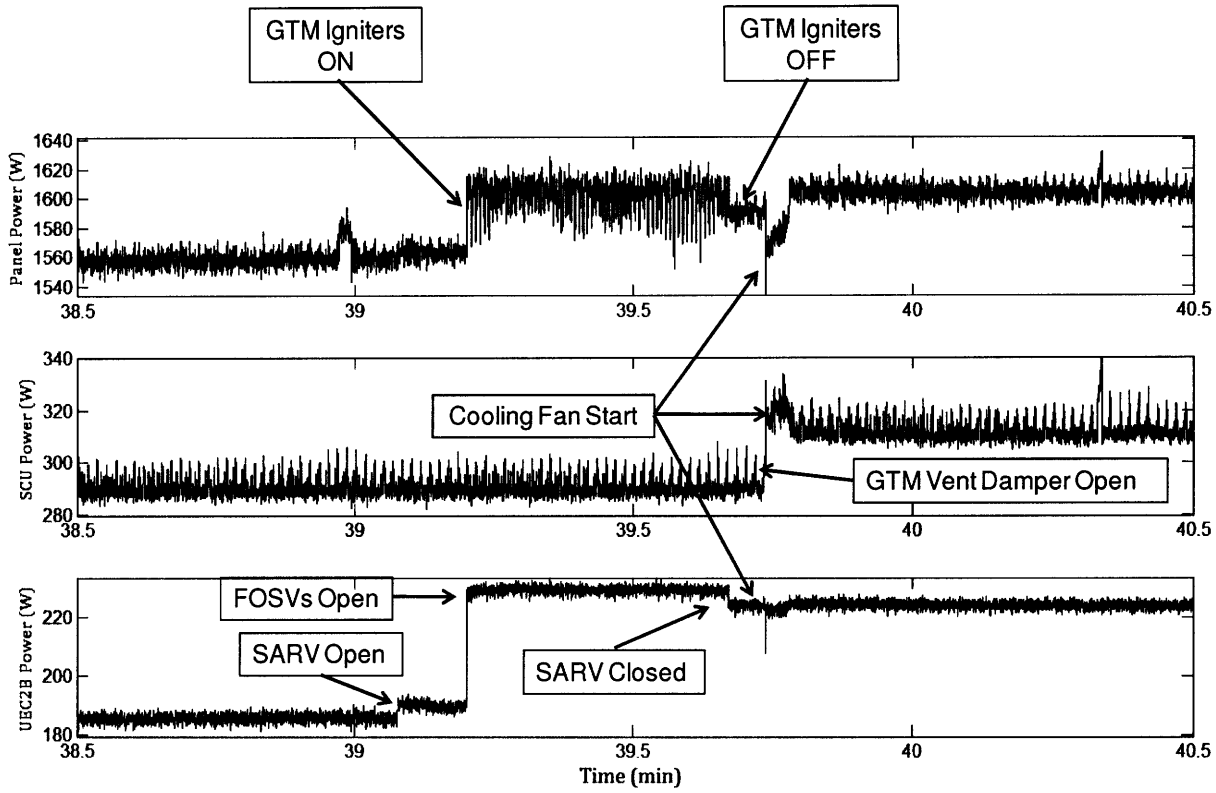

Figure 3-25: Time-aligned spectral plots of a normal GTM start sequence. The large sub-transient voltage sag is a result of the GTM cooling fan start. (4)

3.5.1 GTM Cross-Correlation Results

SCU Transient

First, the SCU was chosen as the downstream candidate. The transient generated by the SCU is due to the +28 VDC signal sent to a relay to open the GTM vent damper. Recall that this is immediately followed by a large voltage droop due to the start-up of the GTM cooling fan. The spectral plots for the upstream and downstream data are provided in Figure 3-26. Each plot contains significant higher frequency content whose origin is unknown.

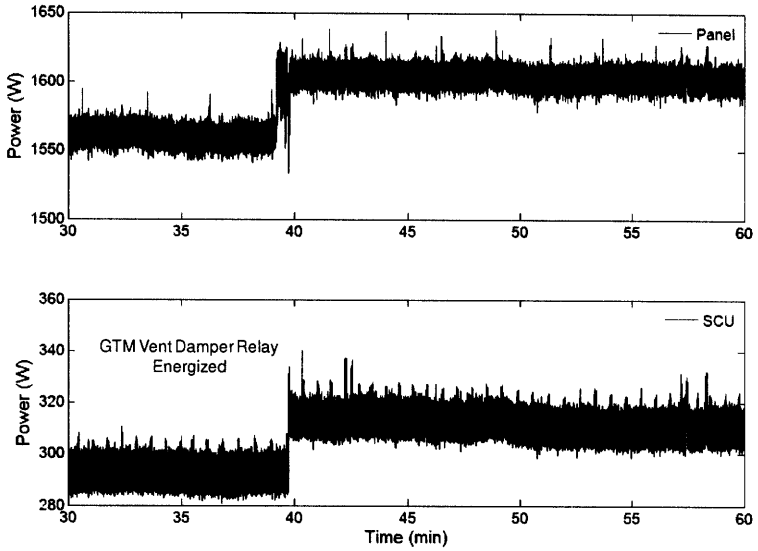

Figure 3-26: Time-aligned plots of Power Panel and SCU. Transient of interest is the relay signal provided by the SCU to open the GTM vent damper.

Several iterations of exemplars were examined using methods previously described. Ultimately, the exemplar shown in Figure 3-27 was chosen. Notice the footprint contains many peaks and valleys and does not provide a smooth curve.

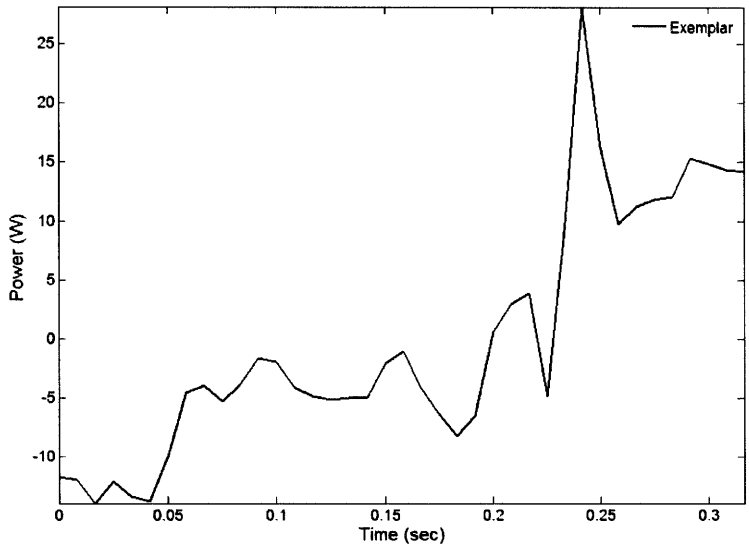

Figure 3-27: Exemplar for GTM damper valve signal.

Downstream and upstream cross-correlation was conducted using the exemplar. Results are provided in Figures 3-28 and 3-29 below. Downstream yielded positive results; however, the upstream failed to correctly identify the event.

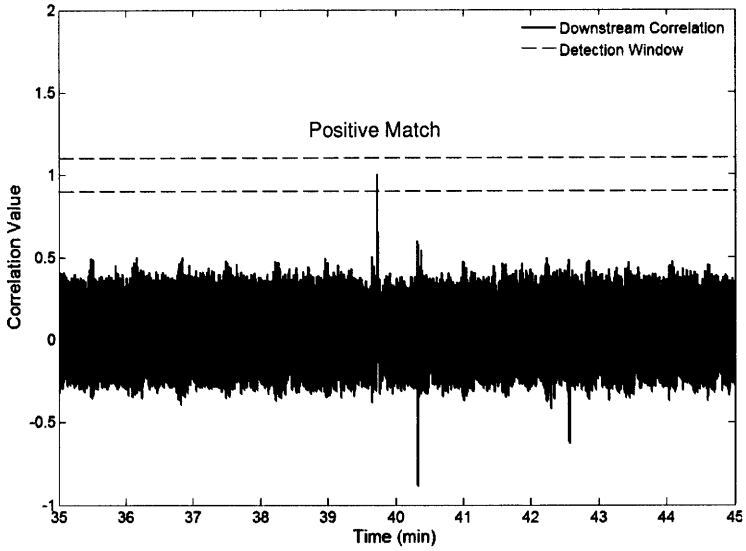

Figure 3-28: Downstream cross-correlation results. Even with significant "chatter", the cross-correlation method correctly identified the transient.

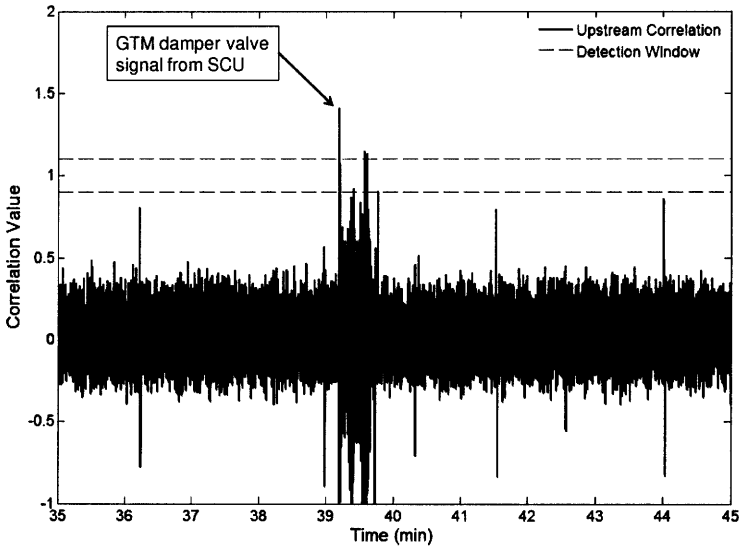

Figure 3-29: Upstream cross-correlation results. Method failed to correctly identify the transient and generated false positives.

Results indicate that the higher frequency "chatter" severely limits the cross-correlation detection method. A simpler approach based on finite state modeling and steady state power levels would be a viable alternative.

UEC SARV Transient

Transients associated with the UEC are captured in the upstream and downstream NILMs in Figure 3-30. The first transient tested is the relay signal provided to open the SARV. This signal only produces a 5 W change in power, which is the smallest transient examined thus far.

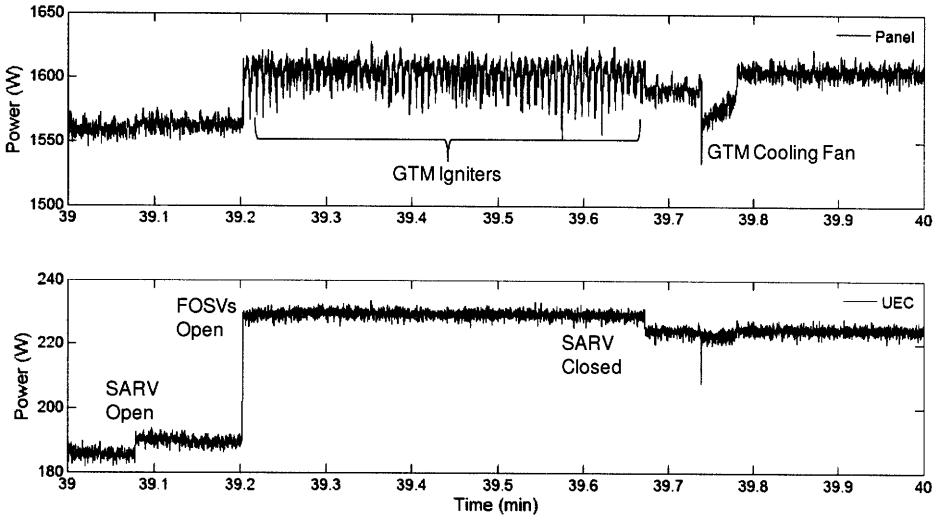

Figure 3-30: Time-aligned plots of Panel (aggregate) and UEC (downstream).

The exemplar for the SARV signal was extracted from the downstream data (Figure 3-31). The downstream data yielded positive cross-correlation results (Figure 3-32). The disaggregation from the upstream data failed again. Figure 3-33 shows how the correlation between the waveforms produced multiple false positives. The SARV opening transient occurs around 39.08 minutes.

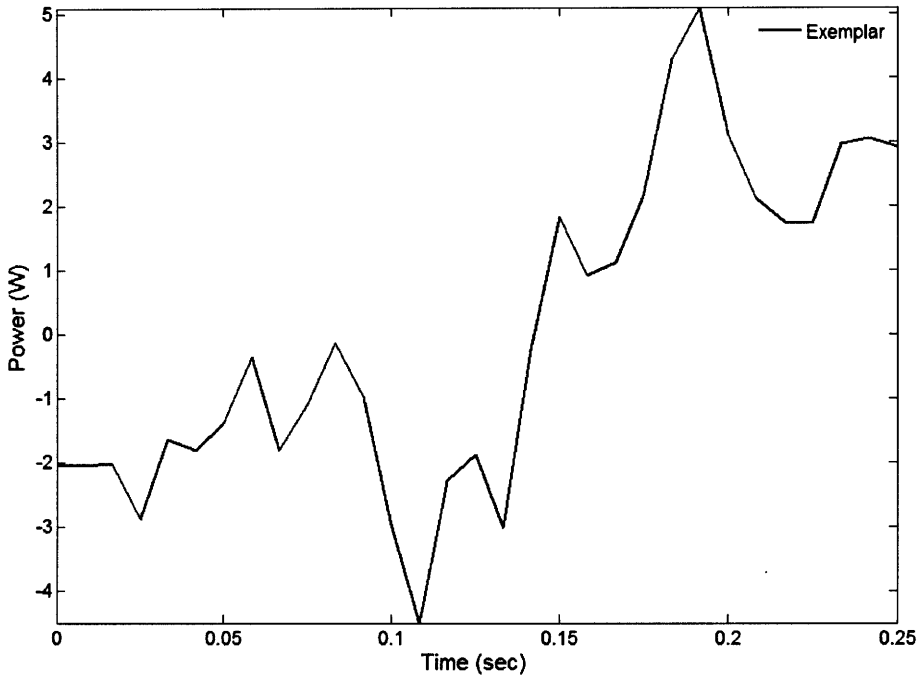

Figure 3-31: Exemplar of UEC SARV transient extracted from downstream data.

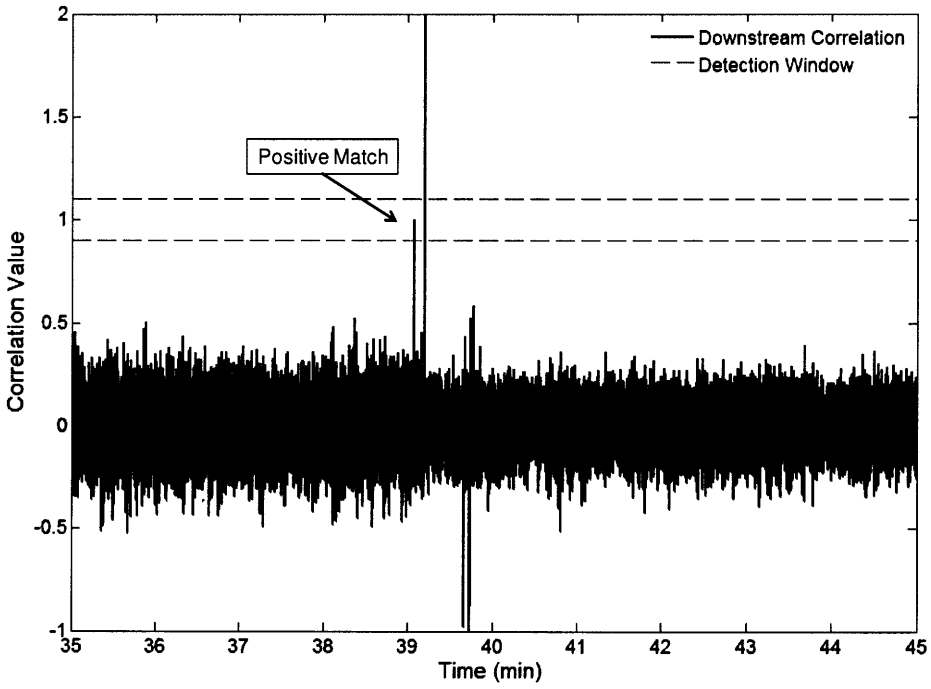

Figure 3-32: Downstream cross-correlation values. The transient was correctly identified.

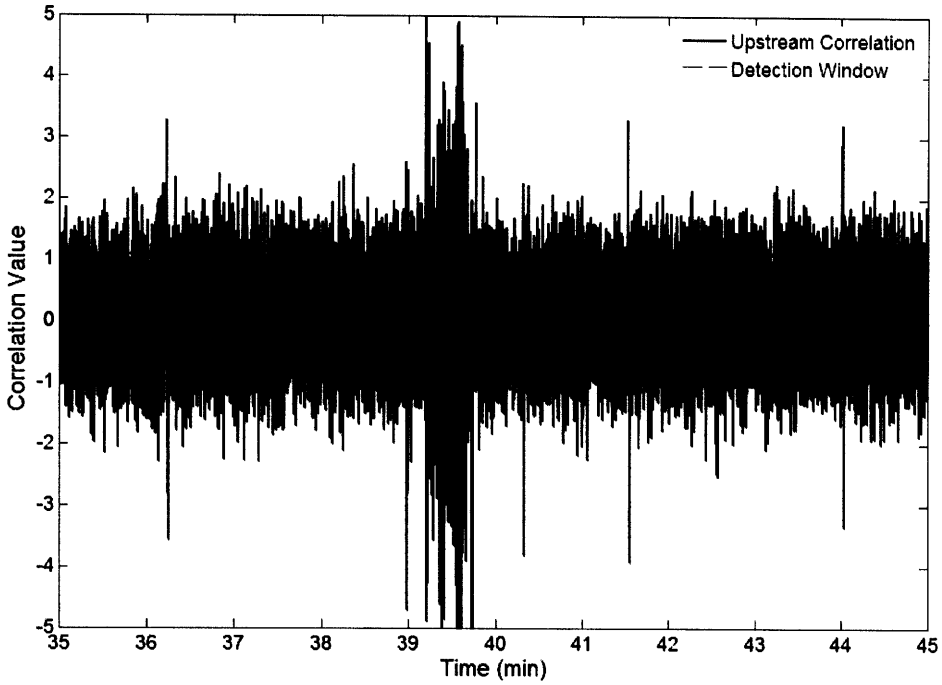

Figure 3-33: Upstream Correlation results for UEC SARV exemplar. Transient of interest is embedded in spikes around 39.08 minutes.

UEC FOSV Transient

Next, the FOSV transient (see Figure 3-30) was extracted from the downstream data and produced the exemplar shown in Figure 3-34.

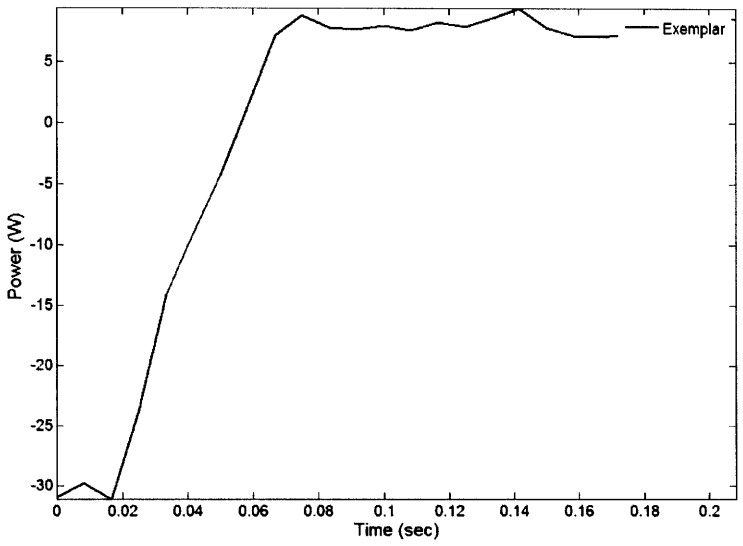

Figure 3-34: UEC FOSV exemplar extracted from downstream data.

Cross correlation results are shown in Figures 3-35 and 3-36. Downstream results were satisfactory. Upstream results revealed strong correlation between the exemplar and the upstream FOSV transient. However, multiple false positives were captured.

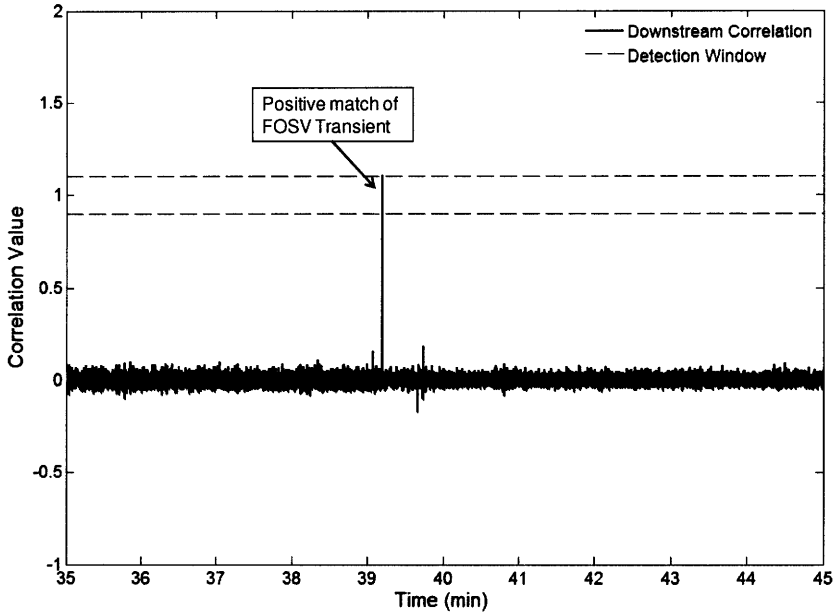

Figure 3-35: Downstream correlation results for FOSV transient. Unique waveform and amplitude produced strong correlation relative to background "chatter".

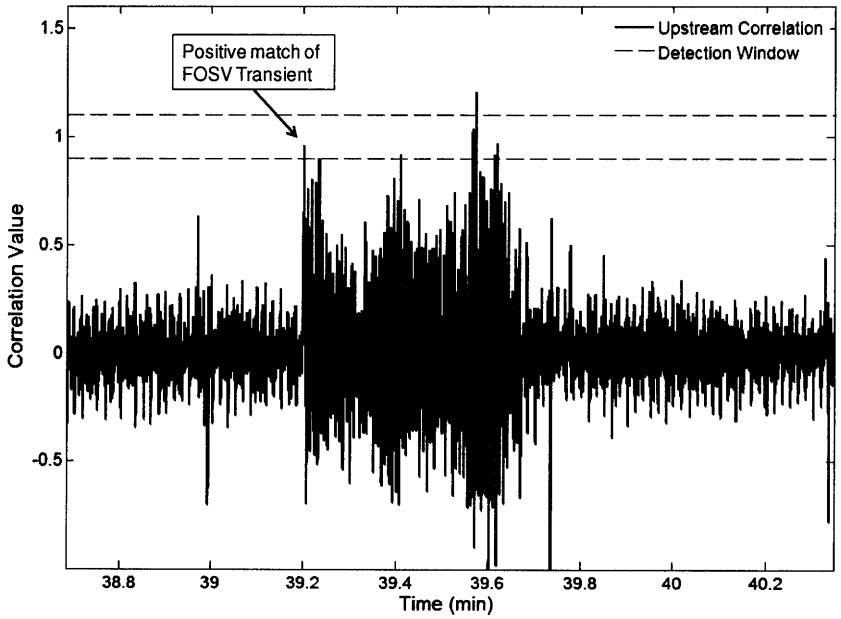

Figure 3-36: Upstream correlation results for FOSV transient. Positive match for event; however, there were multiple false positives as well.

Chapter 4

CHT Classification and Diagnostics Using *Ginzu* NILM

The first operational shipboard NILM application was achieved by Ramsey in 2004. (2) This installation was followed by various trend analyses of cycling fluid systems such as CHT and ASW. (19) Further NILM development focused on creating robust models that enhanced detection of improper pump operations and leaks within fluid systems. (3) In recent years, research teams have continued to gather shipboard system data in efforts to improve detection and diagnostic capabilities. Initially, this data was stored on the NILM computer, and then processed in the laboratory to determine system characteristics. In 2008, the first *Ginzu* NILM[6] configuration capable of real-time detection, classification, and system diagnosis was installed. (5)

In September 2008, the USCGC ESCANABA deployed with the *Ginzu* NILM installed on the CHT system. This marks the second patrol period where the *Ginzu* NILM was installed. This chapter will describe the key characteristics of the *Ginzu* NILM along with some of its capabilities. The methods used for event detection, transient classification, and transient diagnostics are also discussed. Data captured from this period is scrutinized to determine the overall effectiveness of the NILM with regards to trend analyses and diagnostics.

4.1 CHT System Description

The CHT system's function is to collect store, and transfer waste from twenty one locations throughout the ship. Central to the system is the 360 gallon vacuum collection tank (VCT). Drains from the ship's urinals, toilets, and garbage grinder are fed to the VCT. Two alternative vacuum pumps energize to maintain the appropriate vacuum within the tank. Pressure switches

[6] The *Ginzu* NILM was the NILM configuration used by Proper (5) in January 2008 on board the USCGC ESCANABA to monitor the RO and CHT system.

located atop the tank are used to provide low vacuum signals to the control panel. At 14 in-Hg, a single vacuum pump is operated to evacuate the air from the VCT. If vacuum reaches 12 in-Hg, both pumps are energized to increase vacuum level within the tank. When the pressure switches sense 18 in-Hg, all operating vacuum pumps are secured. Two alternating discharge pumps are used to remove waste collection from the collection tank to a holding tank when a high level setpoint probe is energized; the pumps are secured at a low level limit. The local control panel receives its inputs from the various sensors and actuates the appropriate pumps to restore normal operating parameters. The NILM monitors all four pumps via the local control panel power signals. A basic system diagram is illustrated in Figure 4-1below.

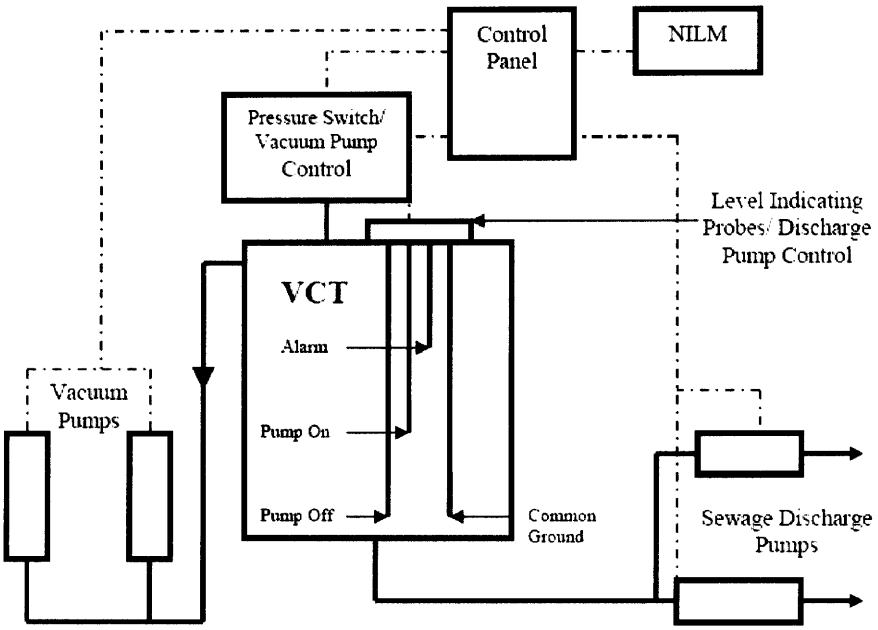

Figure 4-1: NILM Block Diagram. Dashed lines indicate electrical connections within the system. Solid lines represent fluids (air and sewage). (20)

4.2 *Ginzu* NILM Description

Figure 4-2 illustrates the core functions of the hardware and software associated with the *Ginzu* NILM. Raw current and voltage measurements are collected at a sampling rate of 8 kHz via

voltage and current sensing lines. This raw continuous data is collected by the NILM sensor box, where it is converted into a quantized digital signal as it passes through an ADC card.

The quantized digital signal from the ADC is passed via Ethernet to the NILM computer for follow-on processing. This processing includes conversion of the high frequency signal into power envelopes (discussed in Chapter 2), as well as detection and classification techniques used to indicate system status and health information. At the heart of the *Ginzu* NILM is the software package, *Ginzu*. The basic program flow consists of detection, classification, and verification. In its normal mode of operation, *Ginzu* receives preprocessor data at a frequency of 120 Hz. Ten second data windows are loaded and passed to an event detector, which identifies rapid power changes. If an event has occurred, the classifier algorithm is used to identify the transient based on power levels and system state information. The event files created by *Ginzu* are archived for future reference and sent to the user interface for diagnostic functions and user display. The hardware used to perform these functions is shown in Figure 4-3.

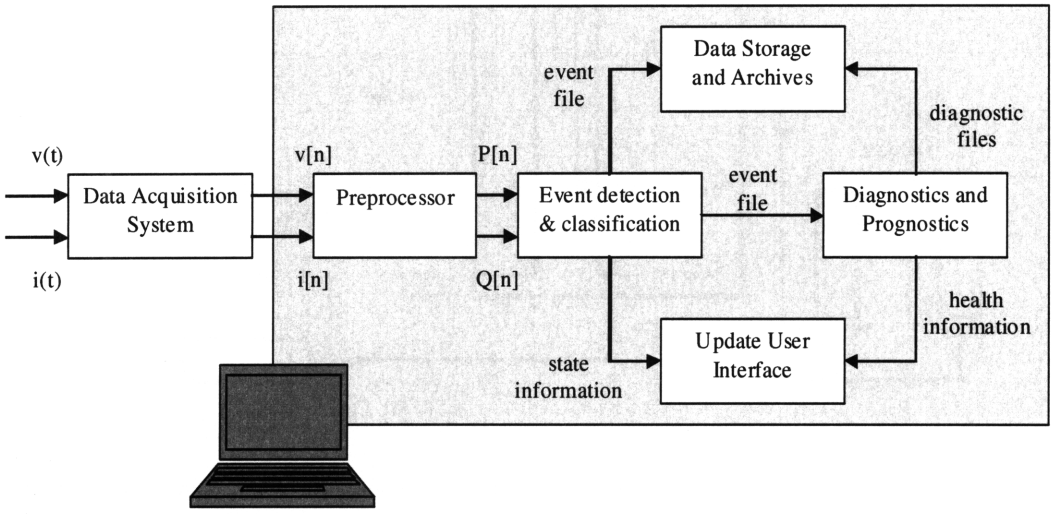

Figure 4-2: Local *Ginzu* NILM Configuration. Highlighted blue area shows the various functions performed following raw data acquisition. Figure courtesy of Proper (5).

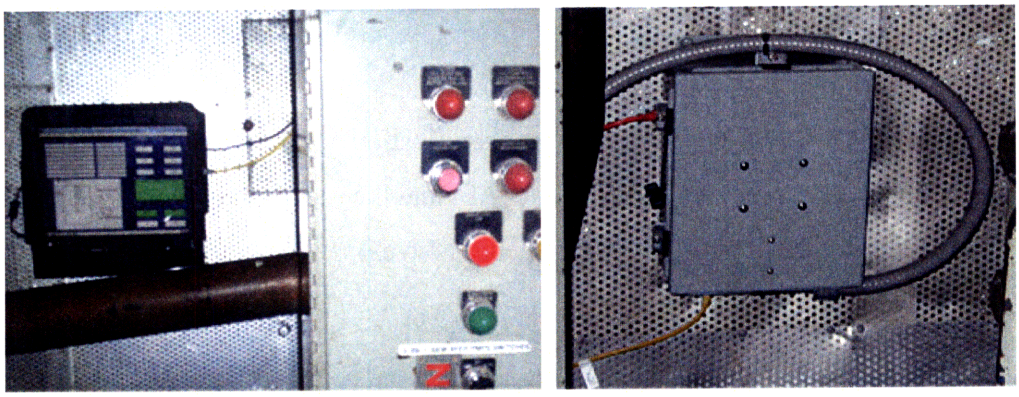

Figure 4-3: NILM Computer (left) collects and processes information received from NILM Sensor Box (right) via Ethernet cable. Grey wire conduit and yellow cable penetrating underneath the NILM box are raw voltage and current measurements received from the control panel.

4.2.1 Detection Method

Events are detected when rapid power changes occur. *Ginzu* uses a change of mean filter to perform this function. A two column power array of real and reactive power is passed to the event detection algorithm, where a low pass filter is used to remove the D.C. level of the incoming data stream. The power signal is then compared to a user-defined detection threshold to determine whether or not an event has occurred. Figure 4-4 shows how the detection algorithm receives the information and produces event detection.

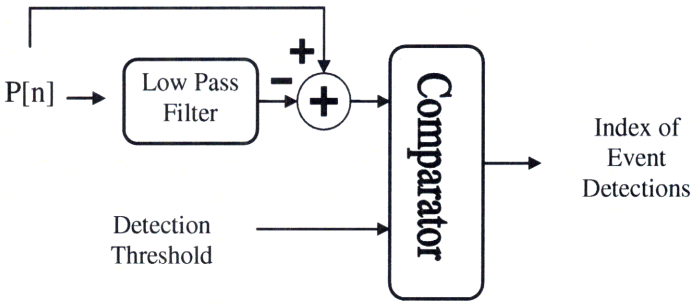

Figure 4-4: Detector Change-of-Mean Filter. (5)

4.2.2 Classification Techniques

When transients are detected, *Ginzu* performs classification via two steps. First, steady state power changes are analyzed in the real envelope (ΔP) and the reactive envelope (ΔQ). Secondly, transient characteristics defined by the power spectral envelope are compared against a library of known system power envelopes.

Steady State

When individual loads are cycled within the system (i.e. pump on/off), they produce a corresponding change in the real envelope and reactive envelope and possibly other spectral envelopes. These changes can be used as a simple classifier to identify loads. *Ginzu* uses only ΔP and ΔQ values to classify events. Since the CHT system is only comprised of four primary loads, the need for higher order harmonics to aid in classification was not required.

Transients

As described in Chapter Two, transient-based recognition permits near-real-time identification of load operation, especially turn-on events. Transients are identified by matching events in the incoming power stream to previously defined transient signatures, or "exemplars." Pre-training has proven to be a reasonable approach for very repeatable loads that show up in large quantities, such as fluorescent lamp ballasts. Each event detected is compared to the full set of exemplars by using a least squares criterion to select the appropriate shifts and gains. The match with the lowest residual norm per number of points is then compared to a threshold. If the fit is good enough, the event is classified as a match to the exemplar. If not, the event is left unclassified.

Correct classification of overlapping transients is possible using properly designed exemplars for a system with as few a number of loads as the CHT system. Fingerprint traces provide positive identification of specific events occurring during system operation. By comparing the shape of the transients to known system events, a numerical score can be assigned to grade the degree of similarity of the two signals; this score is known as the correlation score. It is derived using the

method of least squares in the *Ginzu* algorithm. This method is discussed in detail in Lee (21) and Proper (5).

Event Files

The CHT event classifier generates an ID CODE to represent a specific system event when operating in its normal mode. TABLE 4-1 lists normal system event descriptions along with their associated codes. TABLE 4-2 lists additional system descriptions that were defined to create a more robust classifier. Once a positive event has been identified, an event file is created and stored in the archive directory.

TABLE 4-1: CHT CLASSIFICATION CODES. (5)

Description	ID CODE
Vacuum pump ON	(001)
Discharge pump ON	(003)
Vacuum pump OFF	(002)
Discharge pump OFF	(004)
ALL pumps OFF	(009)

TABLE 4-2: NON-STANDARD CHT CLASSIFICATION CODES. (5).

Description	ID CODE
Vacuum pump ON, but indicates low running power	(005)
Vacuum pump with low running power has turned OFF	(006)
Unclassifiable event (probable noise)	(000)
Unidentified ON event	(007)
Unidentified OFF event	(008)
Vacuum pump cycling [7]	(021)
Discharge pump cycling	(043)
Cycle of Unidentified Load	(087)
2 Vacuum pumps ON	(011)
Vacuum pump ON and Discharge pump ON	(013)

4.2.3 State Verification

If no transients are detected within a given window, the classifier does not need to be called. *Ginzu* uses this opportunity to verify the current state of operation. This is accomplished by calculating the average power level for a ten second window and its standard deviation. These values are used in a state verification function to perform various checks and correct the state status if needed.

4.2.4 CHT *GinzUI* and Diagnostic Package

The *GinzUI* application provides the interface between the event file and the NILM user **(5)**. Its primary functions are:

- To continuously check the user interface directory for newly created *event files*.
- To read *event file* contents and move the *event files* to an archive directory.

[7] A 'Cycling' load is a load which turns on but immediately turns off during the same event window. This occurs when a template match indicates a specific type of pump has started – but no relative power change occurs across the event.

- To peform diagnostics on *event file* data and alert the user if a diagnostic has failed.
- To allow the user to graphically view *event file* contents.

Four CHT *GinzUI* diagnostic packages were available during the September 2008 patrol. Each of these was created based on known system faults that were identified during previous NILM research (2) (20) A general description of the three faults is provided below[8].

Vacuum Pump Clog Diagnostic

In (20), Piber describes a fault where the vacuum pump fails to reach normal steady state power level. This is the result of a clogged suction line or priming line for the associated vacuum pump. This fault results in abnormally long vacuum pump run times as well. Normal vacuum pump run duration is only 1-2 minutes. During this particular event, the vacuum pump remains on for longer periods (several minutes) as it attempts to draw a vacuum. Eventually, the alternating pump energizes to assist in drawing the vacuum. Once the high vacuum set point is reached, both pumps are secured. Figure 4-5 illustrates this sequence of events.

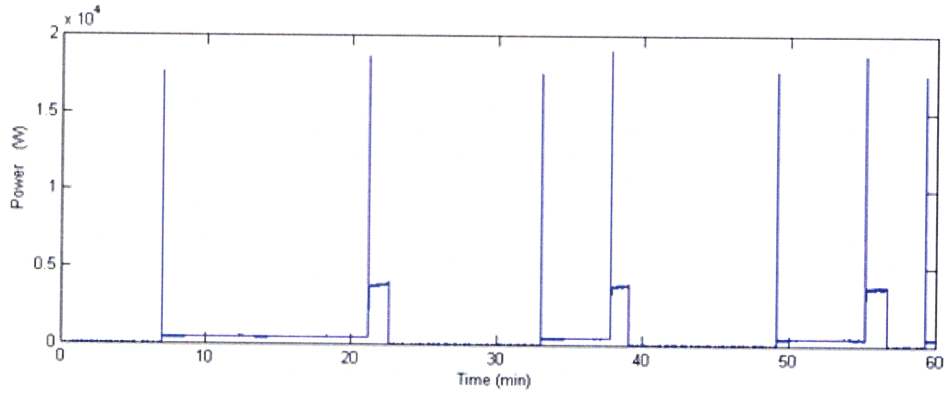

Figure 4-5: Power plot indicating a clogged vacuum pump fault. The first pump energized runs for excessive periods until the low vacuum set point is reached, then the alternating pump assists until the high vacuum level set point is reached. (20)

[8] A detailed description of each fault and its history is provided in Piber. (20)

The clogged vacuum pump is identified in the classifier as 'VP ON with low running power (005). The diagnostic function alarms when five 'low power' vacuum pump runs are identified within the ten most recent vacuum pump starts. This is accomplished by assigning a one to 'low power' starts and a zero to normal pump runs. If the sum of the ten most recent vacuum pump ON events reaches five, the CHT *GinzUI* alarms indicating a clogged vacuum pump has been diagnosed. The alarm clears when eight out of ten of the most recent runs are classified as normal.

Excess Vacuum Pump Runs

The vacuum pumps are controlled via pressure switches located on the side of the sewage retention tank. One switch is set to control the operation of the lead pump by energizing the pump when pressure reaches 14" Hg and securing the pump when pressure reaches 18" Hg. The second switch controls the standby pump to energize it if pressure reaches 12" Hg. If both pumps are energized, the pressure switch de-energizes both pumps upon reaching 18" Hg. (22) Each pressure switch has individual settings that can be adjusted using dials within the switches. If the pressure switch is incorrectly calibrated, the vacuum pumps may run excessively attempting to reach a higher vacuum set point. This fault reveals similar power signatures as those discussed for clogged vacuum pumps. Proper stated *"The CHT UI continuously displays the most recent vacuum pump run duration and the average of the runtimes over the last 50 runs. During normal operation, this value should be between 30 and 60 seconds. The runtimes are calculated and retained as Vacuum Pump OFF (004) or ALL OFF (009) events (sic). The UI alerts the user if the average runtime exceeds 180 seconds. Since a clogged vacuum pump combined with an improperly set or faulty sensor could result in similar system behavior, this diagnostic is disabled if a Vacuum Pump Clog has already been detected".*

Fouled and Damaged Tank Level Indicating Probes

The third diagnostic algorithm pertains to discharge pump operation. In March, 2007, Piber observed erratic discharge pump behavior based on power plots of the CHT system. The

discharge pumps are operated based on tank level control circuitry. This circuitry receives its input via tank level probe indicators located in the VCT. If these probes become fouled or the circuit does not function correctly, erroneous discharge pump operation may occur. Typical discharge pump operation lasts about 3 to 4 minutes while the pump removes 120 gallons of sewage from the VCT to a larger holding tank. Figure 4-6 depicts the short burst associated with a failed probe casualty.

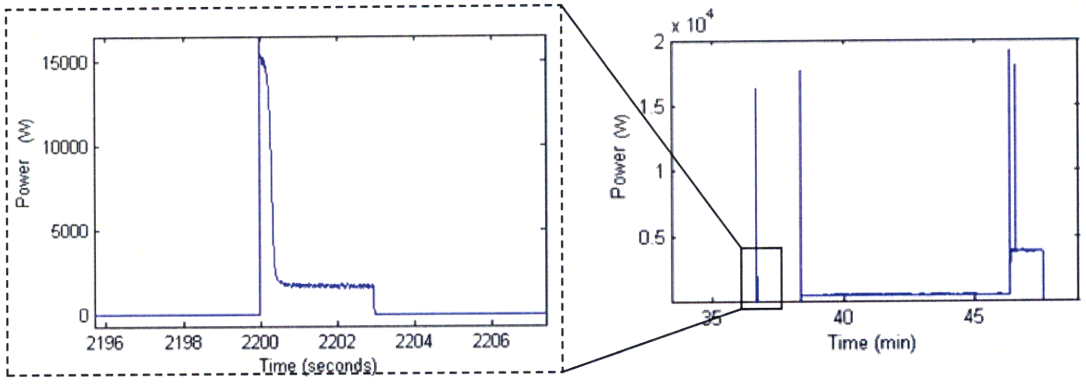

Figure 4-6: Failed probe casualty power response on board the USCGC SENECA. (20)

The *GinzUI* diagnostic algorithm searches for this fault by collecting runtimes for each discharge pump operation. An average healthy runtime is between 3 to 4 minutes. (5) If the average of the last ten discharge pumps is less than 10 seconds, the GUI will alert the user that there is a probable fault by changing the color of the diagnostic log to yellow and indicating 'PROBE FAILURE' in red (Figure 4-7).

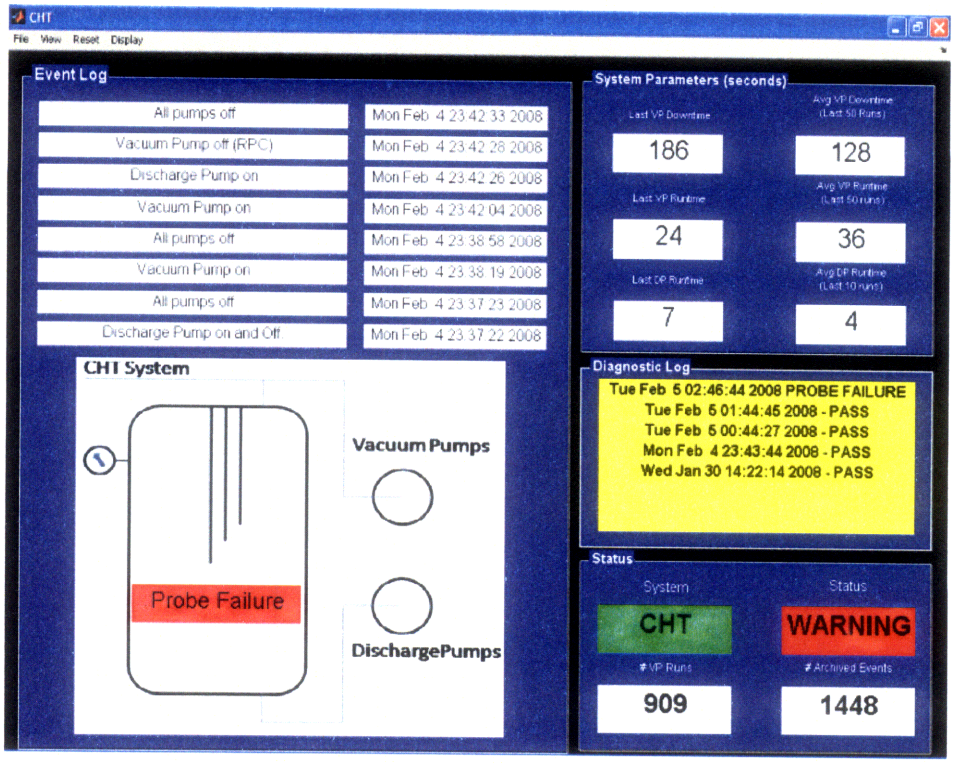

Figure 4-7: ***USCGC Escanaba*** **CHT GUI Illustration. This screen capture indicates a possible probe failure based on indicators. Note the diagnostic log lists the date and time of the potential failure. (5)**

Leak Detection

Vacuum leaks in the CHT system have been documented on multiple occasions during NILM research (3) (20) (5). Mosman noted a major vacuum leak on the USCGC SENECA during his studies (3), which led to further studies on how to determine if a leak is present in the sewage system. Mosman used statistical methods that modeled the time between vacuum pump runs as a Poisson process. Histograms were used to visualize the distribution of the pump times. It was observed that major leaks in the system were visible as shifts in the histogram peaks and change in the general shape. Piber followed this research with field studies on the ESCANABA that revealed the occurrence of a major leak using power data captured by the NILM.

Ginzu Performs leak detection using two separate methods. For larger leaks, *Ginzu* looks for sharp edges in the histograms. If the edge exceeds a tuned threshold, the diagnostic reports a

leak has been detected. For smaller leaks, *Ginzu's* leak diagnostic looks for gradual changes of the distribution over a period of days. (5)

4.3 USCGC ESCANABA Local *Ginzu* NILM Evaluation

In September 2008, the USCGC ESCANABA departed the Boston area with two NILMs installed. A *Ginzu* NILM was installed at the local CHT control panel, while an off-line NILM was placed further upstream to monitor aggregate loads.[9] This chapter will describe how the local NILM provided the crew with at-sea diagnostics, as well as provide a critical review of classifier and diagnostic performance using archived data.

The following quote was taken from a letter of appreciation to the MIT LEES (Laboratory for Electromagnetic and Electronic Systems) team on behalf of the Engineering Department following the patrol:

The NILM provided great support to the crew during our most recent deployment. With the NILM mounted to the shipboard sewage vacuum pumps for vacuum collection tank (VCT) we were able to monitor the run time and frequency of the vacuum pumps in automatic mode...Almost immediately upon installation the NILM indicated that the pumps were in fact operating with a periodicity and duration that suggested excess operation. Further inspection of the VCT system revealed failing check valves and pump deterioration. ***Had the NILM not been installed, the pump most probably would have been run to the point of failure.*** *The NILM provided real time data that allowed maintainers to extrapolate trend performance to avoid a complete system failure that would have required emergency logistic support.* (23)

4.3.1 Ship's Force Use of Diagnostics to Identify Vacuum Leak

On October 19, 2008, while deployed, the crew of the ESCANABA replaced #2 vacuum pump and motor assembly (Figure 4-8) due to excessive wear to the pump and motor that was identified during visual inspections. The cause of the motor and pump degradation was excessive cycling of the vacuum pump due to a major leak in the system. It was determined that

---

[9] The off-line NILM only gathered 'prep' data. It did not provide crew members with a user interface or diagnostic package. Results from the off-line NILM were discussed in Chapter Two.

a faulty check valve downstream of the vacuum pump was not seating properly, thus allowing high pressure air to bleed into the vacuum system.[10]

Figure 4-8: Replacement pump for #2 Vacuum Pump. This photo was taken following the ESCANABA's return to port in November 2008.

One indication of a major leak in the vacuum system is excessive vacuum pump cycling. During routine system events such as toilet flushing, the system pressure drops in a step-like fashion. Leaks, depending upon their size, display more gradual and steady decreases in system pressure. Mosman (3) illustrated this in Figure 4-9 below.

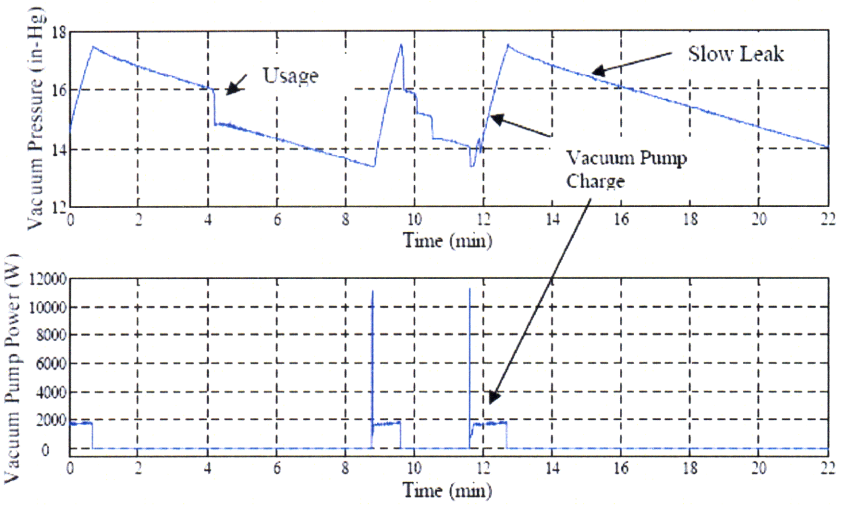

Figure 4-9: Sewage system pressure trace (upper plot) and time-aligned vacuum pump transients (lower plot). Plots illustrate the pressure response of the system due to routine events (flushes) and slow leaks in the system.

[10] The exact events leading up to the replacement were not provided. The reconstruction of events is based on post-patrol analysis of the data and email correspondence with the ship's engineer.

As the leak becomes larger, the slope of the system pressure increases and the vacuum pumps' cycling frequency increases. This system behavior prompted the crew to troubleshoot and identify the faulty check valve.

Figure 4-10 shows the vacuum system behavior prior to and following system repairs. A drastic drop in pump cycles per hour occurred after the repair, since the system was then capable of maintaining vacuum during no-load conditions.

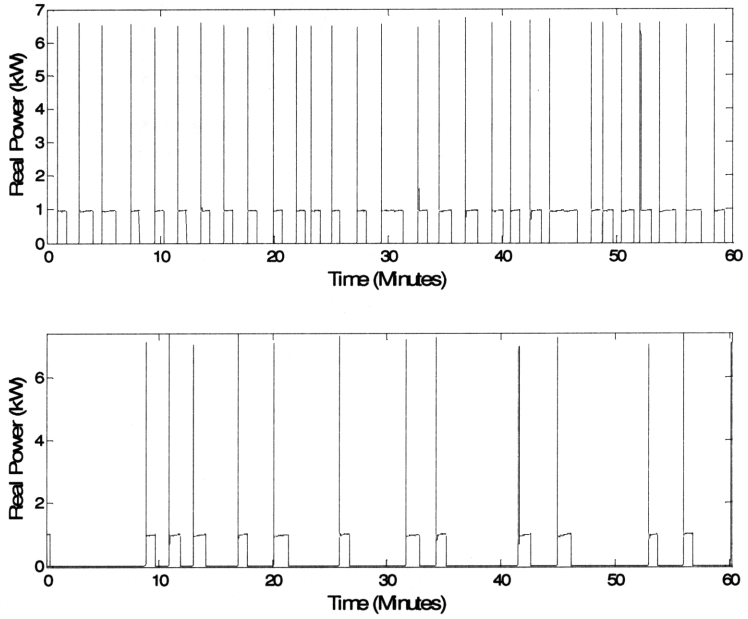

Figure 4-10: Local power plots taken before (top) and after (bottom) repairs. Each plot sample was taken during the 0600 hour for more accurate comparison.

The same information on system cycling was provided to the crew during the patrol via the user interface in a slightly different format. In order to re-create what the crew saw while deployed, one hour of archived events (0600-0700) from September 20, 2008 was processed using *Ginzu*. The screen capture in Figure 4-11 displays the system behavior via statistics gathered by the user interface for the one hour sample. There were 26 vacuum pump cycles with an average of 61 seconds for runtime. The data on the right-hand side of the screen displays information on vacuum pumps and discharge pumps. The average discharge pump runtime displays 'NaN', because there were no discharge pump events during this one hour sample window. This information enabled the crew to note the high vacuum pump run periodicity and led to corrective actions.

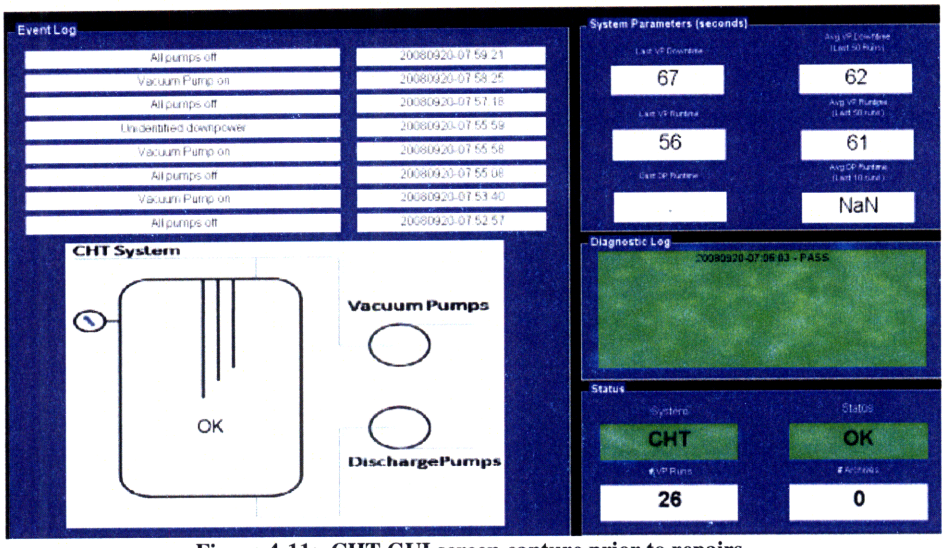

Figure 4-11: CHT GUI screen capture prior to repairs.

Similarly, one hour of post-repair data was processed using *Ginzu*. The screen capture in Figure 4-12 illustrates the results. **The classifier correctly labeled all vacuum pump events.** The average vacuum pump runtime remained around one minute, which is normal. However, the key difference is the number of vacuum pump runs per hour, which was 26 prior to repairs and 10 following repairs.

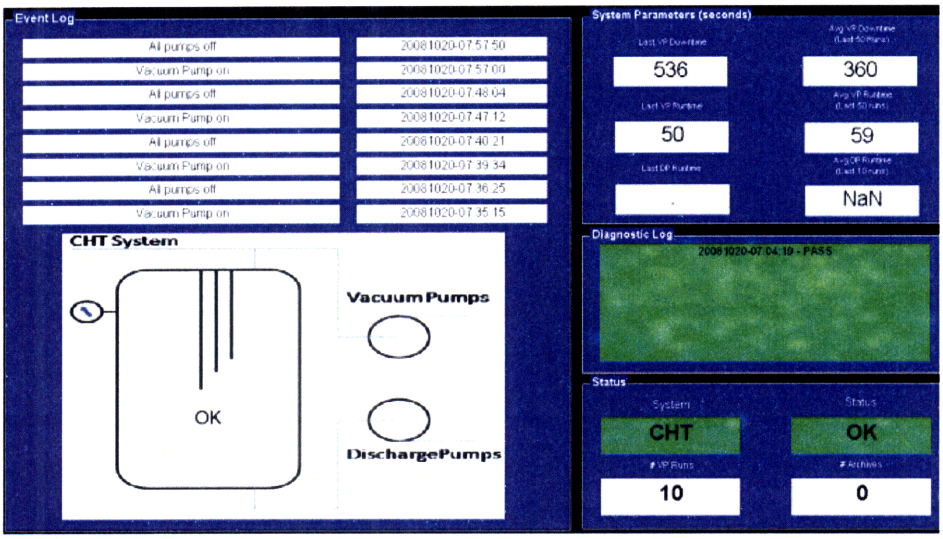

Figure 4-12: CHT GUI display following repairs. Data was taken from October 10, 2008, 0700.

4.3.2 Classifier and Diagnostic Effectiveness

In order to assess the NILM's performance during the patrol period, archived data taken from the NILM laptop was processed using the ViewerUI. *Ginzu's* CHT classifier was used to analyze preprocessed data and generate *event files*. Once the event files were created, the ViewerUI was used to select any *event file* from a list box. Figure 4-13 provides an example of a normal vacuum pump start displayed by the ViewerUI.

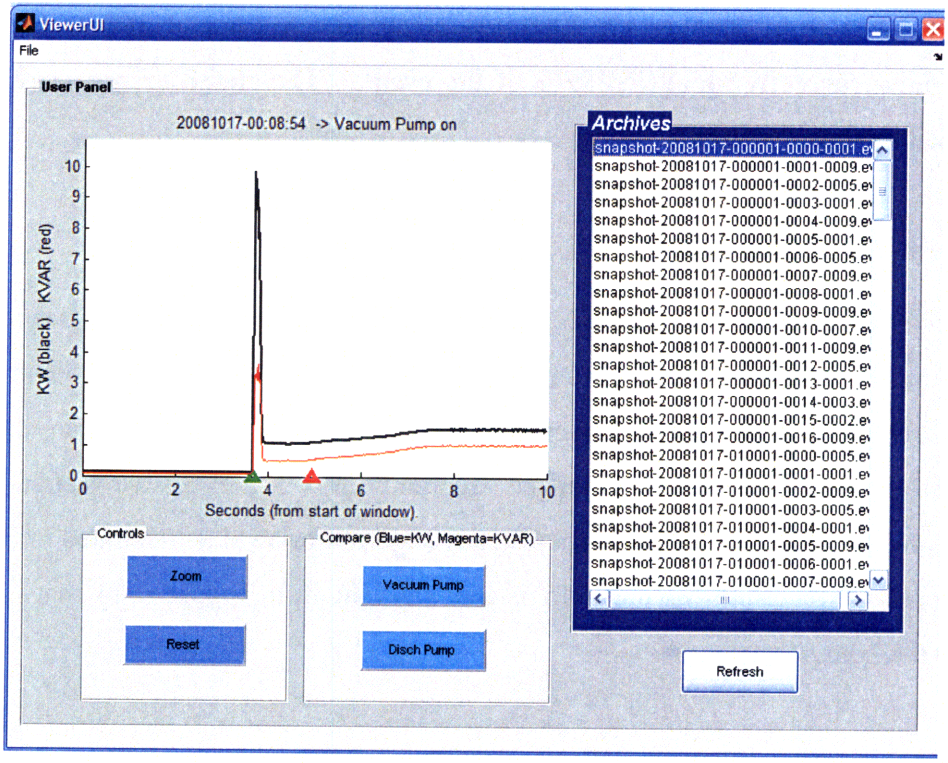

Figure 4-13: A normal vacuum pump On event (001).

The viewer also has the ability to simultaneously display a captured event and either the vacuum pump or discharge pump template, which allows the user to compare events against their exemplars. The right-hand side lists the events that are called from the archive. Note that the event file highlighted has a classification code of (001), which corresponds to a 'Vacuum Pump ON' event. Each event window is ten seconds in length. The green arrow along the time axis indicates when the event is detected; the red arrow corresponds to the end of the lock-out

window. In (5), Proper explained that a 1.25 second lock-out window was invoked to prevent multiple detections during a transient.

Random samples were chosen to analyze the overall effectiveness of the classifier and diagnostic functions of the *Ginzu* NILM. This was only the second time the *Ginzu* NILM configuration was installed for an extended at-sea period.[11] These random sample windows were processed using the CHT classifier, and then *event files* were viewed using the ViewerUI. Eleven hours of archived data taken from October 17, 2008 was analyzed. **A total of 168 *event files* were captured; *Ginzu* correctly identified 99% of the events. The classifier was only unable to recognize two transient events.**

4.3.3 Vacuum Pump Clog Detection

The random sample also revealed that the classifier function correctly identified clogged vacuum pumps on several occasions. Recall from Chapter 3, the classifier labels a potential clogged pump as 'VP ON with low running power'. If five out of the last ten events are classified as such, the *GinzUI* alarms to indicate a clogged vacuum pump. The excessive vacuum pump run duration coupled with the lower than normal steady state power level is illustrated in Figure 4-14 using a spectral power plot. Figure 4-15 is the transient from Figure 4-14 that occurs nine minutes into the hour.

[11] Details of first patrol period are provided in Proper's thesis (5).

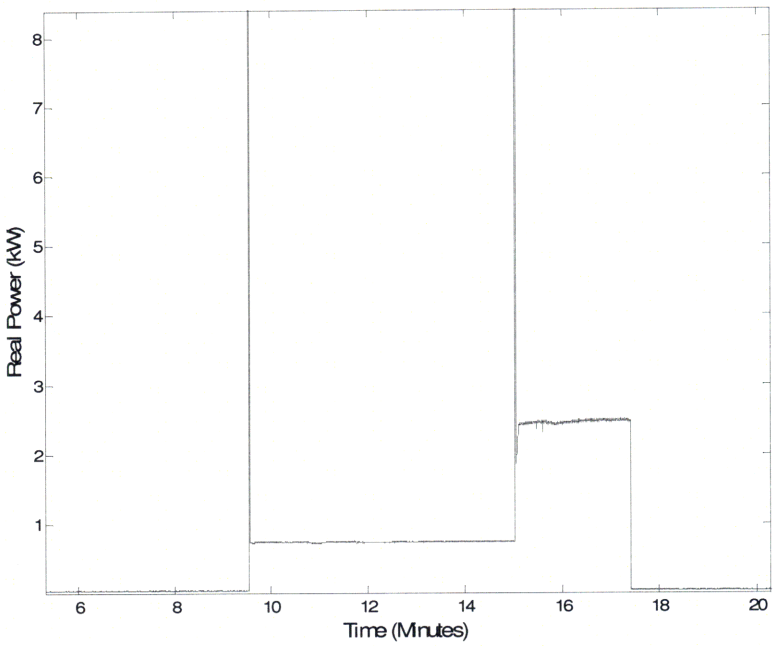

Figure 4-14: Power plot indicating possible clogged vacuum pump. The longer than normal run time of the first pump coupled with the lower than average steady power level causes the *Ginzu* classifier to classify event as 'Vacuum Pump ON, Seal Clogged'.

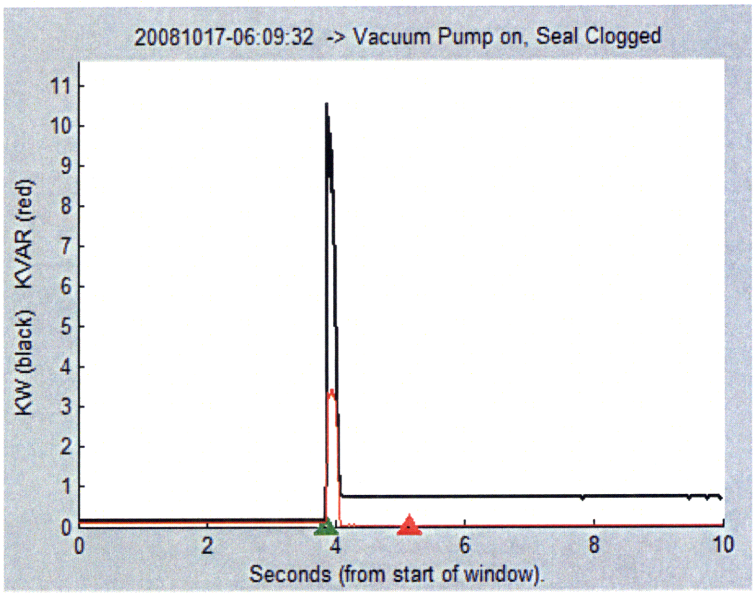

Figure 4-15: Vacuum pump clog fault. The ViewerUI contains *Ginzu's* classification (top stamp) based on the lower than normal power and excessive run-time.

4.3.4 Abnormal Pump Transients and Multiple Events

Data sets prior to the pump and valve repairs were also analyzed. Events captured on September 29, during the 0000-0100 hours revealed unusual pump signatures for one of the vacuum pumps.

(b) Abnormal pump start down transient classification

Figure 4-16 shows two consecutive events captured during this period. The classifier correctly identified the vacuum pump transient even with the unusual up and down transient that occurs as the pump reaches its steady state value. Note the trailing edge of the 'hump' is outside of the lock-out window.

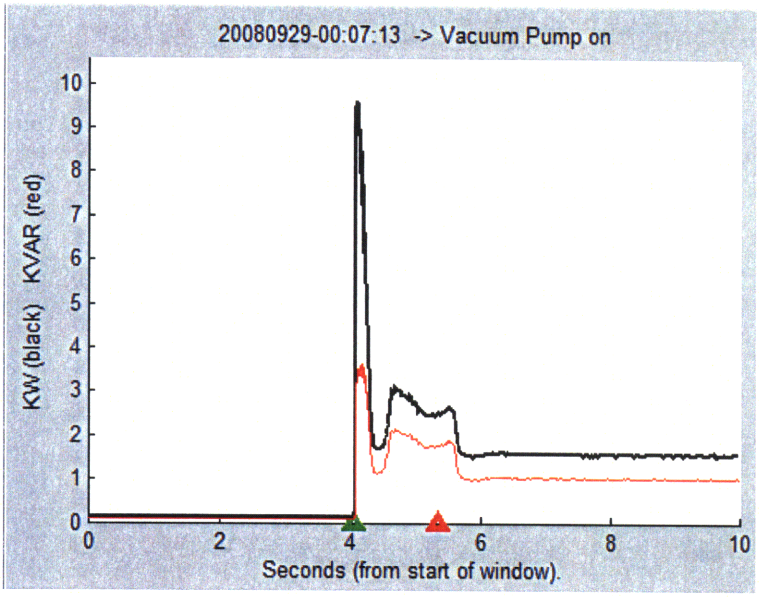

(a) Multiple events detected by classifier.

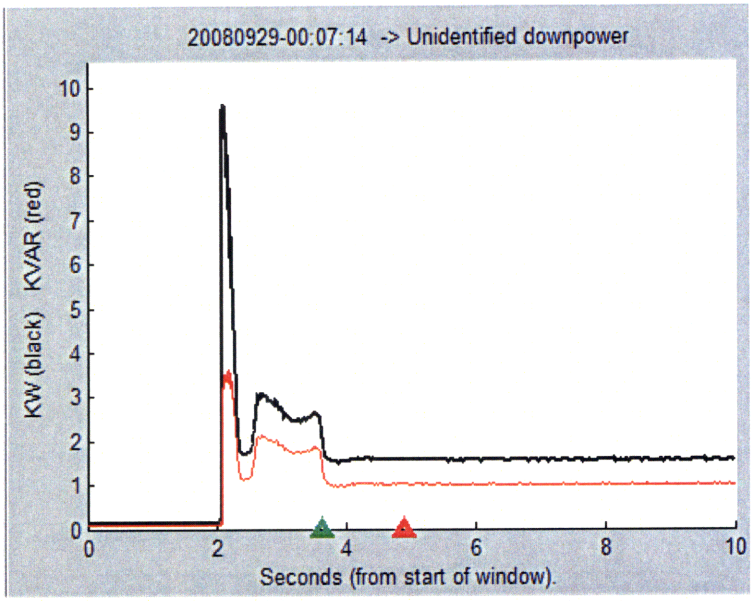

(b) Abnormal pump start down transient classification

Figure 4-16: Classifier performance during abnormal vacuum pump start.

Figure 4-16 (a) is considered a 'multiple event' in a single detection window. If multiple events are determined based on numerical derivatives of the data window, Proper stated "...the event is 'arbitrated' by calculating the ΔP and ΔQ across the lockout window" (5). In this particular case the algorithm functioned properly and classified the event as a vacuum pump start. The transient event (b) is the trailing edge of the unusual 'hump'; correctly labeled as an 'Unidentified Downpower' by *Ginzu*. The power level change due to the trailing edge of the hump did not correspond to the values assigned for either vacuum pumps or discharge pumps, so it was correctly labeled as 'unidentified'.

The next classified event detected was when the vacuum pump was secured. This is illustrated in Figure 4-17. Even with the unusual transient, the classifier eventually self-corrects itself based on power level information, thus returning to an 'All Pumps Off' state. Subsequently, the next event was correctly classified as a vacuum pump start in Figure 4-18.

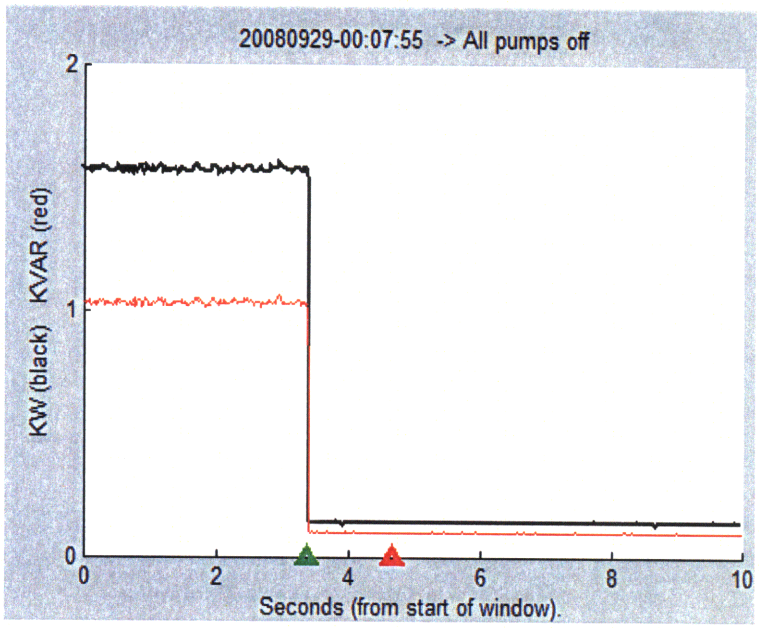

Figure 4-17: Classifier recovery. The 'All Pumps Off' event is followed by the next vacuum pump transient, which is correctly classified.

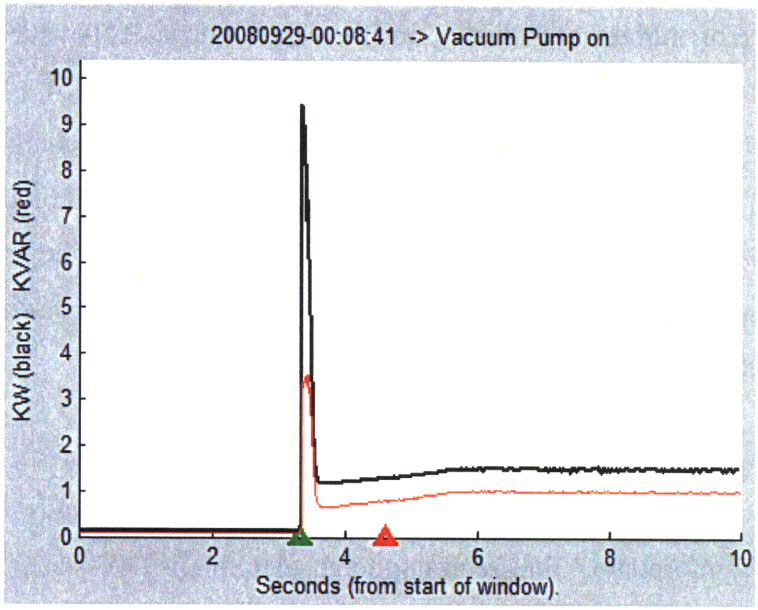

Figure 4-18: Vacuum pump start following state correction.

4.4 Performance Summary

Overall, the performance of the automated classification system was highly successful. The *Ginzu* NILM accurately detected, classified, and diagnosed system transients throughout the patrol period with no system downtime. With little user training, the crew was able to *Ginzu's* real-time user interface to diagnose a vacuum leak, preventing catastrophic at-sea failure.

The detection, classification, and diagnostic methods were relatively simple schemes limited to four operating pumps. As discussed in Chapters Two and Three, as the NILM becomes more 'non-intrusive', the disaggregation becomes more challenging and may require more complex techniques for extracting target information. However, the methods used for power monitoring of the CHT system demonstrate the potential of the NILM as a diagnostic tool.

Chapter 5

Conclusions and Future Work

5.1 Conclusions

Shipboard aggregate power monitoring is a viable solution to sensor count reduction, which will benefit the Navy's efforts in condition based maintenance. However, there are multiple issues that challenge the extension of NILM in efforts to increase its non-intrusive characteristic. Multiple concerns were addressed throughout this thesis. Three more prominent obstacles to NILM aggregate power monitoring include: quantization, measurement distortion, and disaggregation of loads. Chapter 2 revealed that quantization and measurement distortion are less likely to impact aggregate power monitoring when compared to disaggregation.

Effective load disaggregation is very application-specific, thus various methods of extracting loads to perform classification and diagnostics are necessary for successful aggregate power monitoring. Specific methods of disaggregation were examined using ESCANABA and LBES data. Results revealed that the cross-correlation and peak detection method was highly successful on the ESCANBA data. However, LBES data severely challenged this approach of disaggregation.

Chapter 4 provided patrol results from the ESCANABA where the *Ginzu* NILM was installed. An application-specific NILM designed to monitor the CHT system, the *Ginzu* NILM performed exceptionally well. Crew members exploited the real-time user interface to diagnose a leak in the CHT system. This real-world application of the NILM demonstrates the potential of NILM to bridge the gap between data acquisition and real-time user information.

5.2 Future Work

Data acquisition improvements are currently in progress. The NerdJack[12] is one promising aspect of data acquisition that may lead to improved aggregate power monitoring. Its increased voltage range coupled with an increase number of bits will yield higher data resolution. This will enhance the NILM's ability to digitally "zoom" into data and look for key features. Furthermore, the NILM will become more capable of distinguishing unrelated transients from target transients, increasing its ability to disaggregate upstream data.

Another area of current research that may provide fruitful results in aggregate data collection is *Zoom* NILM (24). The primary objective of *Zoom* NILM is to achieve 18-bit resolution over a wide range of currents. In order to achieve this, various hardware changes are being considered. For instance, the dynamic range of the current transducer may be expanded using flux cancellation. Basically, magnetic cancellation of large currents is used to maintain measurement ranges of the current sensor within tolerance.

As with any research, field data collection and analysis must continue in order to test hypotheses. It was shown that disaggregation techniques such as cross-correlation and peak detection work in limited applications. Research throughout this thesis focused on one or two attributes to perform disaggregation. Future work should also consider alternative solutions to extracting target information from aggregate power streams. One possible solution is through machine learning algorithms that group clusters of load features. A cluster approach will provide additional details of a load, increasing the NILM's resolution in the aggregate.

[12] A new Ethernet-based ADC card being developed at MIT. Further description provided in (55).

Bibliography

1. **Paris, James, et al.** *Scalability of Non-Intrusive Load Monitoring for Shipboard Applications.* National Harbor, Maryland : ASNE Day Conference, April 2009.

2. **Ramsey Jr., J.S.** *Shipboard Applications of Non-Intrusive load Monitoring.* s.l. : Master's thesis, Massachusetts Institute of Technology, Department of Electrical Engineering and Computer Science, June 2004.

3. **Mosman, J.P.** *Evaluation of Non-Intrusive Load Monitoring for Shipboard Cycling System Daignostics.* s.l. : Master's thesis, Massachusetts Institute of Technology, Department of Mechanical Engineering, June 2006.

4. **Bennett, Patrick Lawrence.** *Using the Non-Intrusive Load Monitor for Shipboard Supervisory Control.* s.l. : Master's thesis, Massachusetts Institute of Technology, Department of Mechanical Engineering, June 2007.

5. **Proper, Ethan R.** *Automated Classification of Power Signals.* s.l. : Master's thesis, Massachusetts Institute of Technology, Department of Mechanical Engineering, June 2008.

6. **Jones, Richard.** *Improving Shipboard Applications of Non-Intrusive Load Monitoring.* s.l. : Master's thesis, Massachusetts Institute of Technology, Department of Mechanical Engineering, June 2008.

7. **Branch, Perry.** *Development of Real-Time Non-Intrusive Load Monitor for Shipboard Fluid Systems.* s.l. : Master's thesis, Massachusetts Institute of Technology, Department of Mechanical Engineering, June 2008.

8. **Department of the Navy.** Department of the Navy FY 2008 Budget Table of Contents. [Online] February 2007. [Cited: February 11, 2009.] http://www.finance.hq.navy.mil/FMB/08PRES/HIGHBOOK/Highlights_book.pdf.

9. **Chief of Naval Operations.** *CONDITION-BASED MAINTENANCE (CBM) POLICY.* May 1998.

10. **DiUlio, Michael, et al.** Taking the Integrated Condition Assessment System to the Year 2010. [Online] [Cited: February 11, 2009.] http://www.acq.osd.mil/log/mpp/cbm+/Navy/ICAS%202010_paper191.doc.

11. **Fredner, Scott, Imbesi, John and Spaulding, Leslie.** Smart Ship Installations in Full Swing; SSES is Supporting. [Online] November 2000. [Cited: February 11, 2009.] http://www.dt.navy.mil/pao/excerpts%20pages/2000/smartship_Nov.html.

12. **Smith, Jeffrey.** Director Expeditionary Warfare Ships Division NAVSEA 05D3. *email correspondence.* April 15, 2009.

13. **Leeb, S, Shaw, S and Kirtley, J.** *Transient Event Detection in Spectral Envelope Estimates for Nonintrusive Load Monitoring.* s.l. : IEEE Transactions on Power Delivery, vol. 10, no. 3, pp. 1200-1210, July 1995. pp. 1200-1210.

14. **Shaw, S.R.** *System identification techniques and modeling for nonintrusive load diagnostics.* s.l. : PhD, Massachusetts Institute of Technology, Department of Electrical Engineering and Computer Science, February 2000.

15. **Shaw, S.R. and Laughmann, C.R.** *A kalman-filter spectral envelope preprocessor.* s.l. : IEEE Transactions on Instrumentation and Measurement, vol. 56, no. 5, pp. 2010-2017, October 2007.

16. **Remscrim, Z.** s.l. : Master's thesis*(unpublished).*, Massachusetts Institute of Technology, Department of Electrical Engineering and Computer Science, expected June 2010.

17. **McKay, Thomas Duncan.** *Diagnostic Indicators for Shipboard Mechanical Systems Using Non-Intrusive Load Monitoring.* s.l. : Master's Thesis, Massachusetts Institute of Technology, Department of Mechanical Engineering, June 2006.

18. **Greene, CDR William.** *Non-Intrusive Monitoring for Condition Based Maintenance.* s.l. : Master's thesis, Massachusetts Institute of Technology, Department of Mechanical Engineering, June 2005.

19. **DeNucci, T.W.** *Diagnostic Indicators for Shipboard Systems using Non-Intrusive Load Monitoring.* s.l. : Master's thesis, Massachusetts Institute of Technology, Department of Mechanical Engineering, June 2005.

20. **Piber, Mark A.** *Improving Shipboard Maintenance Practices Using Non-Intrusive Load Monitoring.* Cambridge, MA : Master's thesis, Massachusetts Institute of Technology, Department of Mechanical Engineering, June 2007.

21. **Lee, K.** *Electric load information system based on non-intrusive power monitoring.* s.l. : PhD, Massachusetts Institute of Technology, Department of Electrical Engineering and Computer Science, 2003.

22. Instruction Manual for the Envirovac Vacuum Sewage Collection System, United States Coast Guard 270' B Class WMEC. Vol. Technical Publication NO. 2839.

23. **Goshorn, Lieutenant J.A., Engineer Officer, USCGC ESCANABA (WMEC 907).** Command Letter of Appreciation, Ser 5700. 20 NOV 2008.

24. **Wichakool, Warit, et al.** *NILM Progress Report to NASA.* April 27, 2009.

25. **Stanton, Captain M., USN.** *Commanding Officer, Supervising of Shipbuilding, Bath, ME.* [interv.] William Greene. January 21, 2005.

26. **Laughman, C., et al.** *The detection of liquid slugging phenomena in reciprocating compressors vis power measurements.* West Lafayette, IN : In Proc. International Compressor Engineering Conference at Purdue, 2006.

27. *Octoparts Specs.* [Online] [Cited: March Thursday, 2009.] http://sigma.octopart.com/132067/datasheet/LEM-LA-150-P.pdf.

28. *DataSheet Catalog.* [Online] [Cited: March 26, 2009.] http://www.datasheetcatalog.org/datasheet/lem/LA205-S.pdf.

29. **Cox, R, et al.** *Diagnostic Indicators for Shipboard Cycling Systems Using Non-Intrusive Load Monitoring.* Arlington, VA : in American Society for Naval Engineers Day 2006, June 2006.

30. **Cox, R, et al.** *Shipboard fluid system diagnostic indicators using nonintrusive load monitoring.* Philadelphia, PA : in American Society for Naval Engineers Day 2007, June 2007.

31. **Cox, R.** *Minimally Intrusive Strategies for Fault Detection and Energy Monitoring.* s.l. : PhD thesis, Massachusetts Institute of Technology, Department of Electrical Engineering and Computer Science, August 2006.

32. **Mitchell, G, et al.** *Shipboard Fluid System Diagnostic Indicators Using Non-Intrusive Load Monitoring.* s.l. : Naval Engineers Journal, vol. 119, no. 1, November 2007.

33. **Proper, Ethan, et al.** *Field Demonstration of a Real-Time Non-Intrusive Monitoring System for Condition Based Maintenance.* National Harbor, Maryland : in Electric Ship Design Syposium, February 2009.

34. **Shaw, S, et al.** *Nonintrusive Load Monitoring and Diagnostics in Power Systems.* s.l. : IEEE Transactions on Instrumentation and Measurement, vol. 57, no. 7, pp. 1445-1454, July 2008. pp. 1445-1454.

35. *CONDITION-BASED MAINTENANCE (CBM) POLICY.* **Chief of Naval Operations.** 06 MAY 1998, OPNAVINST 4790.16.

36. **Greene, CDR William.** *Non-Intrusive Monitoring for Condition Based Maintenance.* 2005, American Society for Naval Engineers.

37. **Leeb, S, Shaw, S and Kirtley, J.** *Transient Event Detection in Spectral Envelope Estimates for Nonintrusive Load Monitoring.* 1995, IEEE Trans. on Power Delivery, pp. 1200-1210.

38. **Cox, R, et al.** *Diagnostic Indicators for Shipboard Cycling Systems Using Non-Intrusive Load Monitoring.* Arlington, VA : s.n., 2006. In Proc. ASNE Day 2006.

39. **Cox, R, et al.** *Improving Shipboard Maintenance Practices Using Non-Intrusive Load Monitoring.* Philadelphia, PA : s.n., 2007. In Proc. ASNE Intelligent Ships Symposium VII.

40. **Mitchell, G, et al.** *Shipboard Fluid System Diagnostic Indicators Using Non-Intrusive Load Monitoring.* Arlington, VA : s.n., 2007. In Proc. ASNE Day .

41. **Shaw, S, et al.** *Nonintrusive Load Monitoring and Diagnostics in Power Systems.* 2008, IEEE Trans. on Instrumentation and Measurement, pp. 1445-1454.

42. **Piber, Mark A.** *Improving Shipboard Maintenance Practices Using Non-Intrusive Load Monitoring.* Cambridge, MA : Massachusetts Institute of Technology S.M. NAME/S.M. ME Thesis, June 2007.

43. **Ramsey Jr., J.S.** *Shipboard Applications of Non-Intrusive load Monitoring.* s.l. : Massachusetts Institute of Technology NSEE/S.M. EECS Thesis, June 2004.

44. **Mosman, J.P.** *Evaluation of Non-Intrusive Load Monitoring for Shipboard Cycling System Daignostics.* s.l. : Massachusetts Institute of Technology, NE/S.M. ME Thesis, June 2006.

45. **Branch, Perry.** *Development of Real-Time Non-Intrusive Load Monitor for Shipboard Fluid Systems.* s.l. : Massachusetts Institute of Technology, S.M. Engineering Management Thesis, June 2008.

46. **Proper, Ethan R.** *Automated Classification of Power Signals.* s.l. : Massachusetts Institute of Technology, N.E./S.M. E.M, June 2008 Thesis, June 2008.

47. **DeNucci, T.W.** Diagnostic Indicators for Shipboard Systems using Non-Intrusive Load Monitoring. s.l. : Massachusetts Institute of Technology, S.M. NAME/S.M. ME Thesis, June 2005.

48. **Proper, Ethan, et al.** *Field Demonstration of a Real-Time Non-Intrusive Monitoring System for Condition Based Maintenance.* 2008.

49. **Lee, K.** *Electric load information system based on non-intrusive power monitoring, Ph.D. diss.* s.l. : Massachusetts Institute of Technology, 2003.

50. **Jones, Richard.** *Improving Shipboard Applications of Non-Intrusive Load Monitoring.* s.l. : Massachusetts Institute of Technology, Thesis Naval Engineer's Degree/S.M. Engineering and Management, June 2008.

51. **Cox, R.** *Minimally Intrusive Strategies for Fault Detection and Energy Monitoring.* Cambridge : Massachusetts Institute of Technology, Ph.D. Diss.

52. **Bennett, Patrick Lawrence.** *Using the Non-Intrusive Load Monitor for Shipboard Supervisory Control.* s.l. : Massachusetts Institute of Technology, Thesis Naval Engineer, S.M. M.E., 1996.

53. **Paris, James, et al.** *Scalability of Non-Intrusive Load Monitoring for Shipboard Applications.* s.l. : American Society for Naval Engineers (submitted), 2009.

54. **Shaw, S.R.** *System identification techniques and modeling for nonintrusive load diagnostics.* s.l. : PhD, Massachusetts Institute of Technology, Department of Electrical Engineering and Computer Science, February 2000.

55. **Remscrim, Z.** *Masters Thesis (unpublished).* s.l. : Massachusetts Institute of Technology, Department of Electrical Engineering and Computer Science, expected June 2010.

56. **Shaw, S.R. and Laughmann, C.R.** *A kalman-filter spectral envelope preprocessor.* pp.2010-2017, s.l. : IEEE Transactions on Instrumentation and Measurement, October 2007, Vol. 56.

Appendix: MATLAB Script Files

```
%SCRIPT TO PLOT DOWNSTREAM DATA FROM ESCANABA CHT%%%%%%%%%%%%%%%%%%%%%%%%%%%%%%
%Keith Douglas%%%%%%%%%%%%%%%%%%%%%%%%%%%%%%%%%%%%%%%%%%%%%%%%%%%%%%%%%%%%%%%
%%%%%%%%%%%%%%%%%%%%%%%%%%%%%%%%%%%%%%%%%%%%%%%%%%%%%%%%%%%%%%%%%%%%%%%%%%%%%
clc;clear all;

y=textread('snapshot-20081017-060001.1.txt');

%%%%%%%%%%%%%%%Convert to average power and plot%%%%%%%%%%%%%%%%%%%%%%%%%%%%%
%RMS voltage
    V = 440;

%Measurement Resistor Value set with dip switches in NILM box
    Rm = 100;

%Current Transducer Scaling Factor for LEM LA 55-P
%   K = 1/1000;

%Current Transducer Scaling Factor for LEM LA 205-S or LA 150-P
    K = 1/2000;

%Voltage range across ADC; gain code =0 corresponds to +/- 5v
    g = 10;

%ADC bit size or count range
    bits=2^12;

%This takes RMS voltage along with current input and scale factors
%and%converts to 3 phase average power.  The 1/64 accounts for prep FFT that
%samples 128 points
    P1= V*(1/64)*(g/bits)*(1/Rm)*(1/K)*(1/sqrt(2))*y;

%Time vector converted into minutes
    t = [0:1:length(P1)-1]*(1/120)*(1/60);

%Plot Figure in black and white only
figure= figure('Color',[1 1 1]);

% Create plot.  Column 1 corresponds to real power; Col. 2 Reactive Power
plot(t,-P1(:,2)./1000-.1258,'Color',[0 0 0]);

% Create ylabel
ylabel('Real Power (kW)','FontSize',12);

% Create xlabel
xlabel('Time (Minutes)','FontSize',12);

% title('Local CHT NILM');

axis tight;
```

```
%SCRIPT TO PLOT UPSTREAM DATA FROM ESCANABA CHT%%%%%%%%%%%%%%%%%%%%%%%%%%%%%%
%%%%%%%%%%%%%%%%%%%%%%%%%%%%%%%%%%%%%%%%%%%%%%%%%%%%%%%%%%%%%%%%%%%%%%%%%%%%
clc;clear all;

%Read in the prep files for both local and upstream events.  These files
%have already been time-aligned while in raw data format
%upstream power signal
x=textread('snapshot-20081022-020001.1.txt');

%Convert to average power and plot
     V =  440;
     Rm = 30;
     K =  2000;
     g  =   10;
     bits=4096;


%Upstream Power value
%column 1 is real power; column 2 is reactive

     P= V*(1/64)*(g/bits)*(1/Rm)*K*(1/sqrt(2))*x(:,1);
     t = [0:1:length(P)-1]*(1/120)*(1/60);


%Plot Figure
figure= figure('Color',[1 1 1]);

%upstream plot
plot(t,P-868,'Color',[0 0 0]);

title('Power Panel 2-282-3','FontSize',16);
ylabel('Real Power (W)','FontSize',12);

% ylabel('Reactive Power (VAR)','FontSize',12);
xlabel('Time (Minutes)','FontSize',12);
axis tight;
```

```
%SCRIPT TO PLOT DOWNSTREAM AND UPSTREAM DATA FROM ESCANABA CHT%%%%%%%%%%%%%%%
%%%%%%%%%%%%%%%%%%%%%%%%%%%%%%%%%%%%%%%%%%%%%%%%%%%%%%%%%%%%%%%%%%%%%%%%%%%%
clc;clear all;

%Read in the prep files for both local and upstream events.  These files
%have already been time-aligned while in raw data format
%upstream power signal
x=textread('snapshot-20081022-020001.1.txt');

%downstream
y=textread('snapshot-20081022-020001.down.txt');

%Convert to average power and plot
V =  440;
Rm = 75;          %local
Rm1 = 30;         %upstream
K =  2000;        %local
K1 = 2000;        %K for downstream CT
g  =   10;
bits=4096;

%downstream Power value
%cols1 and 2 provide real and reactive coefficients only

P= V*(1/64)*(g/bits)*(1/Rm)*K*(1/sqrt(2))*y(:,1);
t = [0:1:length(P)-1]*(1/120)*(1/60);

%upstream Power value

%column 1 is real power; column 2 is reactive
P1= V*(1/64)*(g/bits)*(1/Rm1)*K1*(1/sqrt(2))*x(:,1);
t1 = [0:1:length(P1)-1]*(1/120)*(1/60);

%Plot Figure
figure= figure('Color',[1 1 1]);

%upstream plot
subplot(2,1,1);
plot(t1,P1-868,'Color',[0 0 0]);
title('Power Panel 2-282-3','FontSize',16);
ylabel('Real Power (W)','FontSize',12);

% ylabel('Reactive Power (VAR)','FontSize',12);
xlabel('Time (Minutes)','FontSize',12);
axis tight;

%downstream plot
subplot(2,1,2);
plot(t+.44,-P,'Color',[0 0 0]);
title('CHT Control Panel','FontSize',16);
xlabel('Time (Minutes)','FontSize',12);
ylabel('Real Power (W)','FontSize',12);
```

```
% ylabel('Reactive Power (VAR)','FontSize',12);
axis tight;
```

```
%Script for plotting 3SA and LOSP2A, SLOW to OFF exemplar, and
cross%correlation plots of upstream %and downstream
%Keith Douglas, April 2009
%MATLAB plot m-file generation was used to determine plot format codes

clear all; clc;

%%%%%%%%%%%%%%%%%%%%%%%%%%%%%%%%%%%%%%%%%%%%%%%%%%%%%%%%%%%%%%%%%%%%%%%%%%%%%%%
%%%%%%%%%%3SA DEFINITIONS%%%%%%%%%%%%%%%%%%%%%%%%%%%%%%%%%%%%%%%%%%%%%%%%%%%%%

 %high and low gain data available; col1 Q, col2 P
x=textread('3SA_fullprepsnapshot-20080619-110001.1.txt');

%RMS VOLTAGE
 V = 440;

%bits
b=4096;

%3SA has two channels-ch.1 VR=5 ch.2 VR=20
%VR = 20;
 VR=5;

%3SA has two amplification levels,G, as well.  Ch.1 G=10; Ch.2 G=100;
 G=10;
%G=100;

%KN is Fluke i3000 conversion ratio of .1 mV/A
k=1e-4;

%3 phase average power
P = sqrt(3)*V*x(1:431900,2)*VR/(64*b*G*k*sqrt(2));

%%%%%%%%%%%%%%%%%%%%%%%%%%%%%%%%%%%%%%%%%%%%%%%%%%%%%%%%%%%%%%%%%%%%%%%%%%%%%%%
%%%%%%%%%%%LOCAL LOAD DEFINITIONS%%%%%%%%%%%%%%%%%%%%%%%%%%%%%%%%%%%%%%%%%%%%%

%LOSP2A

y=textread('LO_fullprepsnapshot-20080619-110002.1.txt');
Rm = 20;
k = 2500;  %K=2500 for LEM LA 305P
VR = 10;
P1 = sqrt(3)*V* y(:,2)*VR*k/(64*b*Rm*sqrt(2));
t = [0:1:length(P1)-1]*(1/120)*(1/60);

%%%%%%%%%%%%%%%%%%%%%%%%%%%%%%%%%%%%%%%%%%%%%%%%%%%%%%%%%%%%%%%%%%%%%%%%%%%%%%%
%%%%%%PLOT OF 3SA VS. VARIOUS LOCAL LOADS%%%%%%%%%%%%%%%%%%%%%%%%%%%%%%%%%%%%%%

% Create figure
figure1 = figure('Color',[1 1 1]);

% Create subplot
subplot1 =
subplot(2,1,1,'Parent',figure1,'FontSize',14,'FontName','CambriaMath');
```

```
% Uncomment the following line to preserve the X-limits of the axes
xlim([33 37]);
box('on');
hold('all');

% Create plot of 3SA
plot(t-.004,-P/1000,'DisplayName','3SA','Parent',subplot1,'Color',[0 0 0]);

% Create ylabel
ylabel({'Power (kW)'},'LineWidth',1,'FontSize',16,'FontName','CambriaMath');

% Create legend
legend1 = legend(subplot1,'show');
set(legend1,'YColor',[1 1 1],'XColor',[1 1 1],'FontSize',14);

% Create subplot
subplot2 =
subplot(2,1,2,'Parent',figure1,'FontSize',14,'FontName','CambriaMath');

% Uncomment the following line to preserve the X-limits of the axes
  xlim([33 37]);

box('on');
hold('all');

% Create plot of downstream load
plot(t,-P1/1000,'DisplayName','LOSP 2A','Parent',subplot2,'Color',[0 0 0]);

% Create ylabel
ylabel({'Power (kW)'},'LineWidth',1,'FontSize',16,'FontName','CambriaMath');

% Create xlabel
xlabel({'Time (min)'},'LineWidth',1,'FontSize',16,'FontName','CambriaMath');

% Create legend
legend2 = legend(subplot2,'show');
set(legend2,'YColor',[1 1 1],'XColor',[1 1 1],'FontSize',14);

%%%%%%%%%%%%%%%%%%%%%%%%%%%%%%%%%%%%%%%%%%%%%%%%%%%%%%%%%%%%%%%%%%%%%%%%%%%%%%%
%%%%%%%%%%%%%%%%%%%%cross correlation%%%%%%%%%%%%%%%%%%%%%%%%%%%%%%%%%%%%%%%%%%

%Define exemplar
%LARGE
% exemplar=-P1(254808:256180);
%SMALL
exemplar=-P1(239050:239100);

%remove DC bias
exemplar=exemplar-mean(exemplar);

%Create new figure
figure2 = figure('Color',[1 1 1]);

% Create axes
axes2 = axes('Parent',figure2','FontSize',14,'FontName','CambriaMath');
```

```
box('on');
hold('all');

% Create plot of exemplar
t_exemp=[0:1:length(exemplar)-1]*(1/120);
plot(t_exemp,exemplar/1000,'DisplayName','OFF to SLOW Exemplar','Color',[0 0
0],'LineWidth',2);
axis tight;

% Create ylabel
ylabel({'Power (kW)'},'LineWidth',2,'FontSize',16,'FontName','CambriaMath');

% Create xlabel
xlabel({'Time (sec)'},'LineWidth',2,'FontSize',16,'FontName','CambriaMath');

% Create legend
legend2 = legend(axes2,'show');
set(legend2,'YColor',[1 1 1],'XColor',[1 1 1],'FontSize',14);

%%%%%%%%%%%%%%%%%%%%%%%%%%%%%%%%%%%%%%%%%%%%%%%%%%%%%%%%%%%%
%Cross correlation of exemplar with Upstream%%%%%%%%%%%%%%%%%%%%%%%%%%%%%

cross=xcorr(exemplar,-P)/norm(exemplar).^2;
M=length(cross);
t_cross=[-M/2:M/2-1]*(1/60)*(1/120);

%Create new figure
figure3 = figure('Color',[1 1 1]);
axes3=axes('Parent',figure3,'FontSize',14,'FontName','CambriaMath');
box('on');
hold('all');

% Create plot of cross correlation
plot(-t_cross,cross,'DisplayName','Upstream Correlation','Color',[0 0
0],'LineWidth',2);
axis tight;

% Comment out to view full data file
xlim([33 37]);
line([0 60],[.9 .9],'LineStyle','--','LineWidth',1,'Color','k');
line([0 60],[1.1 1.1],'LineStyle','--','LineWidth',1,'Color','k');

% Create ylabel
ylabel({'Correlation
Value'},'LineWidth',2,'FontSize',16,'FontName','CambriaMath');

% Create xlabel
xlabel({'Time (min)'},'LineWidth',2,'FontSize',16,'FontName','CambriaMath');

% % Create legend
legend3 = legend('Upstream Correlation','Detection Window');
set(legend3,'YColor',[1 1 1],'XColor',[1 1 1],'FontSize',14);

% Create plot of correlation
```

```
plot(-t_cross,cross,'DisplayName','Upstream Correlation','Color',[0 0
0],'LineWidth',2);
line([0 60],[.9 .9],'LineStyle','--','LineWidth',1,'Color','k');
line([0 60],[1.1 1.1],'LineStyle','--','LineWidth',1,'Color','k');

% Create ylabel
ylabel({'Correlation
Value'},'LineWidth',2,'FontSize',16,'FontName','CambriaMath');

% Create xlabel
xlabel({'Time (min)'},'LineWidth',2,'FontSize',16,'FontName','CambriaMath');

% % % Create legend
legend2 = legend('Upstream Correlation','Detection Window');
set(legend2,'YColor',[1 1 1],'XColor',[1 1 1],'FontSize',14);

 %%%%%%%%%%%%%%%%%%%%%%%%%%%%%%%%%%%%%%%%%%%%%%%%%%%%%%%%%%%%%%%%%%%%%%%%%%%
%%%%%%%%%%%%%%%%Peak Detection Algorithm Peak Detection%%%%%%%%%%%%%%%%%%%%%
%peakdet.m file courtesy of Eli Billauear at
%http://www.billauer.co.il/peakdet.html for %release to public
%domain

%This portion of the script calls the peak detector function,
identifies%where the peaks occur, then plots %the positive i.d.'s (based on
threshold%set by user)

[maxtab1,mintab1]=peakdet(cross,0.1,-t_cross);
k=length(maxtab1);

%preallocate matrix
hold=zeros(k,2);

%look for max values between threshold specified in 'if' statement,
for i = 1:length(maxtab1)
    if maxtab1(i,2) <= 1.1 && maxtab1(i,2) >= 0.9
        hold(i)=maxtab1(i,2);
    else
end
end

%Create new figure and plot output of maxtab col 1, time from t_cross, to
%see spikes

figure4 = figure('Color',[1 1 1]);
axes4=axes('Parent',figure4,'FontSize',14,'FontName','CambriaMath');
box('on');
hold('all');

% Create plot of cross correlation results using peak detector to find them

plot(maxtab1(:,1),hold,'DisplayName','Upstream Correlation Spikes','Color',[0
0 0],'LineWidth',2);
xlim([0 60]);
line([0 60],[.9 .9],'LineStyle','--','LineWidth',1,'Color','k');
line([0 60],[1.1 1.1],'LineStyle','--','LineWidth',1,'Color','k');
```

```
% Create ylabel
ylabel({'Correlation
Spikes'},'LineWidth',1,'FontSize',16,'FontName','CambriaMath');

% Create xlabel
xlabel({'Time (min)'},'LineWidth',1,'FontSize',16,'FontName','CambriaMath');

% % Create legend
legend4 = legend( 'Upstream Positive Detection Spikes');
set(legend4,'YColor',[1 1 1],'XColor',[1 1 1],'FontSize',14);

%%%%%%%%%%%%%%%%%%%%%%%%%%%%%%%%%%%%%%%%%%%%%%%%%%%%
%Cross correlation of exemplar with Downstream%%%%%%%%%%%%%%%%%%%%%%%%%%%%
crossdown=xcorr(exemplar,-P1)/norm(exemplar).^2;

t_crossdown=[-M/2:(M-1)/2]*(1/60)*(1/120);

%Create new figure
figure5 = figure('Color',[1 1 1]);
axes5=axes('Parent',figure5,'FontSize',14,'FontName','CambriaMath');
box('on');
hold('all');

% Create plot of cross correlation

plot(-t_crossdown,crossdown,'DisplayName','Downstream Correlation','Color',[0
0 0],'LineWidth',2);

%Plot threshold window
line([0 60],[.9 .9],'LineStyle','--','LineWidth',1,'Color','k');
line([0 60],[1.1 1.1],'LineStyle','--','LineWidth',1,'Color','k');axis tight;
xlim([33 37]);
ylim([-1 2]);

% Create ylabel
ylabel({'Correlation
Value'},'LineWidth',1,'FontSize',16,'FontName','CambriaMath');

% Create xlabel
xlabel({'Time (min)'},'LineWidth',1,'FontSize',16,'FontName','CambriaMath');

% % Create legend
legend5 = legend('Downstream Correlation','Detection Window');
set(legend5,'YColor',[1 1 1],'XColor',[1 1 1],'FontSize',14);

%Peak Detector Algorithm
[maxtab2,mintab2]=peakdet(crossdown,0.1,-t_crossdown);
k=length(maxtab2);

%preallocate matrix
hold2=zeros(k,2);

for i = 1:length(maxtab2)
    if maxtab2(i,2) <= 1.1 && maxtab2(i,2) >= 0.9
```

```
        hold2(i)=maxtab2(i,2);
    else
    end
end

%Create new figure
figure6 = figure('Color',[1 1 1]);
axes6=axes('Parent',figure6,'FontSize',14,'FontName','CambriaMath');
box('on');
hold('all');

% Create plot of cross correlation

plot(maxtab2(:,1),hold2,'DisplayName','DownstreamCorrelation
Spikes','Color',[0 0 0],'LineWidth',2);
xlim([0 60]);

% Create ylabel
ylabel({'Correlation
Value'},'LineWidth',1,'FontSize',16,'FontName','CambriaMath');

% Create xlabel
xlabel({'Time ( min
)'},'LineWidth',1,'FontSize',16,'FontName','CambriaMath');

% % Create legend
legend6 = legend('Downstream Correlation Spikes');
set(legend6,'YColor',[1 1 1],'XColor',[1 1 1],'FontSize',14);
```